Ageing of the LHCb outer tracker

Investigation of possible solutions and their effects on the detector performance

M. R. Blom
mblom@nikhef.nl

June 8, 2009

Masters Thesis
Master in Particle and astroparticle physics
Faculteit der exacte wetenschappen
Vrije Universiteit Amsterdam
Boelelaan 1083
1081 HV Amsterdam

Supervisor: Dr N. Tuning
Second reader: Dr P.J. Blankert

Project conducted at:
Nikhef, B-physics group
Science Park 105
1098 XG Amsterdam

Abstract

The modules of the LHCb outer tracker have shown to suffer severe gain loss under moderate irradiation. This process is called ageing. Ageing of the modules results from contamination of the gas system by glue, araldite AY 103-1, used in their construction. In this thesis the ageing process will be shown. The schemes known to reduce, reverse, or prevent ageing have been investigated to determine their effect on the detector performance. The addition of O2 to the gas mixture lowers the detector response by an acceptable amount and does not affect the gas transport properties significantly. The ageing rate is decreased after extensive flushing and HV training could eventually repair the irradiation damage. The risks of HV training have been assessed. Furthermore, several gaseous and aquatic additions have been tested for their capability to prevent, or moderate ageing, but none showed significant improvement.

Contents

List of Tables

List of Figures

Chapter 1

Introduction

Matter and antimatter are believed to have been produced in equal amounts during the Big Bang, but the observable universe seems to be matter dominated. There must be a fundamental difference between matter and antimatter. The search for the mechanism behind this asymmetry is one of the unsolved mysteries in contemporary physics.

In 1967, Sakharov formulated three conditions necessary to explain this imbalance [1]. One of these requirements was that the laws of physics may not be invariant under combined parity transformation (reversal of spatial coordinates) and charge transformation (replacing particles with their antiparticles), otherwise known as violation of CP symmetry [2].

Kobayashi and Maskawa [3] showed CP violation can only occur if there are more than two generations of quarks[1]. In 1964, CP violation was discovered in the neutral kaon system[2] [4] and in 2002 also in the B meson system. CP violation is accommodated in the Standard Model, which describes elementary particles and their interactions. However, the amount of CP violation is to small to fully explain the absence of antimatter.

A great research effort is made at the Large Hadron Collider (LHC) at CERN, Geneva, by the LHCb experiment to investigate CP violation and explain the asymmetry between matter and antimatter. A state-of-the-art detector has been built to determine the properties of the particles created in the LHC proton-proton collisions. However, one of its subdetectors, the outer tracker, used for measurement of the particle momenta, suffers from ageing [5]: degradation of the signal response due to radiation.

1.1 The LHCb experiment

Violation of CP symmetry has been observed directly in the decays of B mesons (mesons containing a bottom quark, b, or an anti-b quark, $\bar{b}$). An example is the decay of the B^0 meson (bound state of d quark and $\bar{b}$ quark) into K^+ and π^-. Its CP conjugate, $\bar{B^0} \to K^- + \pi^+$, does not have the same branching ratio.

In the high energy (center-of-mass energy of 14 TeV) proton-proton collisions of the LHC, many B mesons and $b\bar{b}$ pairs, will be created. The LHCb experiment will use these to study CP violation in the B meson system with high statistics and unprecedented precision.

[1] Awarded the Nobel prize in physics 2008
[2] Awarded the Nobel prize in physics 1980

1.1.1 The LHCb detector

The $b\bar{b}$ pairs are mainly produced at small angels with the LHC beam line. The LHCb detector has therefore been designed as a single-arm forward spectrometer. A cross section of the detector is shown in figure 1.1. The acceptance of the detector covers a region from 15 to 300 mrad in the horizontal x-z plane and 15 to 250 mrad in the vertical y-z plane [6]. One third of all produced $b\bar{b}$ pairs will decay within the detectors acceptance.

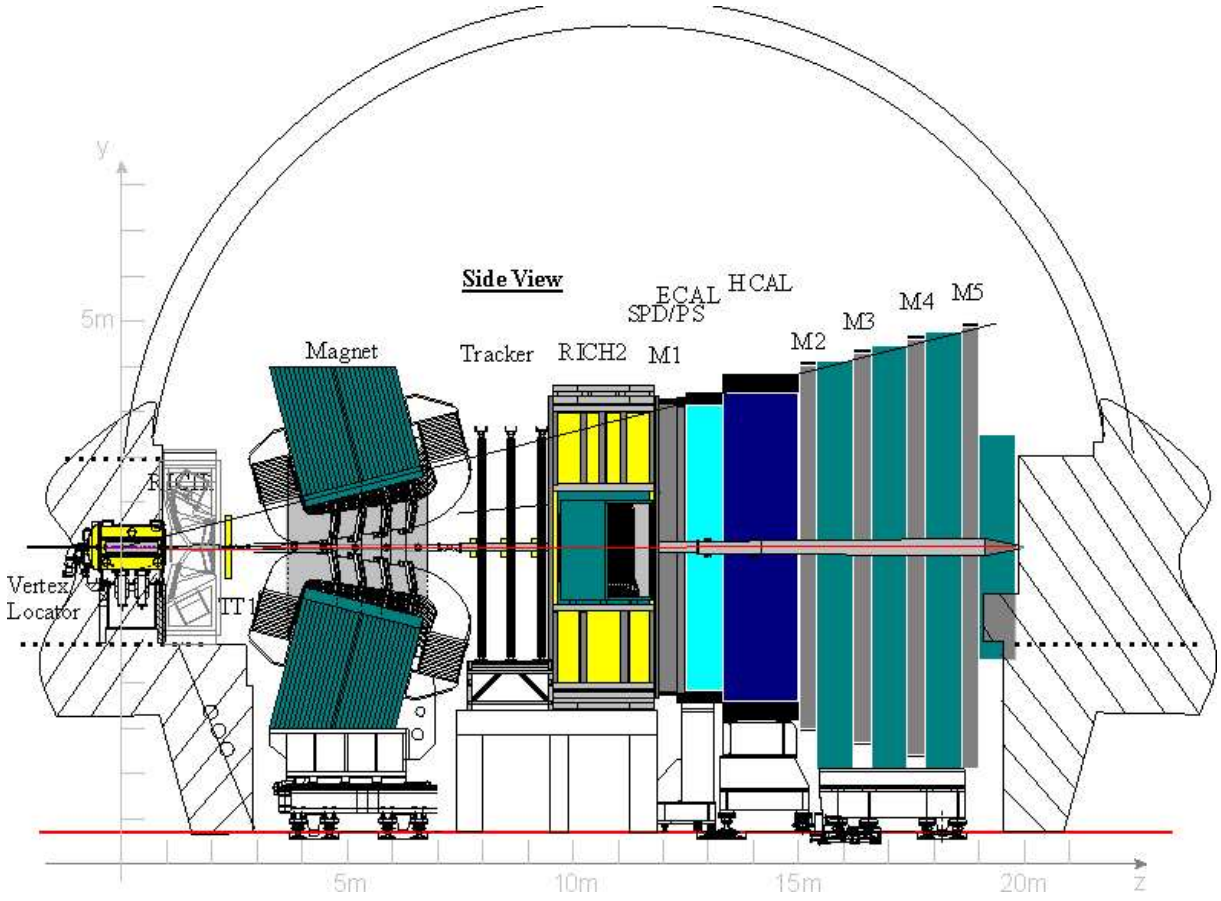

Figure 1.1: *A schematic representation of the LHCb detector in its cavern. It is a single-arm forward spectrometer, 20 m long and 5 m high. The LHC beam pipe is the gray horizontal tube along the axis. The proton-proton collisions will take place in the vertex locator, depicted on the left of the figure.*

The gray horizontal axis is the LHC beam pipe. Collisions will occur in the Vertex Locator (left in figure 1.1), which will determine the proton-proton collision point (primary vertex) and the point at which the produced B meson decays (secondary vertex). The distance between the primary and secondary vertex is used to estimate the lifetime of the B meson. The trigger tracker (TT1), inner and outer tracker (Tracker), are used to reconstruct the flight paths (tracks) of the particles and their decay products. The particle tracks will be bend by the magnetic field of the dipole magnet (Magnet). The curvature of the tracks are used to determine the particle

momenta and reconstruct the B meson mass. The electromagnetic and hadronic calorimeters (ECAL, HCAL) reconstruct the energy and position of the electrons and hadrons, which are used together with data from the Ring Imaging Cherenkov detectors (RICH1, RICH2) for particle identification. The only particles that will be able to traverse the entire detector will be muons (and neutrinos). The muon detector, which consists out of five stations, M1 – M5, measures the charge of the muon, which serves as input for the fast selection of interesting events (triggering) and is used to determine the flavor of the initial B hadron (muon tagging).

1.2 The outer tracker

The LHCb outer tracker consists out of standalone units, built out of small drift cells (see section 2.2). The modules are arranged in planes as depicted in figure 1.2. The three outer tracker stations, labeled T1 – T3 in figure 1.1, consist out of four such planes, oriented at stereo angles of 0°, -5°, +5°and 0°with respect to the y-axis. As can be seen in figure 1.2 (left), four types of modules with different dimensions have been used: F, S1, S2 and S3 modules, so that they may be fitted closely around the beam pipe and inner tracker as shown in figure 1.2 (right).

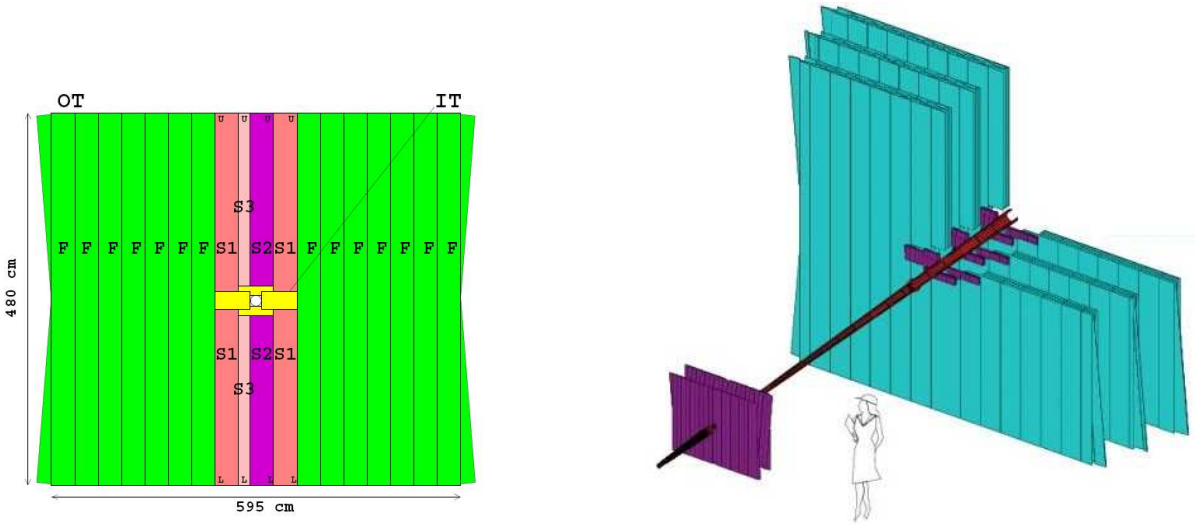

Figure 1.2: *Outer tracker layout.*

Outer tracker modules consists out of two layers of 64 straw tubes (see section 2.2), which are small cylindrical drift chambers. The outside wall is conducting and acts as cathode and a collecting wire along the axis of the tube as anode. They rely on the principle of electron multiplication. A charged particle that traverses a straw, ionizes gas molecules. Due to a potential difference between the cathode and anode, the liberated electrons will move towards the anode wire at a speed characteristic for the gas and free additional electrons on the way. The time it takes the electrons to reach the wire provides the distance at which the primary ionization took place. Hits in consecutive straw tubes, allow reconstruction of the particle track as depicted in figure 1.3.

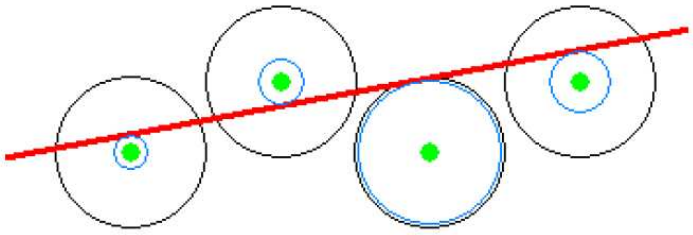

Figure 1.3: *Principle behind track reconstruction from hits in multiple outer tracker straw tubes.*

1.2.1 Ageing

The LHCb outer tracker modules have been designed to be operational for five years. But, when they are irradiated an insulating coating forms on the anode wire, which causes the number of collected electrons to decrease. Such deterioration of the detector response over time as a result of radiation is known as ageing. The ageing of the outer tracker has the potential to limit its lifetime and significantly influence the track reconstruction efficiency. A more thorough description of the outer tracker ageing can be found in section 2.3.

1.3 Outline

In this thesis we investigate the ageing of the LHCb outer tracker with the aim to prevent its occurrence. In chapter 2 the principles on which the operation of the outer tracker is based are summarized and the phenomenon of ageing introduced. Chapter 3 describes the outgassing test of the glue, which was conducted in an attempt to identify exactly which substances are emitted by the glue and may cause ageing. The experimental setup used to conduct ageing tests is described in chapter 4. It has been used to determine the effects on the ageing rate of several gaseous and aquatic additions to the outer tracker gas mixture. The results of these investigations are treated in chapter 5. Addition of O_2 to the counting gas has been shown to reduce the ageing rate, but also lowers the signal response of the detector. Quantification of the loss of signal response and the effects on other gas transport properties are the subject of chapter 6. In chapter 7 schemes we know to prevent, or reverse ageing are further investigated to determine whether their application could cause structural damage of the detector. Finally, the most important conclusions are summarized in chapter 8.

Chapter 2

Drift chambers

A drift chamber is a detector that measures ionization using gas multiplication.A traversing particle with sufficient energy may ionize the gas molecules. This is called the primary ionization. The number of electrons liberated in this process is too small to be measured and has to be increased by electron multiplication. A drift chamber consists of a cathode and an anode. Due to the potential difference, the electrons drift towards the anode. A possible configuration is a cylindrical straw tube, consisting of a conducting wall connected to ground which acts as a cathode, filled with a counting gas at pressure P and a thin anode wire along its axis at some potential V_0 [7]. The primary method of this multiplication and some secondary phenomena are explained in this chapter. In addition the drift chambers which are used in the LHCb outer tracker are discussed and the phenomena of ageing from which these detectors suffer introduced.

2.1 Gas and transport properties

2.1.1 Drift velocity

Due to the potential difference between the cathode and anode an electric field is present in the gas volume. Under the influence of this electric field the electrons that are created in the primary ionization will move towards the positive anode, the ions to the cathode. The average velocity of this motion is called drift velocity, v^+ for ions, v^- for electrons. It is proportional to the reduced electric field, E/P, and depends strongly on the detector configuration. The mobility, μ^+, is a general property of the gas and is defined by:

$$v^+ = \mu^+ \frac{E}{P} \tag{2.1}$$

Table 2.1 gives the mobility of several ions drifting in different gases.

Because electrons are much lighter than ions, they move roughly a thousand times faster. Therefore electrons can substantially increase their energy between collisions with gas molecules.

2.1.2 Avalanche formation

At electric field strengths of a few kV/cm, the electrons from the primary ionization are accelerated to an energy at which they can ionize gas molecules themselves. These extra electrons are

Gas	Ion	Mobility ($cm^2\,V^{-1}\,s^{-1}$)
Ar	Ar^+	1.7
Ar	CO_2^+	1.72
CO_2	CO_2^+	1.7
CO_2	O_2^+	1.32
O_2	O_2^+	2.2

Table 2.1: *Experimental mobilities of several ions in different gases, at normal conditions. [8, 9]*

accelerated and produce more ionizations. This process is the basis of avalanche multiplication (see figure 2.1). The ratio of the charge collected on the anode wire and the amount of charge liberated in the primary ionization is defined to be the gain. It generally assumes values between 10^3 and 10^7.

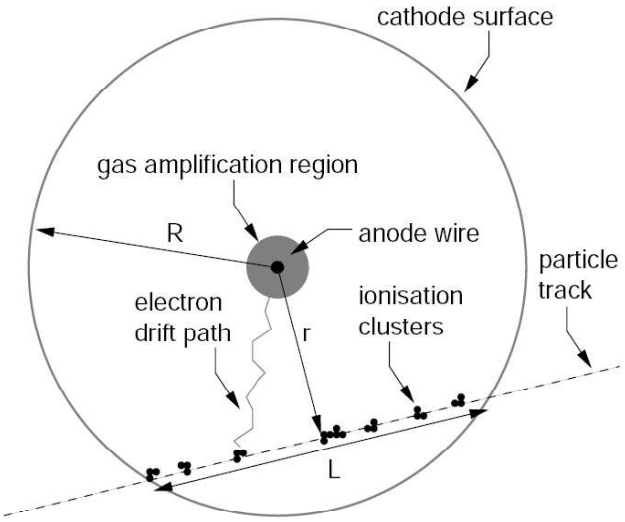

Figure 2.1: *Illustration of working principles of cylindrical drift cell. R is the cell radius, r the radius of closest approach of the particle to the wire and L the length of the particle track inside the cell. [10]*

The mean free path for ionization is defined as the average distance the electrons need to travel to gain enough energy for an ionization. The inverse of this mean free path is called the first Townsend coefficient, α, and represents the number of ion pairs created per unit length.

Let n be the number of electrons at a given position. After a path dx, the increase in the number of electrons will be [8]:

$$dn = n\,\alpha\,dx \tag{2.2}$$

and by integration:

$$M = \frac{n}{n_0} = e^{\alpha x} \tag{2.3}$$

M is the multiplication factor, or gain. In general the electric field will not be uniform. Then $\alpha = \alpha(x)$ and equation (2.3) will become:

$$M = \exp\left[\int_{r_c}^{r_a} \alpha(r)\, dr\right] \tag{2.4}$$

In which r_c and r_a are the radius of the cathode and anode.

This Townsend mechanism is the main mechanism in the formation of an avalanche. Therefore in general equation (2.4) should give the gain. However, other mechanisms that amplify or quench the avalanche take place. Therefore it only gives the size of the so-called Townsend avalanche.

The size of the avalanche at a certain working voltage depends in many ways on the counting gas. The choice of the gas mixture is governed by several factors: low working voltage, high gain and high rate capability. Noble gases are usually chosen as principle gas, because avalanche multiplication occurs at much lower field strengths than in gases with complex molecules. This is a consequence of the many non-ionizing energy dissipation modes available in poly-atomic molecules like vibrations and rotations. Argon is the most commonly used because of its low cost. In most cases a gas mixture rather than a pure gas is used. A so-called quench gas is added to the principle gas to suppress undesirable effects such as photon and ion feedback.

Photon and ion feedback

If pure argon would be used as a fill gas, values of the gain larger than $10^3 - 10^4$ would not be possible. In the avalanche multiplication process excited molecules are formed. Excited molecules can emit a photon that can easily ionize the cathode and start a new avalanche. This process is known as photon feedback. It is remedied by the addition of a polyatomic gas as methane or a inorganic gas as CO_2 that acts like a quench gas. It absorbs the photons and dissipates their energy in a non-radiant way.

The ions formed in the cascade will drift towards the cathode, where they are neutralized by extracting an electron. The excess energy will be lost for instance by radiating a photon. That photon can initiated a new avalanche relatively long after the primary avalanche.

The poly-atomic quench gases have many non-radiative excited states which allows for a efficient photon absorption in a wide range of energies [11, 12]. A small amount of quench gas in the order of 10% can completely change the behaviour of the detector. In this way gains of the order of $10^6 - 10^7$ may be achieved.

Electron attachment

One of the processes that can quench the Townsend avalanche is electron attachment. Free electrons can be captured by electronegative atoms to form negative ions,

$$e^- + X \rightarrow X^- + h\nu \tag{2.5}$$

Electron affinity is a measure for the probability of a molecule to capture an electron in this way. Some gases that are known to be electronegative are: O_2, H_2O and CO_2.

The mean free path for electron capture is defined as the distance an electron can travel before it is captured. The inverse of this mean free path is called the attachment coefficient, η, and represents the number electrons captured per unit length. We can now define an effective Townsend coefficient, α_{eff}:

$$\alpha_{eff} = \alpha - \eta \tag{2.6}$$

Penning effect

The Penning effect is the ionization of gas A by an excited molecule of gas B^*.

$$A + B^* = A + B^+ + e^- \tag{2.7}$$

Penning effects [12] can occur between excited states in the gas mixture which are higher in energy than the lowest ionization potential in the mixture. Molecules of the principle gas (argon in case of the outer tracker) may enter a metastable state. The excited state, unaffected by the electric field, will stay in the gas volume. If the excitation energy of the excited atom is larger than the ionization energy of the quench gas, a collision of the two may produce a secondary electron. Such electrons can significantly increase the size of the avalanche and hence, the gain. Some excitation energies as well as the ionization energy for some relevant gases are listed in tables 2.2 and 2.3.

Gas	Ionization (eV)
Ar	15.76
CO_2	13.77
O_2	12.07

Table 2.2: *Ionization energy for the relevant gases. [13]*

Tables 2.2 and 2.3 show that the excited argon-D state has enough energy (14 eV) to ionize a CO_2 molecule, which needs 13.77 eV.

$$CO_2 + Ar^* = Ar + CO_2^+ + e^- \tag{2.8}$$

Should oxygen be added to the gas mixture [15], the Penning effect is expected to increase, because O_2 molecules (with an ionization energy of 12.07 eV) will be ionized by excited argon-D, CO_2-5 and CO_2-6 states with energies of 14, 13.2 and 15 eV respectively. This effect will be taken into account in gas property simulations as discussed in chapter 6.

Energy level	Excitation energy (eV)
Ar-S	11.55
Ar-P	13
Ar-D	14
CO_2-1	7.9
CO_2-2	8.9
CO_2-3	10.5
CO_2-4	12.2
CO_2-5	13.2
CO_2-6	15

Table 2.3: *Excitation energies for argon and carbon dioxide. [14]*

2.2 Straw tubes

The outer tracker of the LHCb detector comprises 53760 straw tubes. One straw tube is a cylindrically shaped drift chamber with a radius of 2.45 mm.

The wall of these straws is made of two layers of windings. The inner winding consists of a carbon-doped kapton film of 40 μm thickness and acts as cathode. The outer winding is a 25 μm thick kapton-aluminum foil, which insures electric insulation between neighboring straws to prevent cross talk.

The anode wire is made of tungsten with a thin layer of gold and has a radius of 12.7 μm. The wire has to be of high quality. Pores and cracks in the gold layer could allow wire etching, which could lead to breaking of the wire, rendering the straw useless. To keep the gold-tungsten anode wire in the middle of the straw, it is supported by so-called wire locators at regular intervals. These wire locators are plastic cylinders, spaced at intervals of 80 cm, with an aperture of 50 μm for the wire.

One outer tracker module consists of two layers of 64 straws. A cross section of such a module is shown in figure 2.2. The straw tubes are glued to the panel with Araldite AY 103-1. The cathodes of the cells are grounded, the anode wires are kept at 1520 V. This gives every straw tube a gain of about 4×10^4 [16].

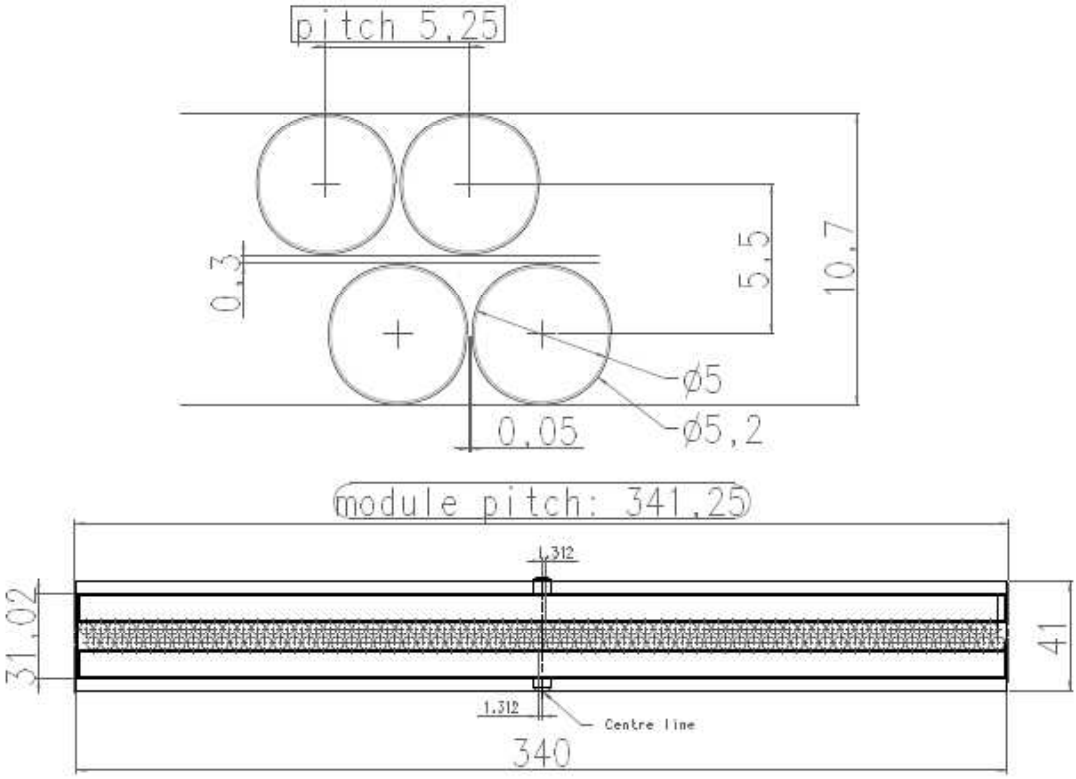

Figure 2.2: *Cross section of straw tube module. [17]*

2.3 Ageing

Ageing generally means that the gain of a drift chamber decreases over time under the influence of radiation. The cathode and anode are damaged by the very radiation which needs to be detected. Ageing is common amongst drift chambers and has been observed in many detectors. Several types of ageing are known. They have been described in [18].

Ageing is a poorly understood phenomenon, despite its long history. It depends on many parameters. The gas composition, irradiation intensity and possible gas pollutants have been observed to be important. When designing and building a detector, it is impossible to be sure beforehand if an ageing effect will take place or not. To determine whether a setup has an acceptable ageing rate or not, so-called ageing tests have to be conducted. To simulate ten years of operation in the hostile environment of the LHC, these tests have been conducted with elevated irradiation levels for shorter times [10], which is the usual procedure for ageing tests. The tests conducted for the LHCb outer tracker showed that no significant ageing took place [19].

However, in 2005 a strong ageing effect has been observed in the outer tracker modules [20]. Apparently no ageing takes place at high irradiation intensities, but for mild intensities significant gain loss has been observed.

Studies have shown that outgassing of the glue, Araldite AY 103-1, used to glue the straw tubes to the panels is the culprit [18, 21, 22]. Before assembling the outer tracker modules, the outgassing properties of the glue had been investigated [23] and Araldite AY 103-1 was classified as save. Since, it has been shown that a small amount of outgassing takes place. When the straw tubes are irradiated, the pollution in the gas forms an insulating carbon-containing layer on the anode wire, which reduces the detector response and ultimately could limit its lifetime.

All outer tracker modules have been built and installed. The glue used for their construction is an integral part of the detector. This means that the ageing of the modules can not be stopped by removing the glue. Therefore ways to either remove the carbon deposit from the anode wire, or prevent its formation, will need to be found.

The rest of this thesis focuses on understanding the ageing process of the outer tracker cells and investigating possible solutions. The outgassing of the glue and additions to the gas mixture that could prevent or limit deposition originating from it, are studied.

.

Chapter 3

Outgassing

Gas emitted by the glue, araldite AY 103-1, pollutes the outer tracker gas system and causes ageing of the detector. We would like to identify exactly which substances are emitted by the glue and determine the total outgassing rate. To achieve that we have placed a sample of araldite in a vacuum chamber and measured the mass spectrum of the residual gas with a quadrupole mass spectrometer. We have done the same for the glue, trabond 2115, which has shown not to cause ageing [22].

3.1 Outgassing test

3.1.1 Setup

To determine the outgassing properties of araldite and trabond, samples (1.0 and 0.58 gr respectively) are placed in a vacuum chamber and the residual gas analyzed with a quadrupole mass spectrometer[1].

Figure 3.1 depicts the setup used to analyze the gas emitted by araldite AY 103-1 and trabond. Two vacuum chambers, a primary one, VA, and a secondary one, VB, are separated by a valve. The two vacuum chambers are both being evacuated by a turbo molecular pump[2] at a rate of 60 $mbarLs^{-1}$. The pressure in both chambers is measured with a pirani pressure gauge[3]. The pressure in VB can be put to atmospheric pressure with dry nitrogen gas, so that a glue sample may be inserted. Dry nitrogen gas can be evacuated efficiently from the vacuum chambers and does not contain pollutants like water, which attaches to the walls.

A sample of araldite AY 103-1, handled with care to avoid contamination, is placed in VB. When the pressures in both VA and VB are of the order of 10^{-8} mbar the valve separating them is opened and the sample is lifted into VA with a special lever. The lever is retrieved and the valve closed. In this way the glue sample is placed into the vacuum vessel with the mass spectrometer with the lowest possible amount of contamination.

The mass spectrometer ionizes gas molecules. A quadrupole mass filter sorts the produced ions according to their mass/charge ratio (M/Z) [24, 25]. In this way a characteristic mass spectrum

[1] Balzers prisma QME 200
[2] Pfeiffer TMU 071 P
[3] Balzers 20 TPR 018 Pirani

is obtained for every gas component. If several substances are present in VA, the measured mass spectrum is the sum of the individual mass spectra of all components.

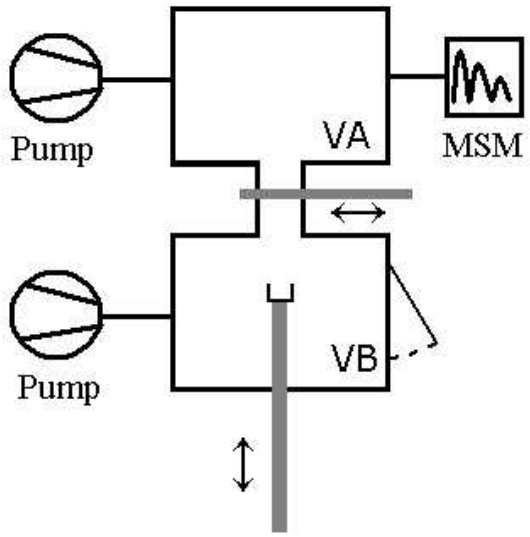

Figure 3.1: *Schematic representation of the vacuum setup to measure the outgassing speed of araldite and trabond and determine which gasses are emitted by these glues.*

3.1.2 Quantifying outgassing

The pressure in the vacuum chamber at any time is a result of a dynamic balance between the ability of the pump to remove gas from the system and the gas released into the system by processes such as: leaks, outgassing and vaporisation [25].

Figures 3.2 and 3.3 depict the pressure in the primary vacuum vessel (VA) as a function of time for three evacuations: one with araldite in the vessel, one with trabond in the vessel, one for an empty vessel. The uncertainties in the measurements correspond to the daily variation in the pressure caused by temperature fluctuations. The evacuation of the empty vessel takes significantly less time than the of one containing a glue sample. A pressure between 10^{-9} and 10^{-8} mbar is reached within 10 hours (see figure 3.2). The glue samples release gasses into the chamber, continuously supplying the pump with a gas load, resulting in a higher pressure.

Immediately after the glue samples have been placed in VA, the pressure increases rapidly to a value of the order of 10^{-6} mbar and decreases again to approximately 10^{-7} mbar. The pressure increase is caused by the mass spectrometer itself. The glue sample in VA is situated in a small metal bucket. The distance between the bucket and the mass spectrometer is small. The filament of the mass spectrometer, which ionizes the gas molecules is hot. It heats up the bucket and the glue, increasing the amount of outgassing. After approximately 100 hours the outgassing speed starts to decrease exponentially with time.

Figure 3.3 shows that the pressure in VA is much higher with trabond than it is with araldite after the same period of evacuation. This means that trabond emits gas at a higher rate than araldite. The material released by trabond does not cause ageing [22] and must therefore be a different, harmless substance. The mass spectra obtained for both glues should then be different (see section 3.2).

The pumping speed, S, is known to be 60 $mbarLs^{-1}$. The absolute outgassing rate, Q, of both glues at any pressure, p, is therefore given by equation 3.1.

$$Q = S \times p \tag{3.1}$$

The ultimate pressure in the vacuum chamber is reached when the pumping speed and the continuous supply of gas are equal. This equilibrium pressure will be higher when a glue sample is present in the the vacuum chamber. But figure 3.3 shows that with glue present no steady pressure is reached. Instead, the pressure keeps declining exponentially, but much slower compared to the empty vessel. This indicates that the outgassing of the glue samples decreases exponentially with time. If outgassing results from the chemical reaction that causes hardening of the glue, less outgassing could mean that the rate at which hardening of the glue takes place decreases. To determine the timescale of this process, the pressure curves in figure 3.3 have been fitted with:

$$p = Ce^{\frac{-t}{\tau}} \tag{3.2}$$

The values of the characteristic time scale, τ, for araldite and trabond are given in table 3.1.

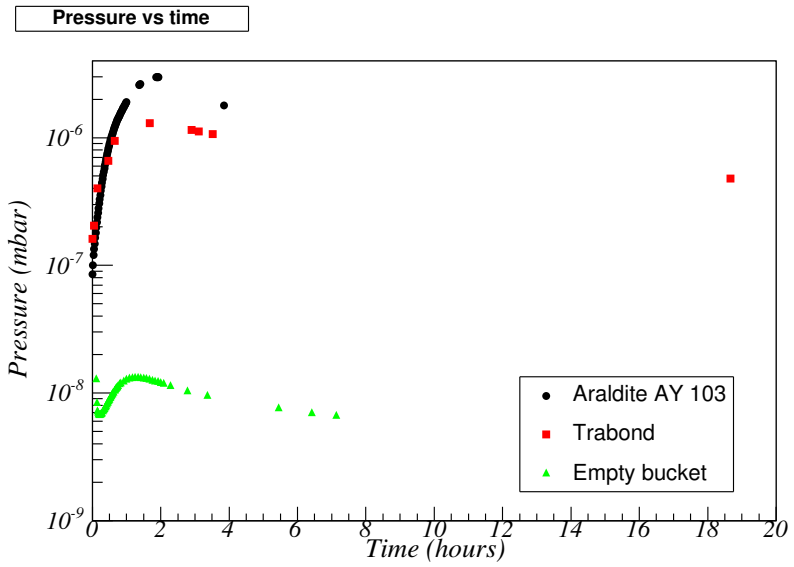

Figure 3.2: *Pressure in the primary vacuum vessel as a function of time for both glues, the first 20 hours. The pressure curves have been fitted with equation 3.2.*

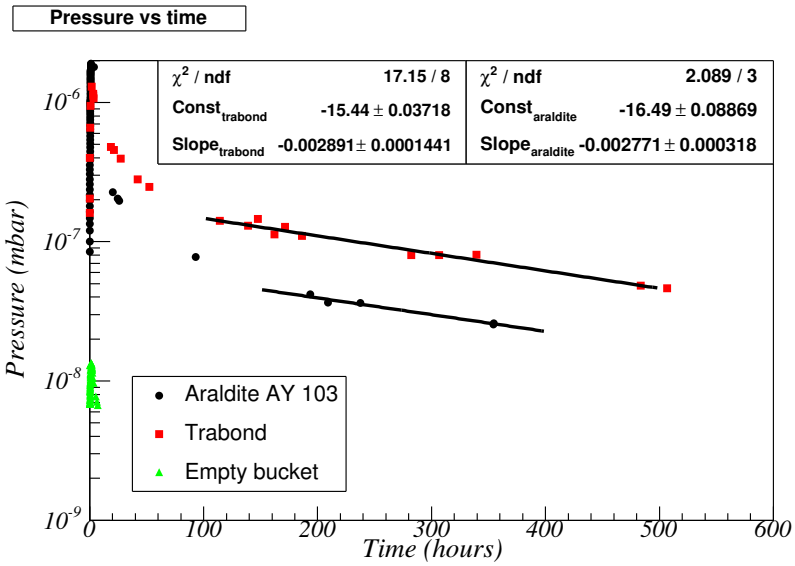

Figure 3.3: *Pressure in the primary vacuum vessel as a function of time for both glues. The pressure curves have been fitted with equation 3.2.*

No ultimate value for the pressure and hence, for the outgassing rate, is reached during the outgassing test. But the lowest pressure reached with glue in the vacuum chamber, does give an upper limit on the outgassing speed of the sample. This upper limit is also given in table 3.1.

Glue	τ (hr^{-1})	τ (days)	Upper limit outgassing speed ($mbarLs^{-1}$)
Araldite	-0.0028 ± 0.0003	14.9 ± 1.6	$2.4\ 10^{-6}$
Trabond	-0.0029 ± 0.0001	14.4 ± 0.7	$9.0\ 10^{-6}$

Table 3.1: *Upper limit for the outgassing speeds of araldite AY 103-1 and trabond.*

The outgassing rates of araldite and trabond seem to decrease with nearly the same characteristic time, about 14.5 days. Maybe, the characteristic timescales, τ, determined in vacuum are not the natural timescales at which trabond and araldite harden in the modules, but the time it takes the vacuum to draw water from the glue samples.

The outgassing tests have been conducted in vacuum, while the glue in the outer tracker modules resides at atmospheric temperature. Assuming that the outgassing speed in vacuum and at atmospheric pressure decrease at the same rate, an estimate can be made for the time it will take the concentration of pollution in the outer tracker modules to reach a certain concentration. The pressure in VA at the start of the exponential decrease in figure 3.3 is $4.0{\times}10^{-8}$ mbar. According to equation 3.1 this corresponds to an outgassing rate of $2.4{\times}10^{-6}$ $mbarLs^{-1}$, which may be used as the initial outgassing rate of the araldite sample at $t = 0$. This outgassing rate would translate to a concentration of 141 ppm in an outer tracker module under atmospheric

pressure with a gas exchange rate of 20 L/hr. After 15 days the outgassing rate would have decreased to 8.8×10^{-7} $mbarLs^{-1}$, which would translate to a concentration of 52 ppm in an outer tracker module. This leads us to believe that either the measured decrease in outgassing rate is not from hardening of the glue, but is caused mostly by dehydration of the glue sample in vacuum, or the assumption that outgassing in vacuum and at atmospheric pressure take place at the same rate is wrong.

3.1.3 Comparison to earlier outgassing test

Outgassing tests [23], designed to predict whether certain materials and substances will cause ageing, qualified araldite AY 103-1 as non-outgassing. The material under investigation was put into a container through which clean gas was flushed. The gas flowing out of the box was analyzed, using gas chromatography and a mass spectrometer. This test had a detection sensitivity up to the ppm level. For some substances, an electron capture devise could be used and a detection sensitivity better than ppb could be achieved, so that concentrations of the order of 10^{-6} mbar could be detected.

The upper limit for the outgassing speed of araldite measured with the quadrupole mass spectrometer is of the order of $2.4\times10^{-6}mbarLs^{-1}$. At this rate it would take the glue sample we used 400 seconds to contaminate a volume of 1 L with 1 ppm pollution, which was the detection sensitivity of the outgassing test [23]. This means that the detection limit of the conducted outgassing test may not have been sufficient to observe outgassing of the glue, depending on the size of their sample and gas flow. We shall see that most of the matter emitted by the glues is water (section 3.2), which does not cause ageing. The concentration of the harmful pollutant may have been below the detection limit of the earlier tests.

3.2 Mass spectra

The absolute outgassing rates of araldite AY 103-1 and trabond 2115 have been measured with the vacuum setup of figure 3.1. The aim was to identify the precise molecules emitted by araldite. To this end mass spectra of araldite and trabond have been measured using a quadrupole mass spectrometer.

A filament in the mass spectrometer ionizes and, in some cases, fragments molecules from the gas under study. The produced ions are separated according to their mass/charge ratio by a time depending, radio frequency electric field. The mass spectra obtained by this process are the sum of the individual mass spectra of the gas components. Identification of the components arises from comparison to their individual mass spectra which have been measured separately or, need to be obtained from literature.

Before the outgassing test, the chamber is baked out at a temperature of 50°C for several hours to remove gas molecules from the wall. This heating procedure cleans the vacuum chamber sufficiently, but some amount of air, water and N_2 is expected to remain in the chamber as a result of earlier contamination of the vacuum. A background spectrum is measured before the glue is placed in VA (see figure 3.1). An example of such a spectrum is shown in figure 3.4. It is understood using the literature spectra of air, water, N_2, CO_2 and H_2.

Water is notoriously difficult to remove from the vacuum system. Its mass spectrum has high peaks at 16, 17 and 18 AMU, that are expected to dominate the spectrum. However, the relative size of the peaks at these masses consistently disagree with the water spectrum from literature. The background spectra in figure 3.4 is therefore used as a gauge measurement for water and the remaining peaks at the mentioned masses, expected to belong to water (16, 17 and 18 AMU), are scaled accordingly.

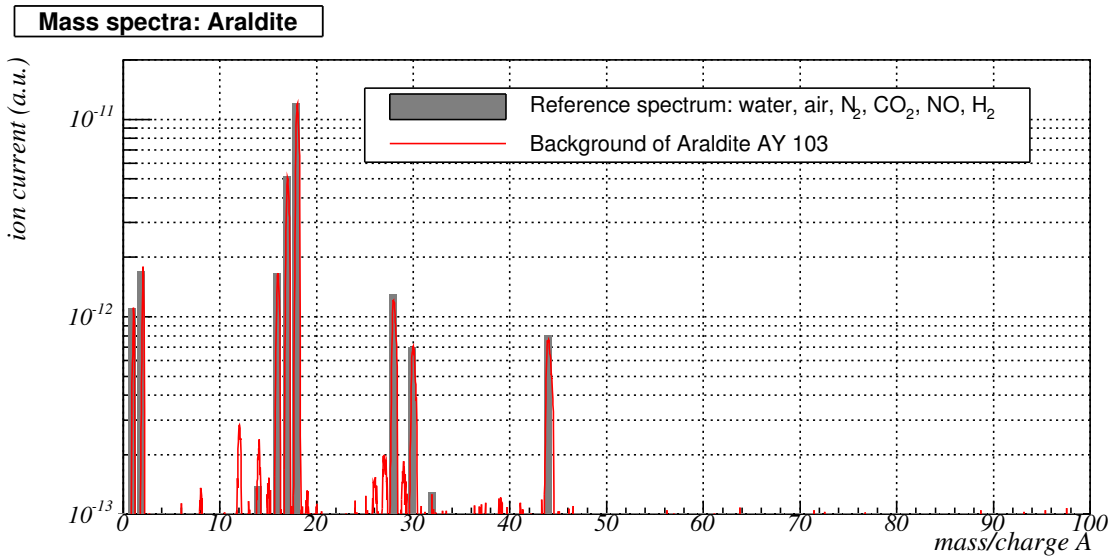

Figure 3.4: *Solved mass spectrum of empty primary vacuum vessel, VA, used as background of the araldite measurement.*

Figure 3.5 depicts the mass spectra measured for araldite AY 103-1 and trabond. The araldite spectrum was measured at a pressure of 2.6 10^{-8} mbar, reached after 93 hours of pumping. The trabond spectrum was measured at a pressure of 4.6 10^{-8} mbar, reached after 139 hours of pumping. Their respective background spectra, that were measured before insertion of the samples, have been subtracted. As expected, the spectra look similar for masses below 50 AMU, since water, air and N_2 should be present in both measurements. For masses above 50 AMU, the spectra differ significantly, due to the different chemical composition of the glue samples. In the next section, the spectra are studied in detail.

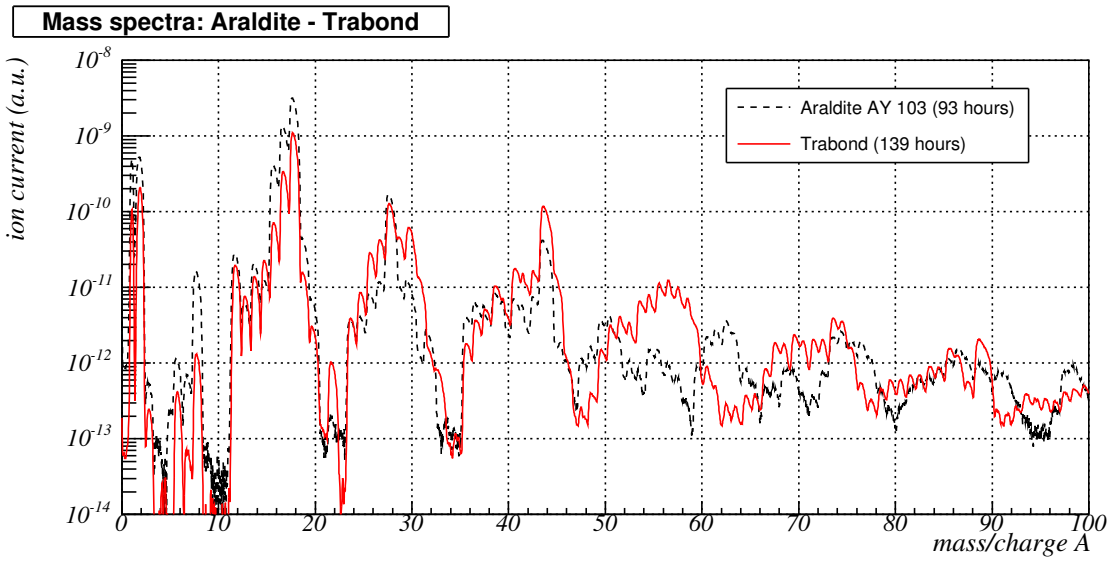

Figure 3.5: *Mass spectra of Araldite and Trabond after 93 and 139 hours of evacuating respectively.*

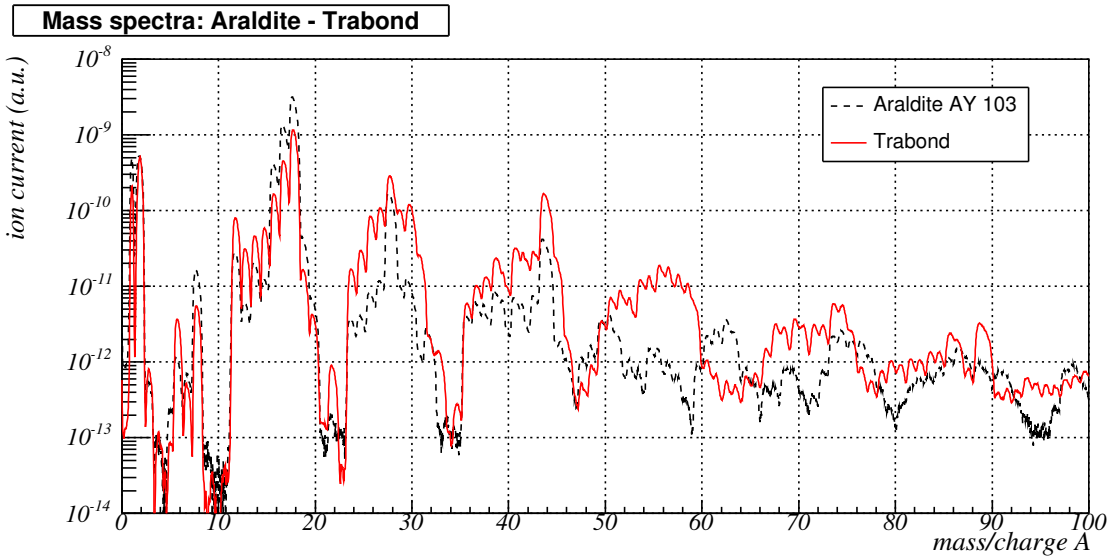

Figure 3.6: *Mass spectra of Araldite and Trabond after 360 and 480 hours of evacuating respectively.*

3.3 Mass spectrum analysis

3.3.1 The amount of water in araldite

The mass spectrum of araldite in figure 3.7, measured at a pressure of 5.55×10^{-8} mbar, shows that the major part of the emitted substances is water (peaks at 16, 17 and 18 AMU). Therefore, the outgassing rate of molecules that cause ageing is much lower than the rate determined in section 3.1.2. Correcting for the outgassing rate of water could increase our knowledge of the outgassing rate of the harmful pollution.

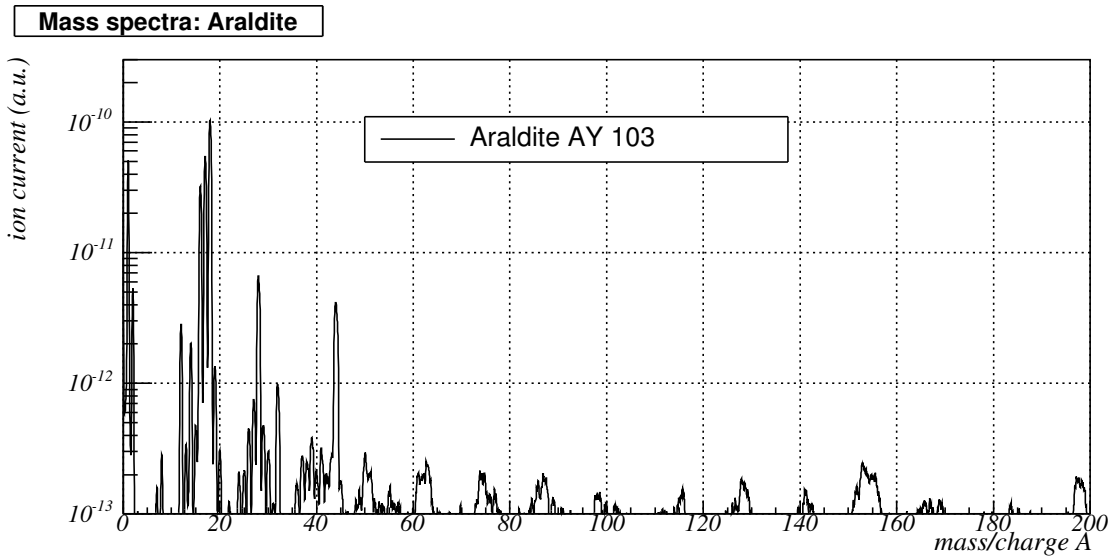

Figure 3.7: *Araldite mass spectrum.*

As mentioned before, water produces peaks in the mass spectrum at 16, 17 and 18 AMU. The ratio of the heights of these peaks is fixed and their absolute size depends on the partial pressure of water in the vacuum. The height of the mass peak at 18 AMU is therefore a measure for the water concentration in the chamber and may be used to determine its partial pressure.

Mass spectra of the empty vacuum chamber, like the one in figure 3.4, may be solved without much difficulty, because they only contain the well known spectra of water, air, N_2 and hydrogen. Such spectra, measured at different pressures between 10^{-8} and 10^{-10} mbar have been solved. This gives the relative concentrations of all its constituents and , since the total pressure is known, their partial pressures. Therefore, the relation between the height of the mass peak at 18 AMU and the partial pressure of water in the chamber is obtained.

Figure 3.8 shows the relation between the mass peak at 18 AMU and the absolute vapor pressure of water in the vacuum chamber. The data points have been fitted with a straight line.

The height of the mass peak at 18 AMU in the araldite spectrum is 1.0×10^{-10}, which, according to the fit in figure 3.8, corresponds to a vapor pressure of 3.8×10^{-8} mbar. This is 68% of the total pressure. The upper limit on the outgassing rate of pollution molecules that cause

ageing in table 3.1 can thus be reduced to 7.5×10^{-7} $mbarLs^{-1}$ and the maximum concentration of the malicious molecules to 44 ppm, when the modules where constructed.

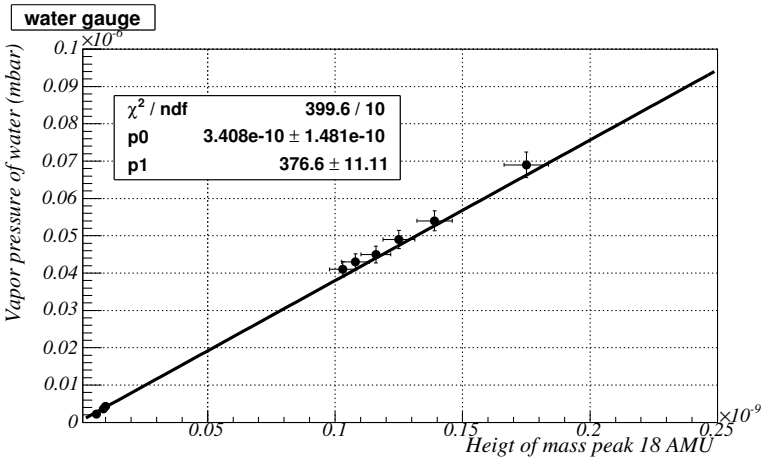

Figure 3.8: *Calibration mass peak 18 and water pressure.*

3.3.2 Molecules possibly emitted by araldite AY 103-1

It is difficult to solve the mass spectrum of araldite, without knowledge of all spectra of the individual gasses. Only the spectra of common gasses are well known and even these may not apply for the settings of our mass spectrometer. We could for instance experience stronger fragmentation of the gas molecules by the ionization filament of the MS, as seems to be the case for water. Individual gauge spectra should in principle be made for the substances which may be expected to be emitted by araldite. However, some molecules, of which the mass is known, are likely to show up in the mass spectrum of araldite.

The coating of the anode wires are hydrocarbons which attach to the wire surface [18]. The araldite mass spectrum should therefore contain the hydrocarbon. The ionization by the mass spectrometer can break the molecules. The spectra of the lightest hydrocarbons: methane, ethane and propane may be expected to be present in the araldite spectrum.

Furthermore, araldite AY 106 (not 103-1, which is used for the outer tracker) has been classified as outgassing: significant outgassing at room temperature has been observed [23]. Pollutants such as: butane, hexane, trimethylpentane and trimethylbutane were detected. These may also be present in araldite AY 103-1. But, since they were not detected in earlier outgassing studies, their concentration should be lower.

Figure 3.9 shows the spectra of methane and ethane taken from literature. The spectra of, for instance, ethane is not one sharp peak at its molecular mass, 30, but also molecules with masses below and above the molecular mass of ethane are present in the spectrum. This is because the ethane molecule may loose one, or several of its hydrogen atoms in the ionization process or may contain heavier isotopes of one of its constituents. Furthermore, fragmentation of ethane

molecules by the mass spectrometer causes a signal at masses associated with methane (14 and 15 AMU). Similar principles hold for heavier hydrocarbons.

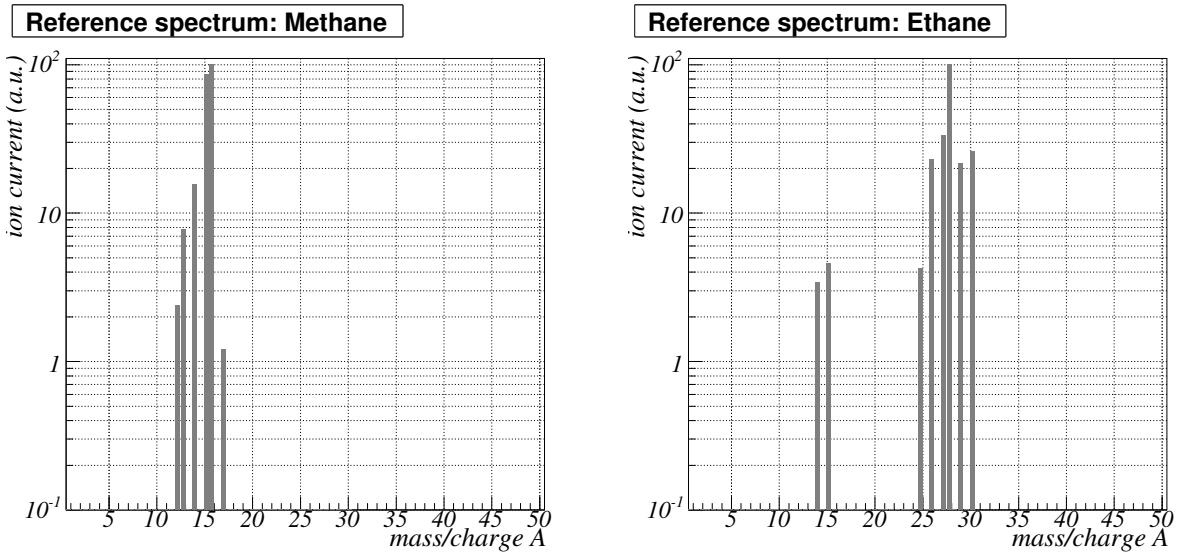

Figure 3.9: *Mass spectra of methane (CH_4) and ethane (C_2H_6) taken from literature.*

Figure 3.10 shows the araldite mass spectrum measured at a pressure of 2.4 10^{-8} mbar and the spectra of methane, ethane, propane and butane. They show that there is good agreement between the spectra and therefore it is likely that the mentioned hydrocarbons are present in the gas. They have either been emitted by the glue directly, or originate from a heavier hydrocarbon which was fractioned in the mass spectrometer.

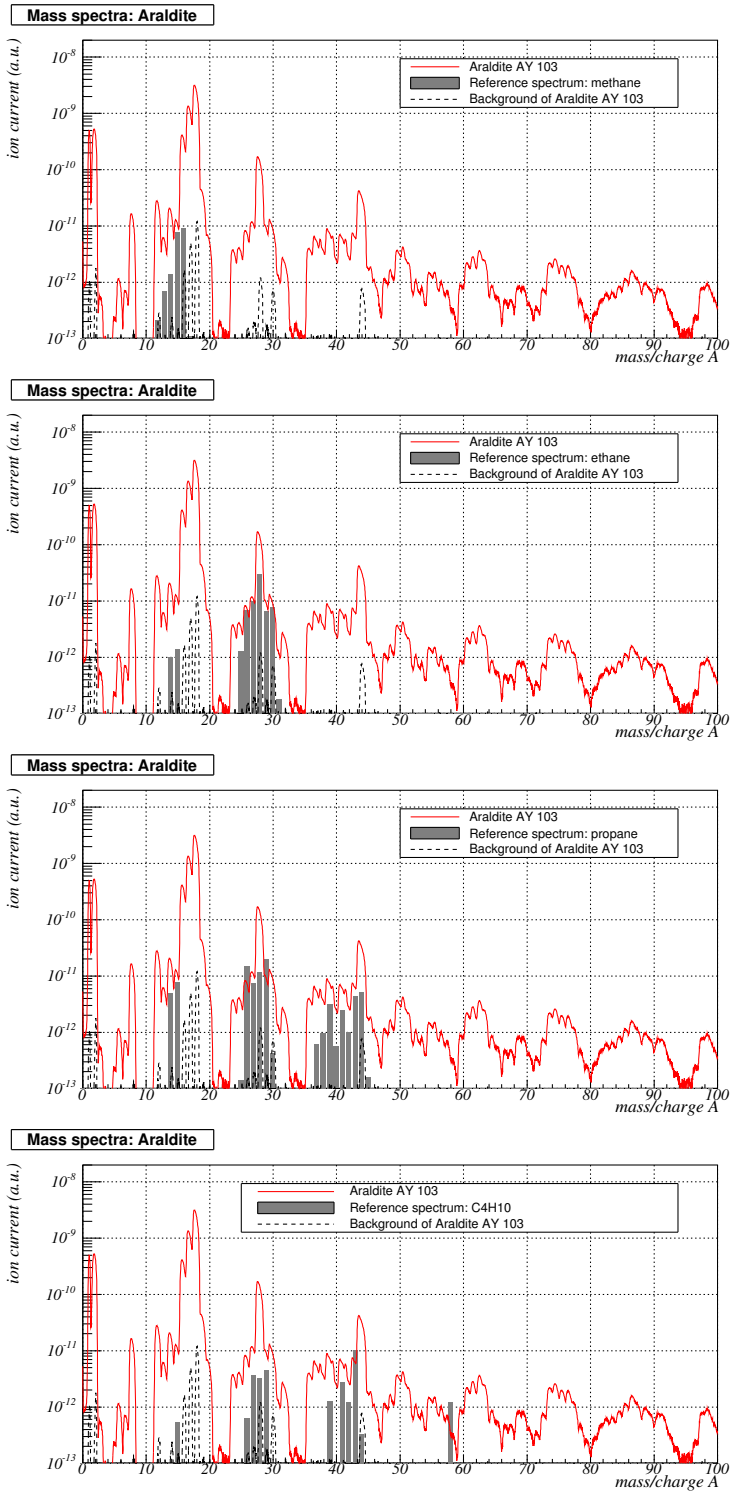

Figure 3.10: *Mass spectra araldite, methane, ethane, propane, butane.*

The gasses so far shown to be present in the araldite mass spectrum have well known mass spectra. Figure 3.11 shows the araldite spectrum solved for the lower masses. The gasses believed to be present in the spectrum together with their concentration relative to that of water (the most abundant constituent) are given in table 3.2. But yet, many substances with high molecular masses have not been identified.

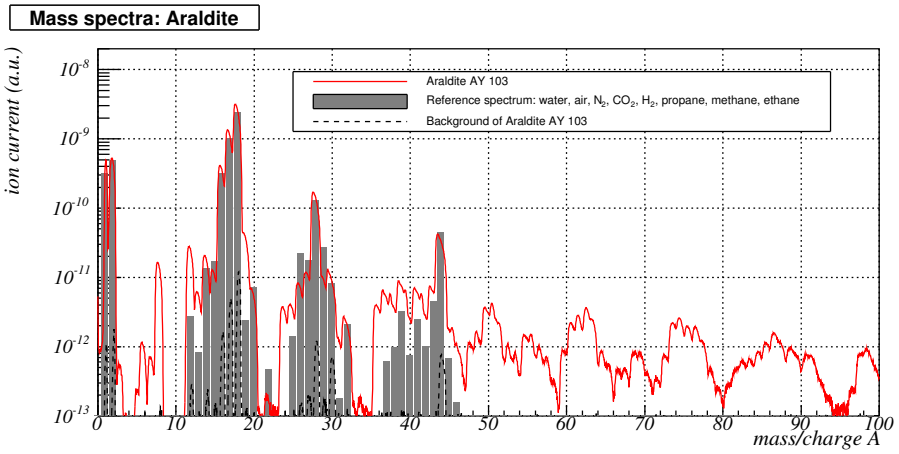

Figure 3.11: *Partially solved mass spectra of araldite.*

Gas	Concentration relative to water
Air	$5.4\ 10^{-3}$
Water	1
N_2	$2.9\ 10^{-2}$
CO_2	$1.6\ 10^{-2}$
Methane	$4\ 10^{-3}$
Ethane	$1.3\ 10^{-2}$
Propane	$8.3\ 10^{-3}$
H_2	0.21

Table 3.2: *Gas components of araldite with low masses and their respective concentration normalized to that of water.*

Epoxy chemistry

Next to small hydrocarbons, other molecules are likely to be present in the araldite mass spectrum. Araldite is an epoxy formed from bisphenol A and epichlorohydrin [26]. In the synthesis of epoxies, the resins are derived by using an excess of epichlorohydrin with respect to bisphenol A, in the presence of sodium hydroxide. The product of this synthesis is a crude diglycidyl ether of bisphenol A, DGEBA. The synthesis reaction is shown in figure 3.12.

In addition to the synthesis of the epoxide, side reactions that produce hydrolyzable chlorine, bound chlorine and α-glycol (see figure 3.13), take place [27]. The content of these by-products in the final composition is usually 20-30%. These compounds may also be present in the araldite glue sample. Their molecular masses are listed in table 3.3. The molecules found to be emitted by araldite AY 106, mentioned in section 3.3.2 are also included.

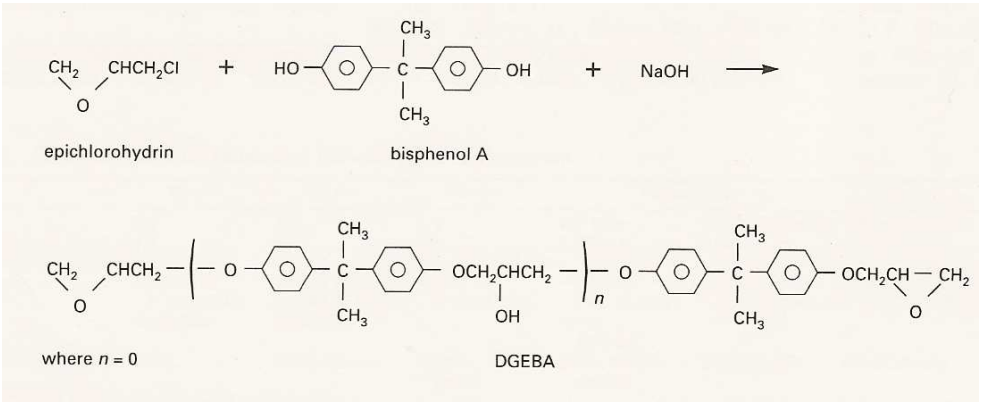

Figure 3.12: *Molecular structure of bisphenol-A [27].*

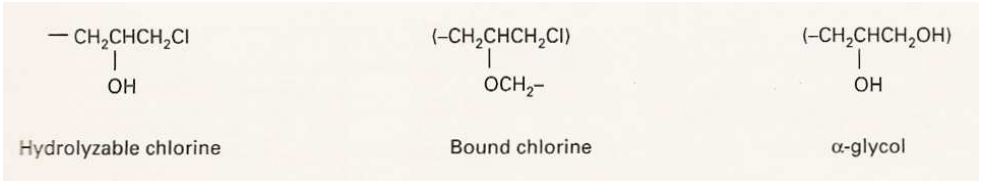

Figure 3.13: *Byproducts that may be produced in the formation of epoxy: hydrolyzable chlorine, bound chlorine and α-glycol [27].*

Solid epoxies form by a chain extension of the liquid resin with bisphenol A. This polymerization is depicted in figure 3.14. The molecular mass of the repetitive group in the solid epoxy has also been added to the list in table 3.3.

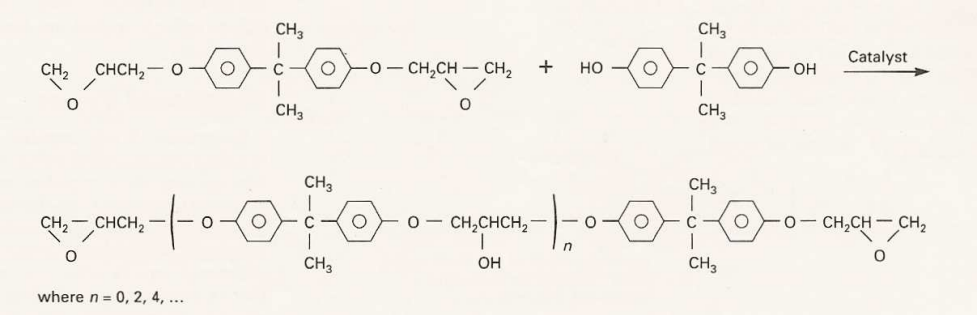

Figure 3.14: *Solid epoxy preparation by polymerization of the resin with bisphenol A [27].*

Molecule	Mass (AMU)
Epichorohydrin	92, 93
Hydrolyzable chlorine	75, 76
Bound chlorine	88, 89
α-glycol	75, 76
Repetitive unit in solid epoxy	168, 169, 170
Trimethylbutane	100
Trimethylhexane	114

Table 3.3: *Gas components of araldite with low masses and their respective concentration normalized to that of water.*

Figure 3.15 shows the araldite spectrum measured up to 200 AMU. The masses of the molecules thought to be present, which are listed in table 3.3, are depicted as red shaded areas. It is clear that many of the shaded areas coincides with a peak, however small, in the mass spectrum of araldite. Table 3.4 shows which of the compounds have masses that are consistent with the araldite mass spectrum and may therefore be present in the araldite sample. But, the before mentioned substances need not be present in the araldite sample. The peaks in the araldite mass spectrum may be caused by some other compound. More confidence could be gained by measuring the mass spectra of the compounds individually and comparing these with the araldite AY 103-1 spectrum.

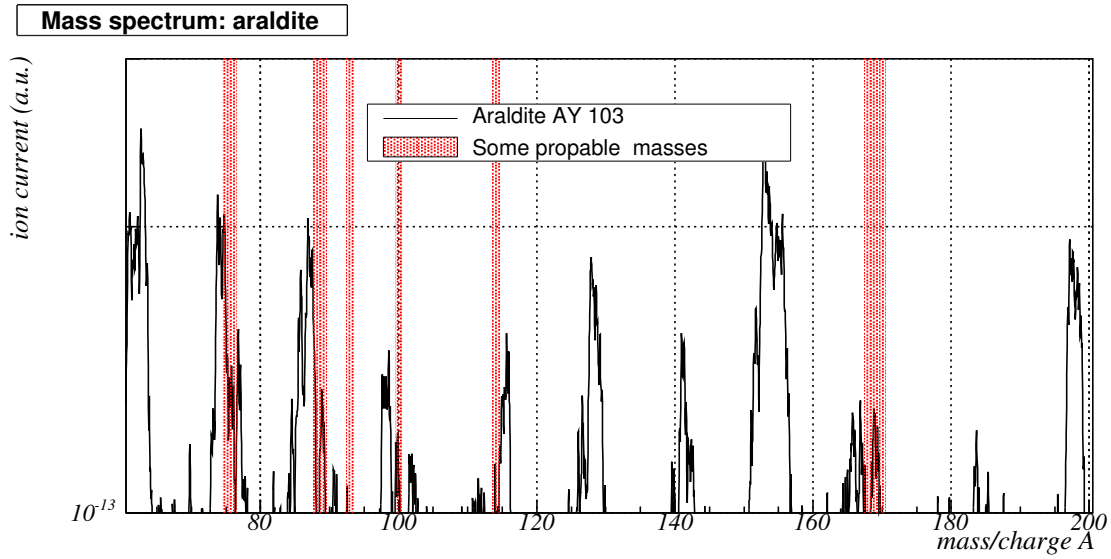

Figure 3.15: *Partially solved mass spectra of araldite.*

Molecule	Mass (AMU)	Present in araldite mass spectrum (y/n)
Epichorohydrin	92, 93	No
Hydrolyzable chlorine	75, 76	Yes
Bound chlorine	88, 89	Yes
α-glycol	75, 76	Yes
Repetitive unit in solid epoxy	168, 169, 170	Yes
Trimethylbutane	100	Yes
Trimethylhexane	114	No

Table 3.4: *List of compounds whose molecular masses are, or are not consistent with mass peaks in the araldite spectrum.*

3.4 Summary

The outgassing rate of the glue in vacuum decreases exponentially with time. The time scale at which it decreases is small compared to the the time scale at which improvement of the ageing rate from flushing is observed. This indicates that the observed reduction in outgassing rate is not only due to the less hardening of the glue, but needs to be, at least partially, attributed to removal of water from the glue.

The pressure in the vacuum chamber containing an araldite, or trabond sample, provides an upper limit of the outgassing rate of the glues. These limits are measured to be 2.4 10^{-6} and 9.0 10^{-6} $mbarLs^{-1}$ for araldite and trabond respectively. For the outer tracker modules, containing approximately 330 times more glue and flushing at 20 L/hr, the maximum level of contamination is 141 ppm. Approximately 68% of which is water. The maximum concentration of harmfull molecules is therefore 44 ppm.

Analysis of the mass spectrum of araldite is consistent with, but does not prove, the presence of:

- Water
- Air
- N_2
- H_2
- CO_2
- Methane
- Ethane
- Propane
- Butane
- Hydrolyzable chlorine
- Bound chlorine
- α-glycol
- Repetitive unit in solid epoxy (figure 3.14)
- Trimethylbutane

Chapter 4

Measurement of signal response

To investigate possible solutions to ageing and determine their effects on the operating efficiency, special setups to measure the signal response of outer tracker modules were used. In this chapter is explained how the gain loss of the modules is measured and quantified. Furthermore, the setup used to measure the pulse height spectrum of individual straw tubes, necessary to determine their energy resolution and gain, is shown.

4.1 Ageing test

4.1.1 Setup

The amount of ageing of an outer tracker module is determined by measuring the response of the detector before and after irradiation. A special setup for this purpose is shown in figure 4.1.

A module is secured to the table and its response to a 20 mCi ^{90}Sr source is measured. ^{90}Sr is a $\beta-$source, which emits electrons up to an energy of 2.3 MeV. The full width of the module is irradiated through a slit of 1×34 cm^2, which results in an irradiated area of 2×35 cm^2. The source is moved over the full length of the module in steps of 1 cm. At each step the induced current is measured separately for all 64 wires. Its strength depends on the gas gain at each position, producing a 2-dimensional map of the signal response of the entire module. An example of such a measurement can be seen in figure 4.2. The induced current is lower at the edges of the module. This is caused by the radiation profile of the source, which can be seen in figure 4.1 (left).

4.1.2 Measurement

To invoke ageing the modules are irradiated with a 2 mCi ^{90}Sr source. A collimator with a diameter of 6 mm results in an irradiated area of approximately 6×6 cm^2 and a distance between the source and the module of 5 mm. Typically a module is irradiated for 20 hours, with the high voltage at 1600 V and a 70/30 Ar/CO_2 gas mixture flowing at 20 L/hr, which corresponds to one volume exchange per hour. Under these conditions the ageing rate of the outer tracker is of the order of 4.4 10^4%/C/cm. Before and after irradiation a 2-dimensional current profile is measured. Two such measurements are shown in figure 4.2.

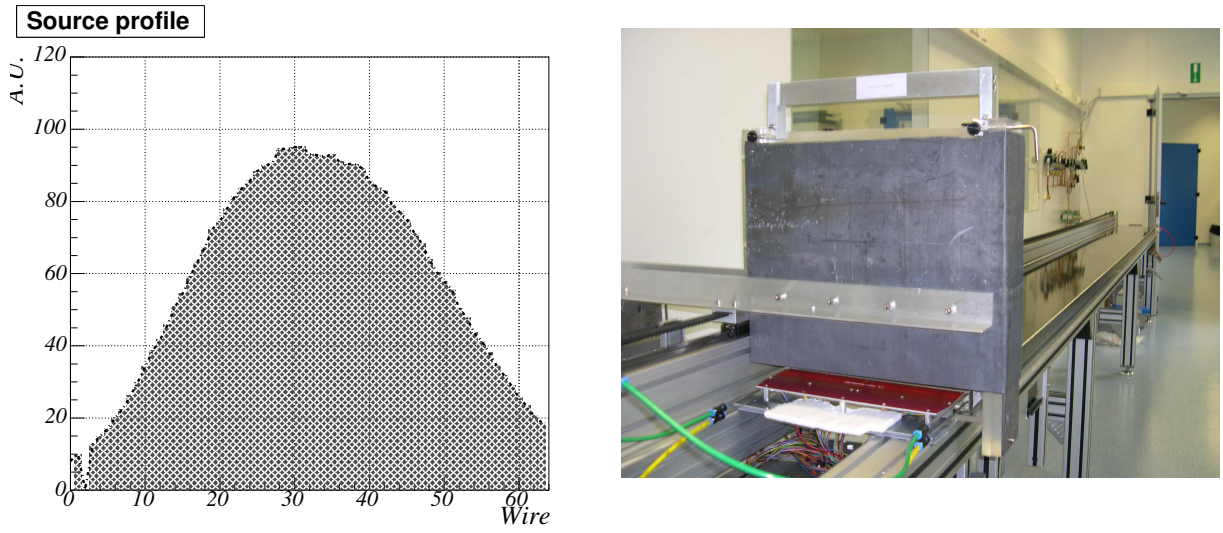

Figure 4.1: *(left) Intensity profile of the ^{90}Sr scanning source. The scale is proportional to the current measured for a high voltage of 1600 V and an Ar/CO_2 70/30 gas mixture. (right) Photo of the setup with an automated 20 mCi ^{90}Sr source used to measure ageing.*

To see if the wires which were irradiated have aged, the ratio of the two current profiles is taken and normalized for a part of the module that was not irradiated. This process removes effects of changing atmospheric pressure and temperature on the gain and produces a damage profile as shown in figure 4.3. The color coding indicates the value of the relative gain at each point of the module. A value of 1 means no ageing occurred, a value of 0.8 means a gain reduction of 20% at that particular spot.

The source used to produce ageing has a spherical radiation profile (see figure 4.4). The expected shape of the aged area is therefore a circle. However figure 4.3 shows this is not the case. Instead it shows a characteristic crescent-moon-shaped ageing spot, which has several distinguishing features:

- Ageing does not take place directly below the irradiation source, where the intensity is highest.
- Ageing only occurs upstream of the irradiation source.
- The ageing rate is high: 4.4 10^4%/C/cm.

In the figure the gas flow is from right to left. Apparently something prevents ageing downstream of the irradiated area. The cause of this phenomena is discussed in section 5.1.

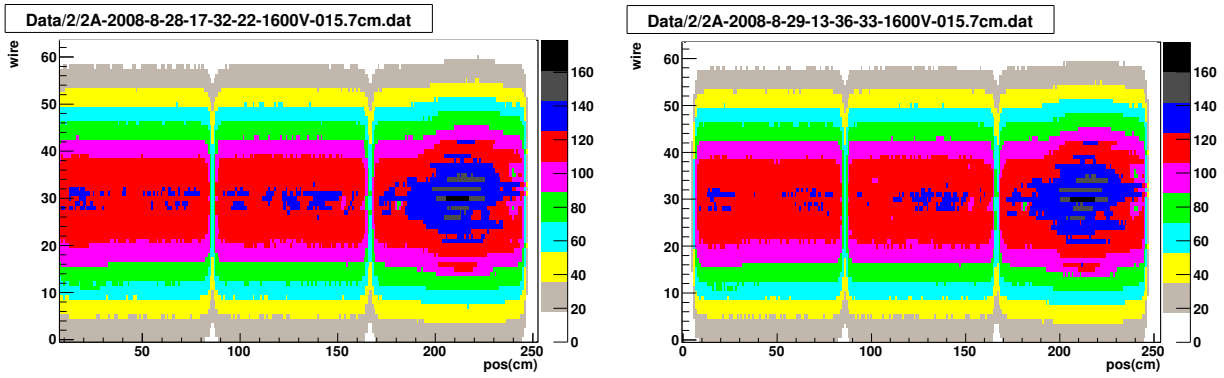

Figure 4.2: *Two current profiles of module 2, measured before (left) and after (right) an irradiation of 20 hours with a 2 mCi ^{90}Sr placed 100 cm from the gas exhaust, with the gas flowing from right to left. [Module 2, 28/08/2008 – 29/08/2008]*

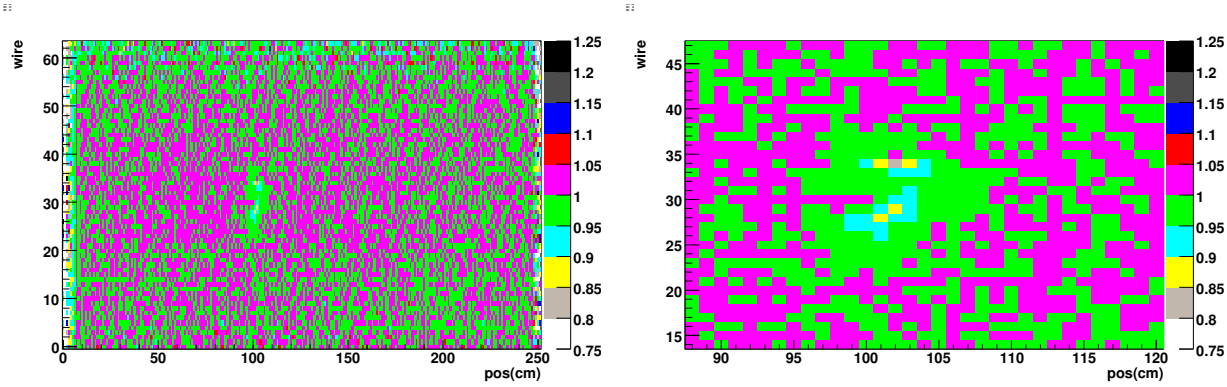

Figure 4.3: *(left) A ratio plot of the currents before and after an irradiation of 20 hours with 2 mCi ^{90}Sr source. The source was placed 100 cm from the gas outlet. The gas flows from right to left. (right) A close up from the irradiated area. The maximum damage is 16%. [Module 2, 28/08/2008 – 29/08/2008]*

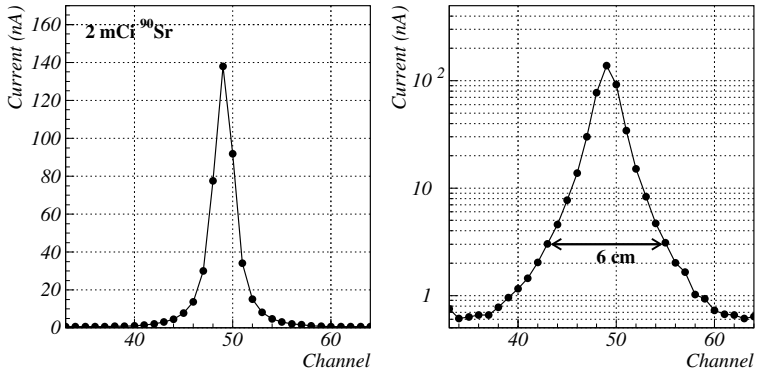

Figure 4.4: *The source profile of the 2 mCi ^{90}Sr source that is used to irradiate the detector to invoke ageing. The operating high voltage is 1600 V.*

4.1.3 Quantifying the ageing

Several schemes of quantifying the amount of ageing exist. An extensive description of these methods can be found in [18, 21]. One way of quantifying the ageing that has been shown to work well is the minimum method. With the minimum method the amount of ageing is the maximum gain loss induced. This value is normalized to that of an area that was not irradiated. The value thus produced is defined to be the amount of ageing. The maximum gain loss in figure 4.3 is estimated to be 16%.

4.2 Pulse height spectrum

Measuring the response to a ^{55}Fe source is a common way to obtain the energy resolution and gain of gas based detectors.

^{55}Fe emits photons with a well defined energy of 5.9 keV. One photon will ionize one argon atom by means of photo-electric effect. Every liberated electron will induce approximately 220 primary electrons [8] and via gas multiplication result in a pulse on the anode wire. If the multiplication factor remains constant the height of the induced pulse should always be the same. In general though, the size of the avalanche and hence that of the induced pulse, will fluctuate. A histogram of the measured pulse heights is called a pulse height spectrum. The width of this spectrum gives the energy resolution of the straw tubes. The maximum of the distribution is a measure for the gain. The smaller peak of the spectrum is called the escape peak, which is characteristic for argon. Its formation is explained below.

4.2.1 Setup

A photo of the setup used to measure pulse height spectra is shown in figure 4.5. A small 74 MBq ^{55}Fe source is placed above a given wire. The pulses induced by the source are read out by a special preamplifier constructed in Heidelberg, which is described in [16, 21, 22]. Only one channel can be read out at a time.

Figure 4.5: *Photo of the experimental setup to measure pulse height spectra with an* ^{55}*Fe source.*

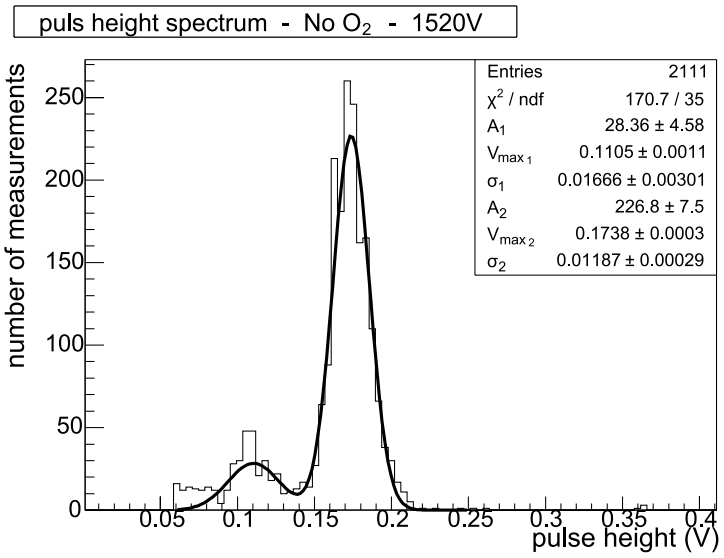

Figure 4.6: *Pulse height spectrum of module 2, wire 32, with a gas mixture of 70/30* Ar/CO_2 *and a high voltage of 1520 V. The main and escape peak have been fitted with a double Gaussian.*

Figure 4.6 shows a pulse height spectrum that was measured for module 2A for a high voltage of 1520 V and a 70/30 Ar/CO_2 gas mixture. It shows two peaks. The principal peak, called the photo-peak, is caused by full absorption of the 5.9 keV photons, emitted by the ^{55}Fe source. The second, smaller peak is known as the X-ray argon escape peak [12]. In some cases of photo-electric absorption a photon, with an energy characteristic for the absorber atom, is emitted. If this secondary photon escapes the detector volume, the energy deposited in the detector is decreased by an amount equal to the X-ray photon energy.

The spectrum comprises of a photo- and an escape peak and is therefore fitted with a double Gaussian:

$$N(V) = A_1 \exp\left[- \left(\frac{V - V_{max_1}}{\sigma_1} \right)^2 \right] + A_2 \exp\left[- \left(\frac{V - V_{max_2}}{\sigma_2} \right)^2 \right] \tag{4.1}$$

The value around which the main Gaussian is centered, V_{max}, is proportional to the gain. The energy resolution, R, is given by:

$$R = \frac{\sigma_i}{V_{max_i}} \tag{4.2}$$

For the fit shown in figure 4.6 this results in an energy resolution of 6.3%.

To determine the gain [16] both the rate of the ^{55}Fe pulses, f_{tot}, and the DC current, I_{tot}, have to be measured so that the average charge per pulse can be computed. The average charge of a pulse is given by:

$$< Q >_{pulse} = \frac{I_{tot}}{f_{tot}} \tag{4.3}$$

The total rate and current are, however, caused by the combined effect of pulses from the photo-peak and the escape peak. The fraction of the total charge and rate originating from photo-peak pulses, $I_{p.p.}$ and $f_{p.p.}$, can be extracted from the pulse-height-spectrum. The average charge of a pulse of the photo-peak is than given by:

$$< Q >_{p.p.} = \frac{I_{p.p.}}{f_{p.p.}} \tag{4.4}$$

A 5.9 keV photon emitted by the ^{55}Fe source creates approximately 220 primary electrons [1] that have a combined charge of 3.52 10^{-17} C. The gain, M, is then given by:

$$M = \frac{< Q >_{p.p.}}{n_p e} \tag{4.5}$$

where n_p is the number of primary electrons and e the elementary charge.

Some values for the gain at different high voltages are given in table 4.1

However, to characterize the performance of the detector with O_2, only the relative change of the pulse height is of interest, rather than the determination of the absolute gain.

[1] 220 is the theoretical value [8]. Recently it has been determined experimentally for the first time and was measured to have a value of 205 [28].

HV (V)	Gain
1400	13000
1450	20300
1500	36800
1550	54900
1600	83600
1650	118000

Table 4.1: *The gain at different values of the high voltage. Measured for module 9B, wire 34, 190 cm from lower end. [16]*

4.2.2 Comparison with ^{90}Sr scan

As was explained in section 4.1, the amount of ageing is determined by the relative response to a ^{90}Sr source before and after irradiation. Instead of these ^{90}Sr scans, the described method to measure the gain using ^{55}Fe , may also be used to determine the amount of ageing.

Figure 4.7 shows two measurements of the relative gain after an irradiation of 20 hours of module 1A, wire 32, as a function of position along the wire. One measurement was conducted with the ^{90}Sr setup of section 4.1, the other by measuring the pulse height spectrum of a ^{55}Fe source, as described in section 4.2, but with an 1 mm slit as collimator. The gas flow was from right to left. It shows that both methods to measure ageing agree well upstream of the ageing source, but disagree significantly downstream. With the ^{90}Sr source as much as 50% gain loss is observed, when the ^{55}Fe measurement shows none at all. This is due to the fact that the ^{90}Sr source illuminates a larger piece of the anode wire than the ^{55}Fe source with the 1 mm collimator. The ^{55}Fe source only irradiates a small area, resulting in a sharp separation between aged and unaffected part of the wire. The ageing observed with ^{90}Sr is the average ageing of a larger area. The edge of the ageing damage is less pronounced, because, with the ^{90}Sr source, ageing upstream contributes to the measurement, that was undetected with the ^{55}Fe source.

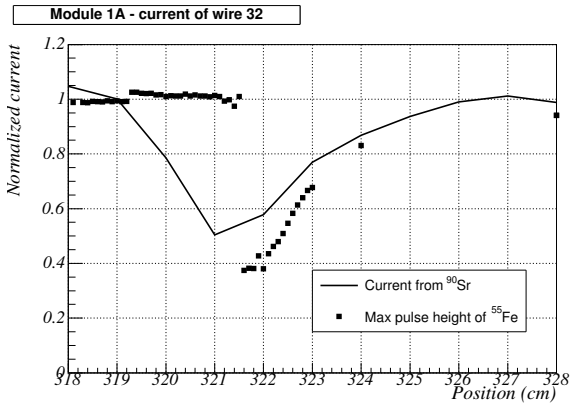

Figure 4.7: *Signal response of module 1A, wire 32, as a function of position along the wire, measured with a ^{90}Sr and a ^{55}Fe source. Gas flow right to left.*

4.2.3 Gain of damaged area

A peculiar effect was observed at CERN [29] when the pulse height spectra of a damaged wire was measured. The spectrum does not always look like the one depicted in figure 4.6, but depending one the place on the ageing spot, the spectra contained one, two, or even three peaks. For the damage depicted in figure 4.8, pulse height spectra measured on different places along the wire are shown in figure 4.9.

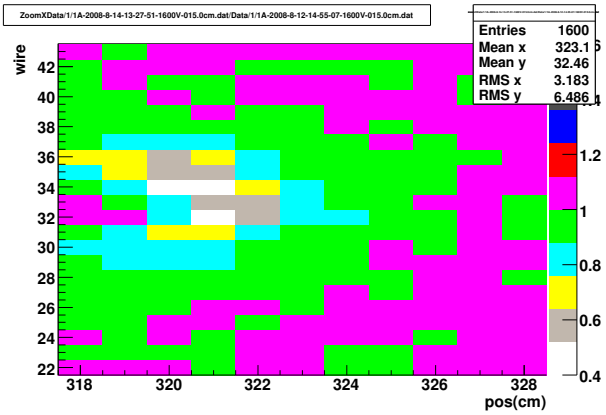

Figure 4.8: *Relative gain of module 1A after an irradiation of 20 hours. Gas flow right to left. [Module 1A, 12/08/2008 – 14/08/2008]*

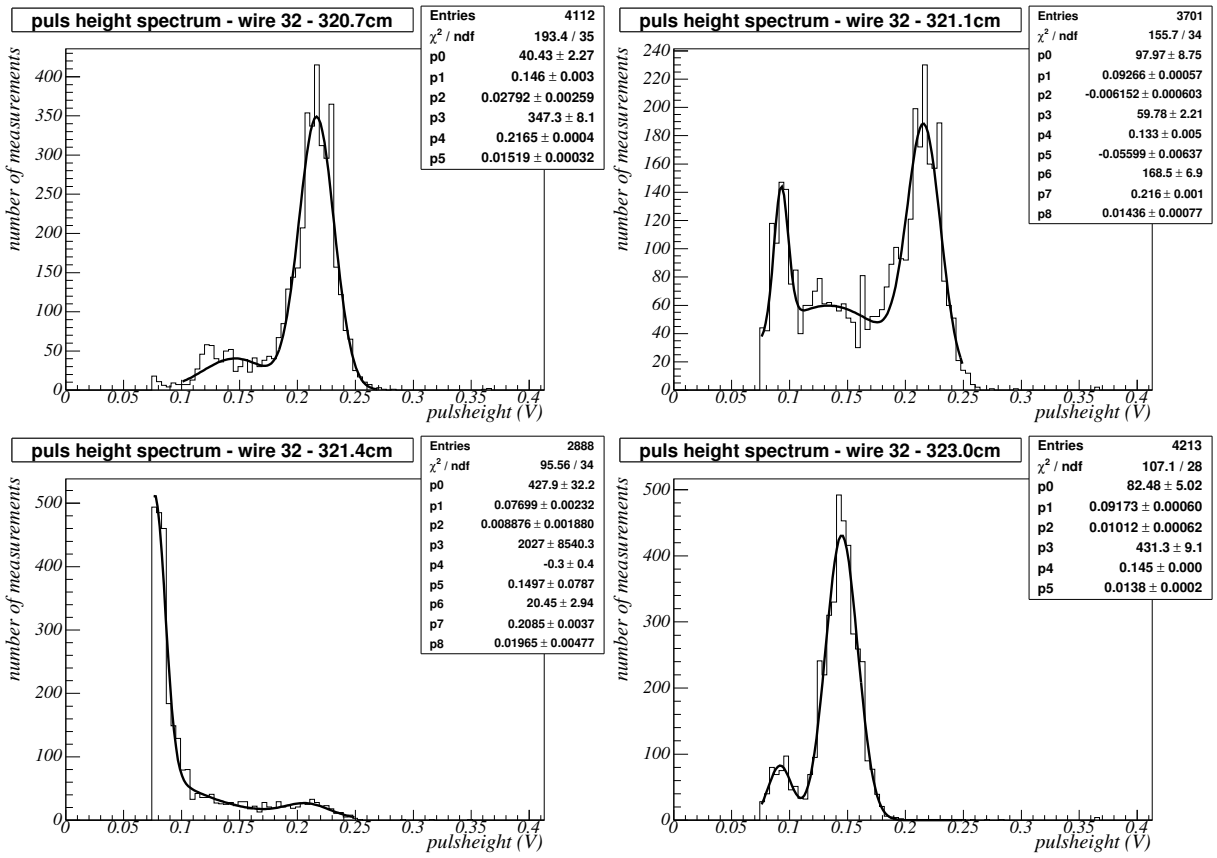

Figure 4.9: *Examples of pulse height spectra at several positions on the aged wire: (upper left) 320.7 cm, (upper right) 321.1 cm, (lower left) 321.4 cm, (lower right) 323.0 cm. Depending on the position on the ageing spot one, two, or even three peaks are observed. This effect was first observed by Y. Bagaturia.*

The pulse height spectrum was measured for every mm of wire. These spectra have been fitted with a double or triple Gaussian, as shown in figure 4.9. The result of this analysis is summarized in figure 4.10. It shows for each position along the wire the maximum pulse heights of the peaks in its spectrum. The size of the data points corresponds with the amplitude of each peak. The gas flow was in the negative direction (from right to left).

Figure 4.10 shows that approaching the damaged area from upstream (from the right in figure 4.10), the height of the induced pulses decreases and the number of pulses in the main peak remains the same. This is expected as more ageing allows less electrons to be collected on the anode wire, thus reducing the height of the pulse, but not the number of pulses. Approaching the damaged area from downstream (from the left in figure 4.10) however, the pulse height of the main peak does not decrease, but the number of pulses in the main peak does decrease. As the number of pulses decreases, a third peak appears in the spectrum. This may indicate that the deposit on the anode wire is not distributed evenly across its surface, so that two values for the

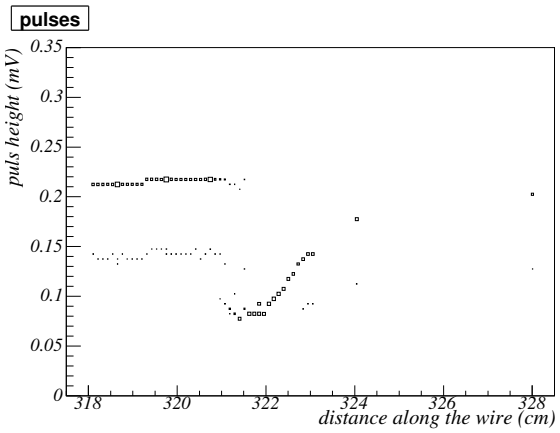

Figure 4.10: *The pulse height of the pulse height spectra as a function of the position along the wire where the spectrum was measured. The size of the data points correspond to the amplitude of the peaks in the spectrum.*

gain are present on this part of the wire. The signal produced by an arriving avalanche may have one of two distinct heights, depending whether it strikes a clean, or aged part of the wire. This should decrease the amplitude of both the main and escape peak and give rise to two additional, smaller peaks in the spectrum. But as the smaller escape peak will not be above threshold, only three peaks are observed in the pulse height spectrum.

In Heidelberg the average height of the pulses induced by a ^{55}Fe source is used to determine the amount of ageing. This method will give a lower estimate of the signal response, compared to when the maximum pulse height (as in figure 4.7) is used. To compare the methods to determine the amount of ageing, used by Nikhef (current induced by ^{90}Sr source) and Heidelberg (average pulse height ^{55}Fe source), measurement of the same damaged wire (wire 32, mod 1A) with both methods is depicted in figure 4.11. When the average pulse height is used, there is better agreement as when the maximum pulse height is used.

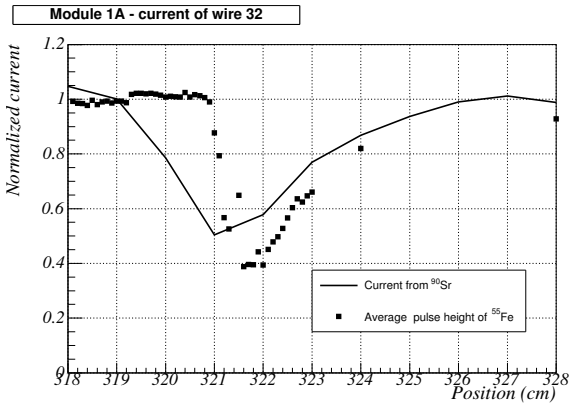

Figure 4.11: *Signal response of module 1A, wire 32, as a function of position along the wire. Once measured with a ^{90}Sr source, the second is the average pulse height of a ^{55}Fe source. Gas flow right to left.*

4.3 Summary

In this chapter two methods have been presented to invoke ageing in a reproducible manner and to attribute a value to its amount: determining the decrease of the response to a ^{90}Sr source and a ^{55}Fe source. Comparison of the two methods shows that with the ^{90}Sr source a larger area is illuminated, significantly influencing the amount of ageing produced by the test.

A ^{90}Sr source is used at Nikhef to test any possible solution to, or treatment of, the deterioration of the outer tracker modules. By measuring pulse height spectra we can determine their consequences for the energy resolution and gain. In particular studies of the effects of gaseous and aquatic additions to the gas mixture have been undertaken, the results of which are the subject of the next chapter.

Measurement of the pulse height spectra of aged wire samples of one mm indicates that part of the anode wire is not evenly damaged. In these regions of the detector, two values of the gain exist at the same time.

Chapter 5

Preventing ageing with additives to the gas

Ageing of the LHCb outer tracker only occurs upstream and is prevented downstream of the irradiated area. Two mechanisms that could prevent ageing downstream of the source seem viable: all the pollution emitted by the glue has already been deposited on the anode wire upstream and none is left to cause damage downstream, or some substance that binds the pollution molecules, making them chemically inactive, is produced in the electron multiplication process. It turns out that the latter theory is the correct one and that the active substance is ozone [30].

In this chapter the measurements done in Heidelberg that led to the determination of the correct prevention mechanism and discovery of ozone being the active substance, are shown, which is the motivation to test the effects of adding several gaseous and aquatic oxidizers to the gas mixture, in the hope to find capabilities similar to those of ozone. The results of these investigations are the subject of the second part of this chapter.

5.1 Ageing prevention mechanism

To determine whether ageing downstream of the radioactive source was prevented by the lack of pollution or the presence of a reactive substance that binds it, the following test was devised in Heidelberg. A strong and a weak radioactive source (primary sources), that both produce crescent-moon-shaped ageing spots are placed next to each other on an outer tracker module. The fact that the ageing profile is crescent-moon-shaped, proves that if downstream prevention is caused by lack of pollution, all malicious molecules have been deposited on the anode wire. Two radioactive sources of equal strength (secondary sources) are used to attempt to induce ageing downstream of the first two sources. If the mechanism of the observed prevention is lack of pollution molecules, both primary sources should prevent ageing equally and ageing by the secondary sources should occur at the same distance from the primary ones. Should prevention be caused by some chemical compound created by radiation, the large primary source should produce more of this substance, bind more pollution and hence, ageing from the secondary source should occur at a larger distance. The setup used for this experiment is shown in figure 5.1.

The measurements of the gain loss, which are depicted in figures 5.2 and 5.3, clearly show

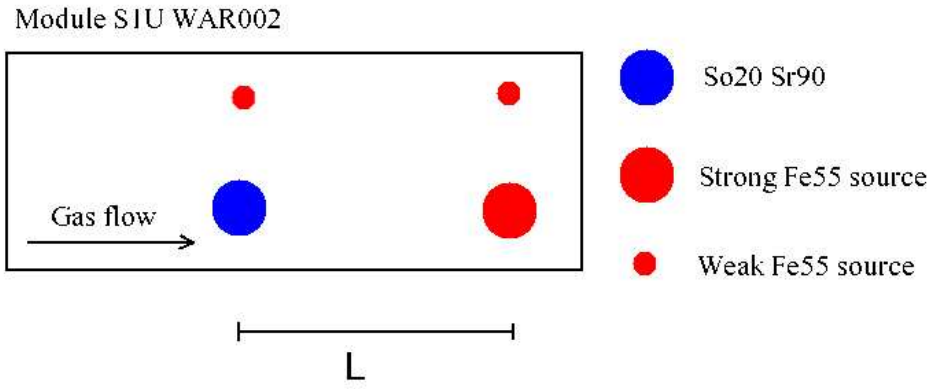

Figure 5.1: *Schematic representation of the setup used in Heidelberg, to distinguish between two mechanisms that could prevent ageing [30]. L is the distance between the primary and secondary sources.*

that none of the secondary sources produce ageing at a distance of 8 cm from the primary ones and the small secondary source at a distance of 25 cm behind the small primary source produces ageing, when behind the large primary source no significant amount can be observed. However, in figure 5.3 the small source does not produce the desired crescent-moon-shaped ageing spot. Nevertheless, it does prevent ageing 8 cm downstream as can be seen in figure 5.2. Therefore, if ageing would have been prevented by the lack of pollutants, no pollutants are present 8 cm downstream of the source. This and measurements that will follow shortly, convince us that ageing downstream of the irradiated area is prevented by a substance produced by the radiation itself.

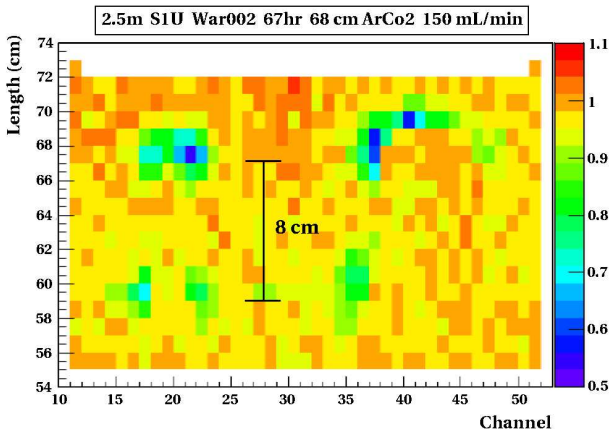

Figure 5.2: *The relative gain of module WAR002 after it has been irradiated for 67 hours by four sources. Two primary sources, one small, one big, invoke ageing in such a way that ageing is prevented downstream. Two secondary sources are placed 8 cm downstream of the primary ones. Ageing under the secondary sources does not take place. [30]*

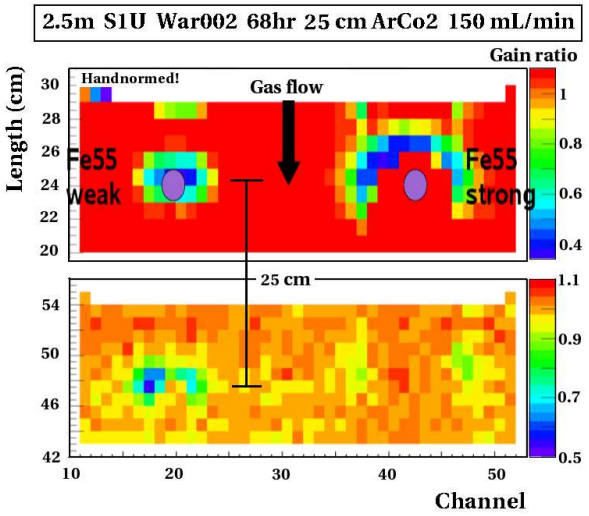

Figure 5.3: *The relative gain of module WAR002 after is has been irradiated for 68 hours by four sources. Two primary sources, one small, one big, invoke ageing in such a way that it is prevented downstream. Two secondary sources are placed 25 cm downstream of the primary ones. Ageing only takes place behind the small primary source; the large source prevents ageing stronger. This indicates pollution is bound by some substance created by the source. [30]*

The measurements in figure 5.2 and 5.3 show that ageing from the secondary source could occur after a distance of 25 cm. The gas speed is about 2 cm/min, therefore the chemical compound that prevents ageing has a lifetime in the order of minutes. A candidate is ozone, which has a lifetime of five to ten minutes. Some ozone was indeed measured using an ozone monitor placed at the gas outlet. As an additional test, the dependence of ozone production on the O_2 concentration was examined.

5.2 Dependence of ozone production on O_2 concentration

To test this hypothesis a second test was devised. Some amount of oxygen was added to the counting gas and an ozone monitor, that could measure the ozone concentration of the counting gas, was placed at the gas outlet (see figure 5.4). Both the oxygen concentration and irradiation intensity were varied, with the following result: the ozone concentration decreased with decreasing irradiation intensity and increased with increasing oxygen concentration (see figures 5.5 and 5.6). From these observations it was concluded that ozone is produced under the source and prevents ageing downstream of the irradiated area.

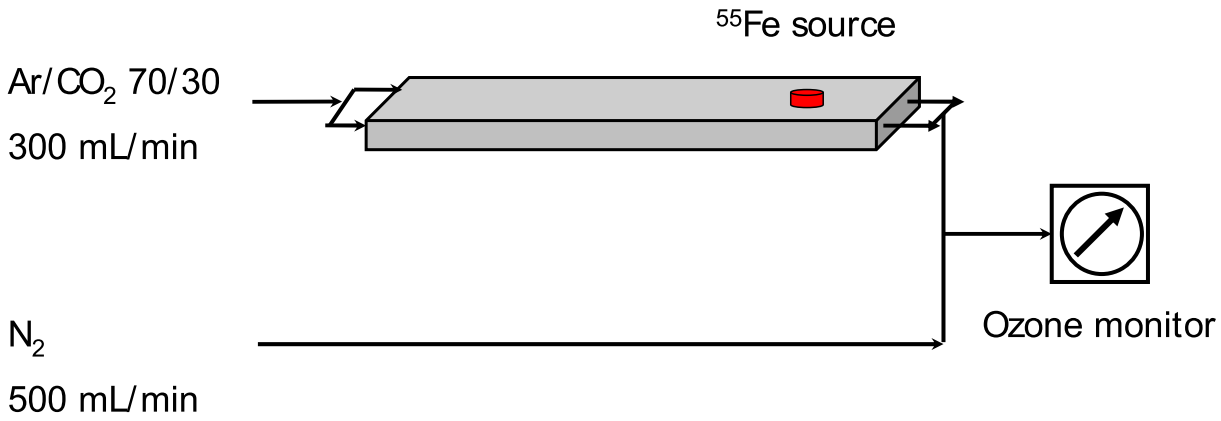

Figure 5.4: *Schematic representation of the setup used by Christian Färber in Heidelberg, to test if ozone is the substance that binds the pollution molecules, thus preventing ageing. [30]*

Although ozone is in principle capable of preventing ageing of the outer tracker modules, it has a fundamental flaw that makes it unpractical to implement. Ozone is an unstable substance, with a lifetime between five and ten minutes. This means that a bottle of ozone transforms to a bottle of oxygen in a few hours, making it difficult to add it to the gas mixture. The only possible way to introduce ozone into the outer tracker modules would be to place ozone generators in the gas system. This would still leave the undesirable effect that the ozone concentration and hence, the properties of the counting gas, would not be constant throughout the whole outer tracker. We would like a substance with similar capabilities as ozone, but stable.

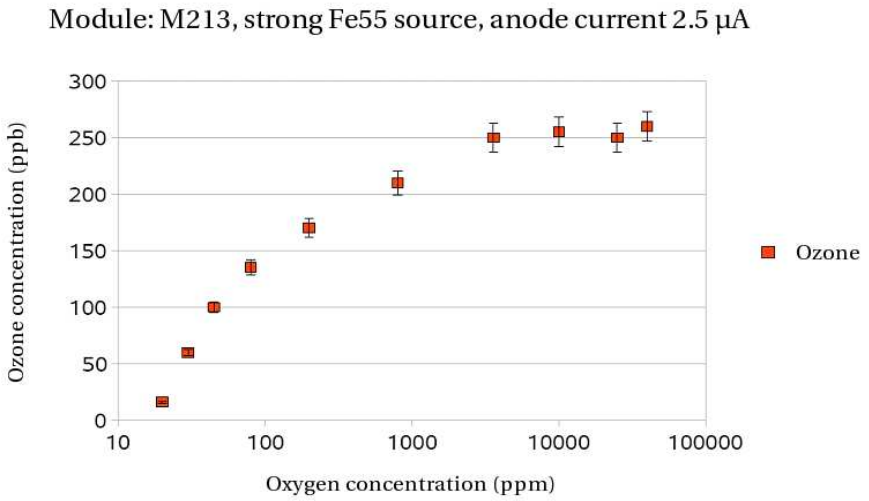

Figure 5.5: *Measurements of the ozone concentration of the gas mixture as a function of the added amount of oxygen. [30]*

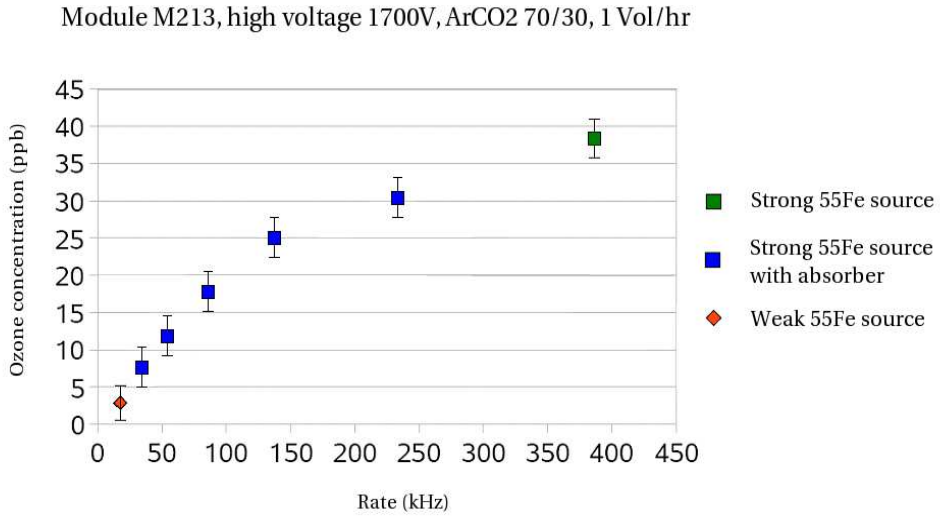

Figure 5.6: *Measurements of the ozone concentration of the gas mixture as a function of irradiation intensity. [30]*

5.3 Nitrogen dioxide

In the hope that nitrogen dioxide (NO_2) had properties similar to ozone, a module that was being flushed with the normal gas mixture plus 100 ppm NO_2 was irradiated in Heidelberg for 46 hours. The results of this irradiation is shown in figure 5.7. After irradiating for a period of 46 hours no significant amount of ageing could be observed. The effects of the addition of NO_2 are still under investigation [30].

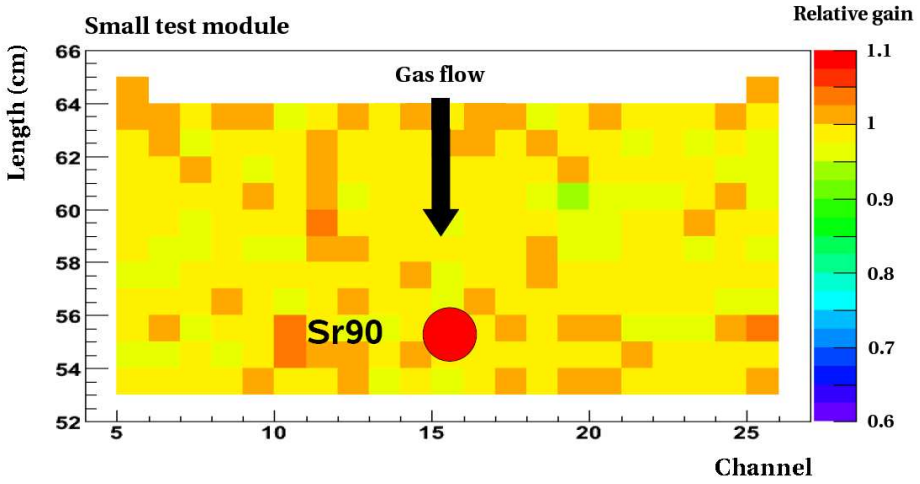

Figure 5.7: *The relative gain of a test module after it has been irradiated for 46 hours, while being flushed with a Ar/CO_2 gas mixture to which 100 ppm NO_2 is added. No significant amount of ageing can be observed. [30]*

NO_2 prevents ageing just as ozone and is a stable molecule. However, nitrogen dioxide is toxic with a MAC value[1] of 2 ppm [31] and prolonged exposure can be lethal.

Two agents that prevent ageing of the outer tracker modules have been found, but both seem to have insurmountable implementation problems. Both substances are oxidizers, so maybe a strong enough oxidizer will prevent ageing. For this reason we have tested other known gaseous and aquatic oxidizers that are stable and (nearly) non-toxic for its ageing preventing capabilities.

5.4 Hydrogen peroxide

Hydrogen peroxide, H_2O_2, is an aquatic oxidizer solved in water. H_2O_2 is a semi-stable molecule that breaks up into water and atomic oxygen, which becomes molecular oxygen. The atomic oxygen created in this process might react with the pollution, rendering it harmless. Because it is a liquid substance, we can not add it directly to the gas mixture, but the gas has to be led

[1]The MAC value of a substance is the maximum, time averaged concentration of the substance a person, by Dutch law, is allowed to be exposed to for more than eight hours a day.

through a bottle filled with 50% water and 50% H_2O_2. To monitor the concentration of H_2O_2 in our counting gas, a dew point meter is placed at the gas outlet of the module. The dew point meter measures the temperature at which the liquid in a gas condensates, which depends on the partial pressure of the liquid. With the partial pressure of water and H_2O_2 combined known, their individual partial pressures can be calculated using Raoults Law, which states that: for weak solutions, the vapor pressure of the individual liquids is proportional to mass-weighted concentration of the components (that is, the concentration in mole) in the solution.

However, it is known that H_2O_2 only exists solved in liquid H_2O. Nevertheless, this measurement was tried, hoping that a small fraction of H_2O_2, or alternatively, the combination of H_2O and O_2, has a beneficial effect on the ageing rate.

A representation of the setup used to add H_2O_2 to the module, measure its amount and determine its effect on the ageing rate is shown in figure 5.8.

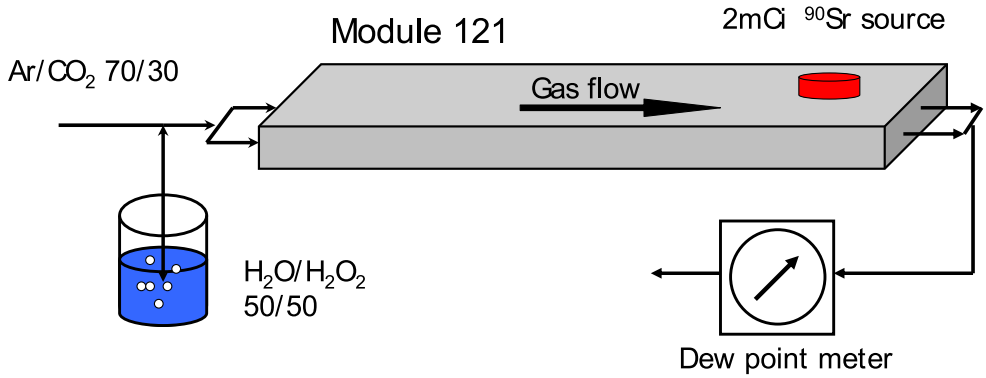

Figure 5.8: *Schematic representation of the setup used to add hydrogen peroxide (and water) to the counting gas. The hydrogen peroxide concentration is monitored with a dew point meter at the gas exhaust.*

A module, being flushed with the normal gas mixture and 2000 ppm H_2O_2, was irradiated for 20 hours. The damage profile of that irradiation is shown in figure 5.9 (left) in which the maximum gain loss is 17%. But part of the damage is masked by the H_2O_2 and H_2O. After the liquids are removed from the system a new measurement of the signal response shows the damage is more severe as was first observed (see figure 5.9 (right)). Apparently the liquid makes the insulating layer on the anode wire more conductive and in this way hides some gain loss in the first measurement. When both effects are taken into account the total gain loss from the irradiation is 24.1%.

Figure 5.10 summarizes all the ageing measurements for H_2O_2. It shows the relative gain after irradiations of 20 hours at different times, under different circumstances. Two irradiations of a dry module (one before it was hydrated, one after) are represented by circles and connected by a line. This, because the ageing rate decreases with increasing flush time. The line therefore indicates the amount of improvement expected from flushing.

The triangle indicates the relative gain after irradiating a H_2O_2 filled module for 20 hours,

measured while it is still hydrated. The square is the real signal response on that spot, which can only be measured after the module has dried. These measurements show that the observed improvement of the ageing rate is significantly larger than would be expected based on flushing alone and thus, adding H_2O_2 and water to the counting gas slightly decreases the ageing rate. This improvement can be attributed to the presence of O_2 in the counting gas (see section 5.7).

Furthermore, the fact that water makes the damage more conductive might be useful in the future. Once the outer tracker has aged, part of the signal response may be regained by introducing water into the module.

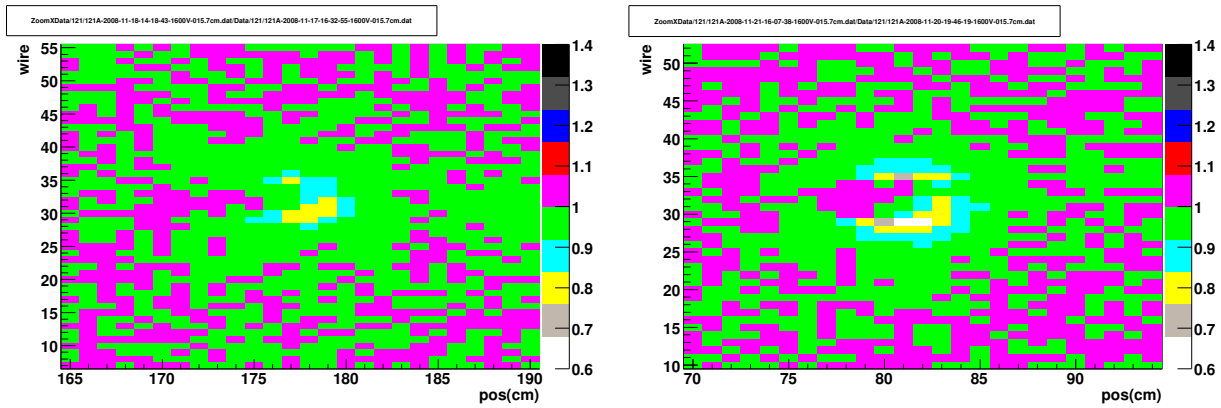

Figure 5.9: *(left) Relative gain after irradiating module 121A with 1500 ppm H_2O_2/H_2O for 20 hours. The maximum gain loss measured while the H_2O_2 and H_2O are still present is 17%. (right) Relative gain of same module after the H_2O_2 and H_2O have been removed. The maximum gain loss then measured is 24.1%. The difference in gain loss is caused by the fact that insulating layer around the anode wire becomes more conductive when it is wet, thus hiding part of the damage. [Left: Module 121A, 17/11/2008 – 19/11/2008. Right: Module 121A, 20/11/2008 – 21/11/2008]*

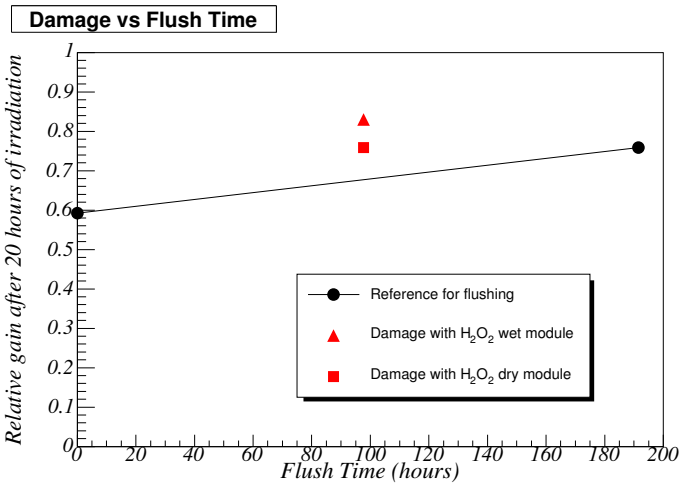

Figure 5.10: *Relative gain vs flush time. The triangle is the relative gain of the module after irradiating for 20 hours, measured when the H_2O_2 and H_2O are still present, the square is the same damage measured when the module has dried, the circles connected by a line are two reference irradiations to estimate the improvement of the ageing rate caused by flushing the module.*

5.5 Nitrous oxide

Nitrous oxide, N_2O, although weaker than NO_2, is also a well known oxidizer. Since it is gaseous at room temperature, N_2O can be added to the counting gas without difficulty.

Module 121A, being flushed with a gas mixture of $Ar/CO_2/N_2O$ 70/29.6/0.4, was irradiated for 20 hours. The damage induced by this irradiation is shown in figure 5.11. The maximum gain loss is 24.5%.

Figure 5.12 shows the amount of gain loss caused by the irradiation with 0.4% N_2O (triangle) and that of two reference irradiations (circles), plotted versus flush time. As before, the line indicates the decrease of the ageing rate from flushing. It clearly shows that all observed improvement of the ageing rate is consistent with the increased flush time of the module and not by the addition of N_2O. The addition of nitrous oxide to the counting gas does not have a significant effect on the ageing rate.

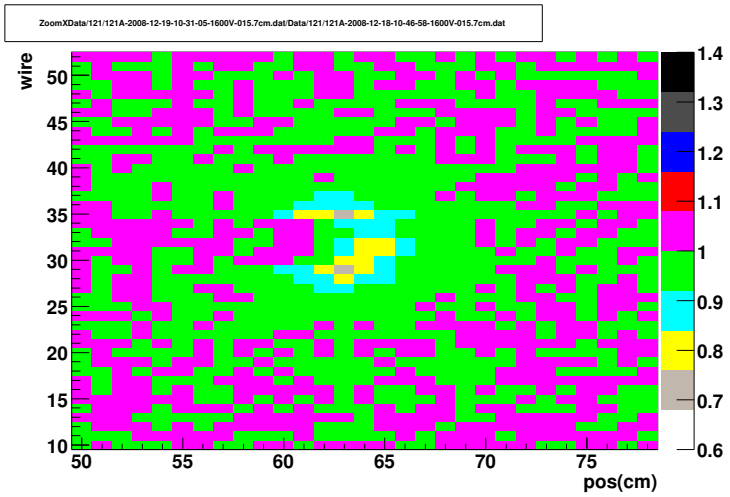

Figure 5.11: *Relative gain after a 20 hour irradiation of module 121 while being flushed with a 70/29.6/0.4 $Ar/CO_2/N_2O$ gas mixture. The maximum gain loss is 24.5%. [Module 121A, 18/12/2008 - 19/12/2008]*

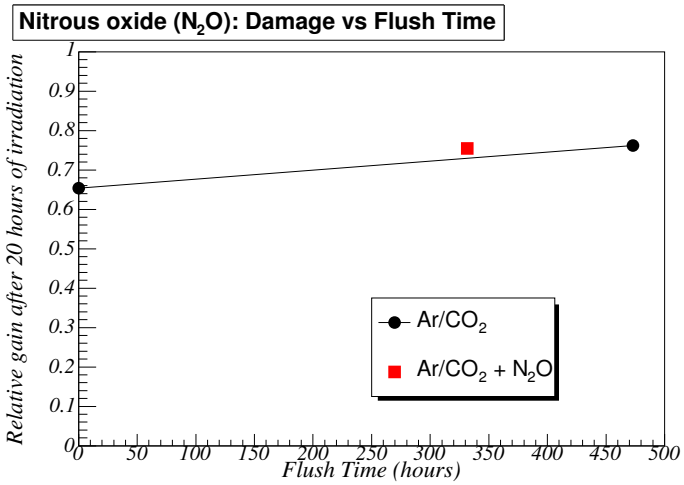

Figure 5.12: *Relative gain vs flush time. The square is the relative gain of module 121 after an irradiation of 20 hours while being flushed with a 70/29.6/0.4 $Ar/CO_2/N_2O$ gas mixture, the circles connected by a line are two reference irradiations to estimate the improvement of the ageing rate caused by flushing the module.*

5.6 Ethanol

Ethanol is known to slow down a certain form of ageing, known as whisker growth [32]. A carbon deposit forms on the anode wire, but in stead of a uniform layer, as in the LHCb outer tracker, whiskers have the shape of individual hairs. No prevention of other types of ageing has ever been attributed to ethanol, but since the insulating layer on the straw tube anode wires are possibly also carbon polymers, ethanol could produce interesting results.

Ethanol is a liquid at room temperature. Adding it to the counting gas is therefore done in the same way as hydrogen peroxide (figure 5.8). The Ar/CO_2 gas mixture is led through a bottle containing a solution of 95% ethanol and 5% methanol. An indication of the concentration is provided by the dew point meter. The dew point meter is designed to measure the condensation of water, not ethanol, but since we are not interested in the precise concentration of ethanol and ethanol evaporates easily, the dew point meter is used as an indication that ethanol is present.

Figure 5.13 (left) shows the relative gain of outer tracker module 121A, after is was irradiated for 42 hours, while being flushed with an Ar/CO_2 gas mixture containing roughly 2000 ppm ethanol[2]. The maximum gain loss from the irradiation is 26%. This is, however, not the true amount of gain loss. The insulating layer around the anode wire absorbes ethanol, thus making it more conductive. Figure 5.13 (right) shows the relative gain of the module when all ethanol has been removed. The real amount of gain loss is measured to be 70.4%.

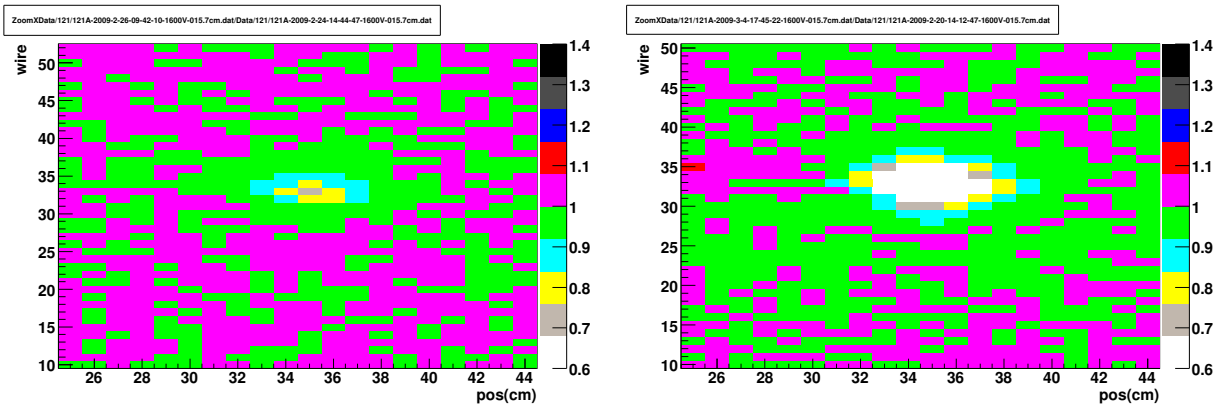

Figure 5.13: *(left) Relative gain after irradiating a module with ethanol added to the gas mixture for 42 hours. The maximum gain loss measured while the ethanol is still present is 26%. (right) Relative gain of same module after the ethanol has been taken out. The maximum gain loss then measured is 70.4%. The difference in gain loss is caused by the fact that insulating layer around the anode wire becomes more conductive when it has obsorbed some ethanol, thus hiding part of the damage. [Left: Module 121A, 24/02/2009 – 26/-2/2009. Right: Module 121A, 20/02/2009 – 04/03/2009]*

Figure 5.14 shows the relative gain versus irradiation time. The circle indicates the gain loss

[2]Also, the effect of an HV training procedure on wires 1 – 32 can be observed in figure 5.13 as damage is prevented in this part of the module. Remarkably, prevention is less clear after the ethanol is removed.

induced by a 20 hour irradiation under normal operating circumstances, the squares the gain loss caused by the irradiation while ethanol is present in the module, the triangle the relative gain loss from the same irradiation (42 hours), measured when no ethanol is present in the module. Based on these measurements we conclude that ethanol does not prevent ageing, but aggravates it.

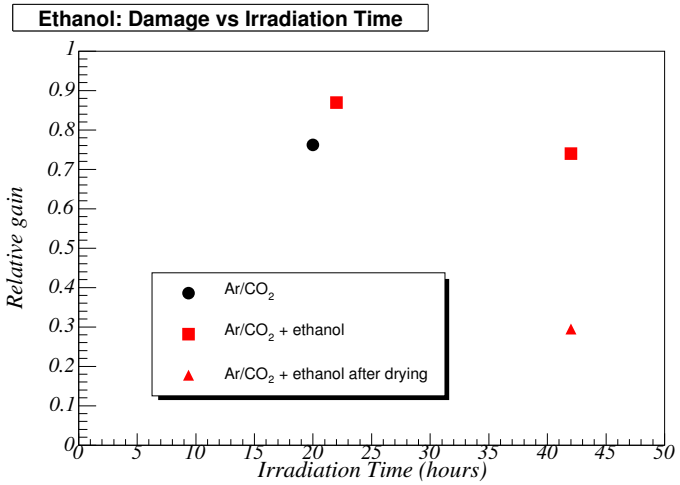

Figure 5.14: *Relative gain vs irradiation time. The circle indicates the relative gain after irradiating module 121 for 20 hours under normal circumstances, the square the relative gain after 42 hours of irradiation, with ethanol added to the gas mixture, measured when the module is still wet, the triangle the relative gain after the same irradiation, but measured when the module has dried.*

5.7 Oxygen

It has been shown [18,21] that adding a small amount of O_2 to the gas mixture decreases the ageing rate with approximately a factor two. Oxygen, however, is notorious for its electronegative nature [9]. Adding O_2 to the gas mixture would not only decrease the ageing rate of the outer tracker drift chambers, but also reduce its signal response. The drifting electrons can be captured by the O_2, before reaching the avalanche region, thereby, effectively reducing the number of primary electrons. Before O_2 can be added to the gas mixture, its effects on the detector performance has to be investigated. Many gas properties are obtained from simulations, which are treated in chapter 6. The precise decline in signal response due to O_2 has been determined by measuring pulse height spectra, as explained in section 4.2, for gas mixtures containing 0%, 2.5% and 4.5% O_2.

Based, in part, on these measurements and the simulations in chapter 6 the decision to add 3% O_2 to the outer tracker gas mixture was made, resulting in the gas mixture $Ar/CO_2/O_2$ 70/27/3.

5.7.1 Influence on gain: Pulse-height-spectra measurements

Measuring pulse height spectra is a way to obtain the energy resolution and gain of a gaseous detector (see section 4.2). The pulse height spectra for several O_2 fractions and values of the high voltage are shown in figure 5.15. The main and escape peak have been fitted with a double Gaussian. The position of the main peaks, V_{max_2}, are a measure for the gain and are listed in table 5.1. The relative gain is shown in table 5.2 and shows that it does not depend on the value of the high voltage, as expected. Adding 2.5% and 4.5% O_2 to the counting gas causes a reduction of the gain of 11% and 28% respectively.

Gas composition	Gain - ^{55}Fe			
	1500 V	1520 V	1550 V	1600 V
Ar/CO_2 70/30	0.148	0.174	0.224	0.319
$Ar/CO_2/O_2$ 70/27.5/2.5	0.130	0.154	0.196	0.286
$Ar/CO_2/O_2$ 70/25.5/4.5	0.106	0.124	0.161	0.229

Table 5.1: *Maximum of pulse height spectrum of the outer tracker straw tubes for several oxygen concentrations and values of the high voltage, measured with a ^{55}Fe source.*

Gas composition	Gain - ^{55}Fe				Gain - ^{90}Sr
	1500 V	1520 V	1550 V	1600 V	1600 V
Ar/CO_2 70/30	1	1	1	1	1
$Ar/CO_2/O_2$ 70/27.5/2.5	0.88	0.89	0.88	0.90	0.80
$Ar/CO_2/O_2$ 70/27.5/4.5	0.72	0.71	0.72	0.72	0.55

Table 5.2: *Relative gain of the outer tracker straw tubes for several oxygen concentrations and values of the high voltage, measured with a ^{55}Fe source.*

The response to a ^{90}Sr source has also been checked and differs from the measurements with the ^{55}Fe source. The response to the ^{90}Sr source is reduced by 20% and 45% when 2.5% and 4.5% O_2 is added to the gas mixture (see table 5.2). This was unexpected.

The difference could be caused by the different nature of the sources. The Fe source emits monochromatic photons of 5.9 keV, the Sr source, electrons with an energy up to 2 MeV. The response to photons and electrons seems to be affected in different ways.

5.8 Summary

Ozone, that is produced in the avalanche process, prevents ageing of the straw tubes downstream of the irradiated area and nitrogen dioxide has been shown to posses similar capabilities. Both gases have properties that make them unsuited to be used in the outer tracker gas system.

Hydrogen peroxide also shows prevention of ageing, but is not as potent. The addition of nitrous oxide to the counting gas does not have a significant effect on the ageing rate and adding ethanol even accelerates the ageing process. After testing these additions to the gas mixture, oxygen is still the most successful ageing moderating substance, even though it reduces the signal response of the detector.

Before O_2 could be added to the gas mixture, its influence on the detector performance has been investigated. The reduction of the gain has been quantified by measuring the pulse height spectra for several O_2 concentrations and has been shown to be acceptable. Other effects on the gas properties, such as the drift velocity, have been identified using simulations. The results of these studies are the subject of the next chapter.

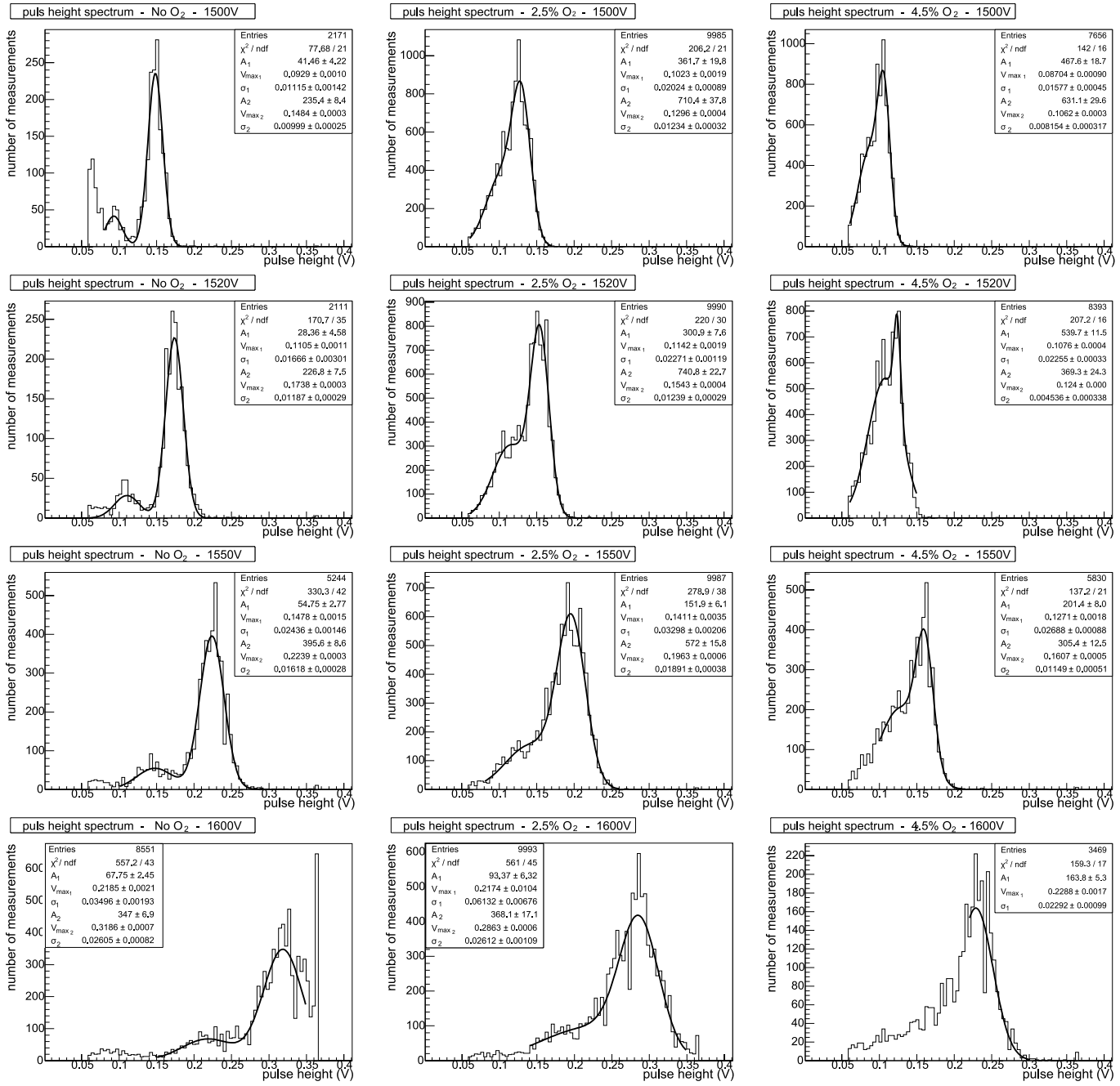

Figure 5.15: *Pulse-height-spectra obtained with ^{55}Fe for several values of the high voltage and varying O_2 concentrations of the counting gas. The main and escape peak have been fitted with a double Gaussian. The large number of entries at 0.365 mV is due to the saturation of the preamplifier.*

Chapter 6

Simulation of the outer tracker

Adding O_2 to the outer tracker gas mixture moderates ageing, but also influences the detector performance. Effects on the signal response have been treated in chapter 4.2. The consequences for the gain and drift gas properties have been obtained by simulating the straw tubes using MAGBOLTZ v7.07 and GARFIELD v9. The results of these simulations are the main subject of this chapter.

In this chapter the programs used to simulate the outer tracker, MAGBOLTZ and GARFIELD, will be introduced. To gain confidence in the results data from various sources for various gas mixtures has been reproduced by simulation. In addition simulated data for the straw tube with Ar/CO_2 has been compared to test beam measurements.

Finally, simulations of the outer tracker arrival time distribution, Townsend coefficient, attachment coefficients and gain for several O_2 concentrations are performed.

6.1 Drift cell simulation: GARFIELD

GARFIELD [33] is a computer program for the detailed simulation of the drift parameters of two- and three-dimensional drift chambers. The program was originally designed to simulate two-dimensional chambers with many wires and planes, but can nowadays also be used for three-dimensional configurations. The author has augmented GARFIELD with a function that can simulate a tube geometry with the wire parallel to the tube, which is used to simulate the outer tracker straw tubes.

GARFIELD takes as input the geometry of the tube, position of the wire, wire diameter, working voltage and the electron transport properties of the fill gas and uses these to compute the electric field in the tube. The drift parameters have to be read in as a function of the reduced electric field E/p [34]. For some commonly used gases and gas mixtures GARFIELD has the properties readily available. For these, GARFIELD will compute the electric field in the tube and calculate the gas transport properties. For other gases or when a higher degree of accuracy is desired, an interface to the MAGBOLTZ program (section 6.2) is available for the computation of electron transport properties in nearly arbitrary gas mixtures.

Because MAGBOLTZ is a dedicated program for the computation of drift properties and determines them with higher accuracy compared to GARFIELD, MAGBOLTZ is used to simulate

the drift velocity, transverse and lateral diffusion, Townsend and attachment coefficient.

6.2 The gas properties: MAGBOLTZ

MAGBOLTZ [14] is a computer program that numerically solves the Boltzmann transport equation for electrons in an electric field. By tracking how far the virtual electron propagates, the program can for instance compute the drift velocity. Table 6.1 shows the input and output parameters of MAGBOLTZ. They are produced as a function of the reduced electric field, which is practical for comparison with simulations of experiments with various geometries. The electric field in the tube is given by equation 6.1 and can be used to determine the parameters as a function of radius, which is necessary to estimate the gain.

$$E(r) = \frac{HV}{r \log(\frac{r_{cathode}}{r_{anode}})} \tag{6.1}$$

Input parameters	Output parameters
E-field	Drift velocity
B-field	Longitudinal diffusion
Angle between E and B	Transverse Diffusion
Gas components	Lorentz angle
Gas component fractions	Attachment coefficient
Temperature	Townsend coefficient
Pressure	Rates of ionization
Cut off for electron velocity	Rates of excitation

Table 6.1: The possible input and output parameters of MAGBOLTZ. [35]

In order to find macroscopic parameters like the drift velocity, MAGBOLTZ needs to know about the microscopic nature of each gas under study. The most important quantities are the scattering cross sections, which measure the probability of collisions to occur and the energy loss per collision. In some cases, for the noble gas helium for instance, the excitation energies are so high that in our experimental range, the drifting electrons lack the energy to excite the atoms, thus making all collisions elastic hard-sphere interactions. Other gases, like the organic quenchers CO_2, CH_4, have vibrational and translational modes which the program must also take into account. It is possible to obtain an accuracy of better than 1% on the drift velocity and 2% on the diffusion coefficients [36, 37].

6.3 Validating the simulation

Before analyzing the consequences of adding a few percent of oxygen on the drift gas properties, the simulation is validated by comparison to data from literature.

6.3.1 Comparison to literature

To validate the simulation, data from several sources [38–41] was used. The experimental parameters, such as gas mixture and geometry of the setup, of the respective experiments were taken as input for the simulation. The experimental and simulated data for drift velocity, Townsend coefficient, attachment coefficient and effective Townsend coefficient are shown as a function of the reduced electric field in figures 6.1 – 6.5. Presenting the experimental parameters as a function of reduced electric field strength is a practical way to compare data from different experiments as it does not depend on the geometry of the setup. Figures 6.1 - 6.5 show that we have good agreement between simulation and experiment.

Figure 6.1 shows reduced Townsend coefficient as a function of reduced electric field. The reduced Townsend coefficient is higher for larger field strengths or lower pressures. At lower pressures the electron can reach larger speeds between collisions and in stronger electric fields the electron is accelerated more rapidly. Both effects allow the drifting electron to liberate more additional electrons in collisions.

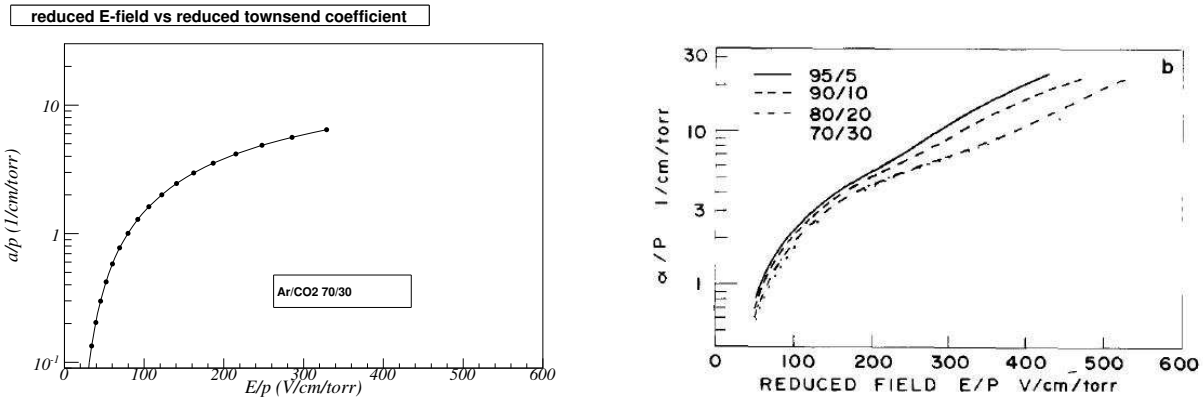

Figure 6.1: *(left) Reduced Townsend coefficient α/P as a function of the reduced electric field E/P from simulation, (right) from experiment [39].*

Figure 6.2 shows that the drift speed is higher for higher electric fields and lower CO_2 concentrations, while figure 6.3 shows that the drift speed is lower for gasses containing less CH_4 and higher electric fields. The difference must be attributed to the different nature of the two quenchers. The collisions cross sections, and therefore the mean time between collisions, can vary strongly for different gasses and depends heavily on electric field strength. The deviating cross sections for different values of the electric field for CO_2 and CH_4 cause variation in the time between collisions and therefore, in drift speed.

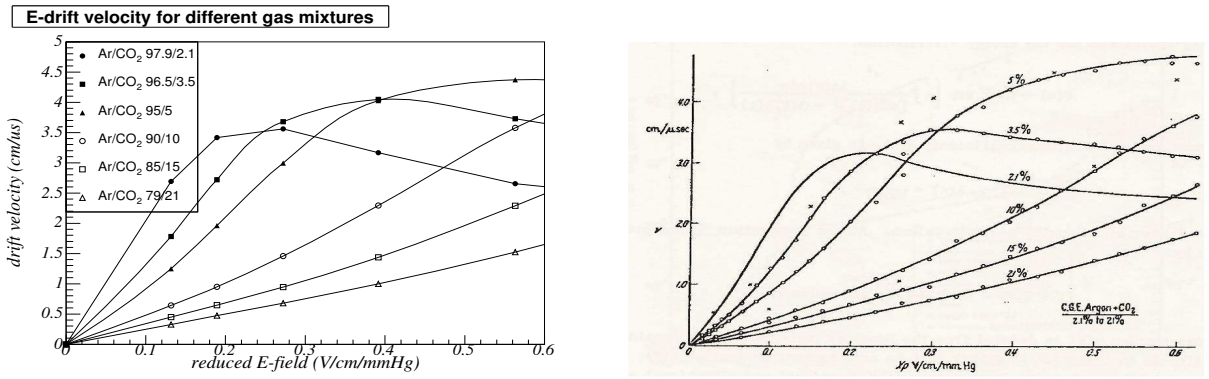

Figure 6.2: *(left) Drift speed vs reduced E-field for different Ar/CO_2 mixtures from simulation, (right) from experiment [41].*

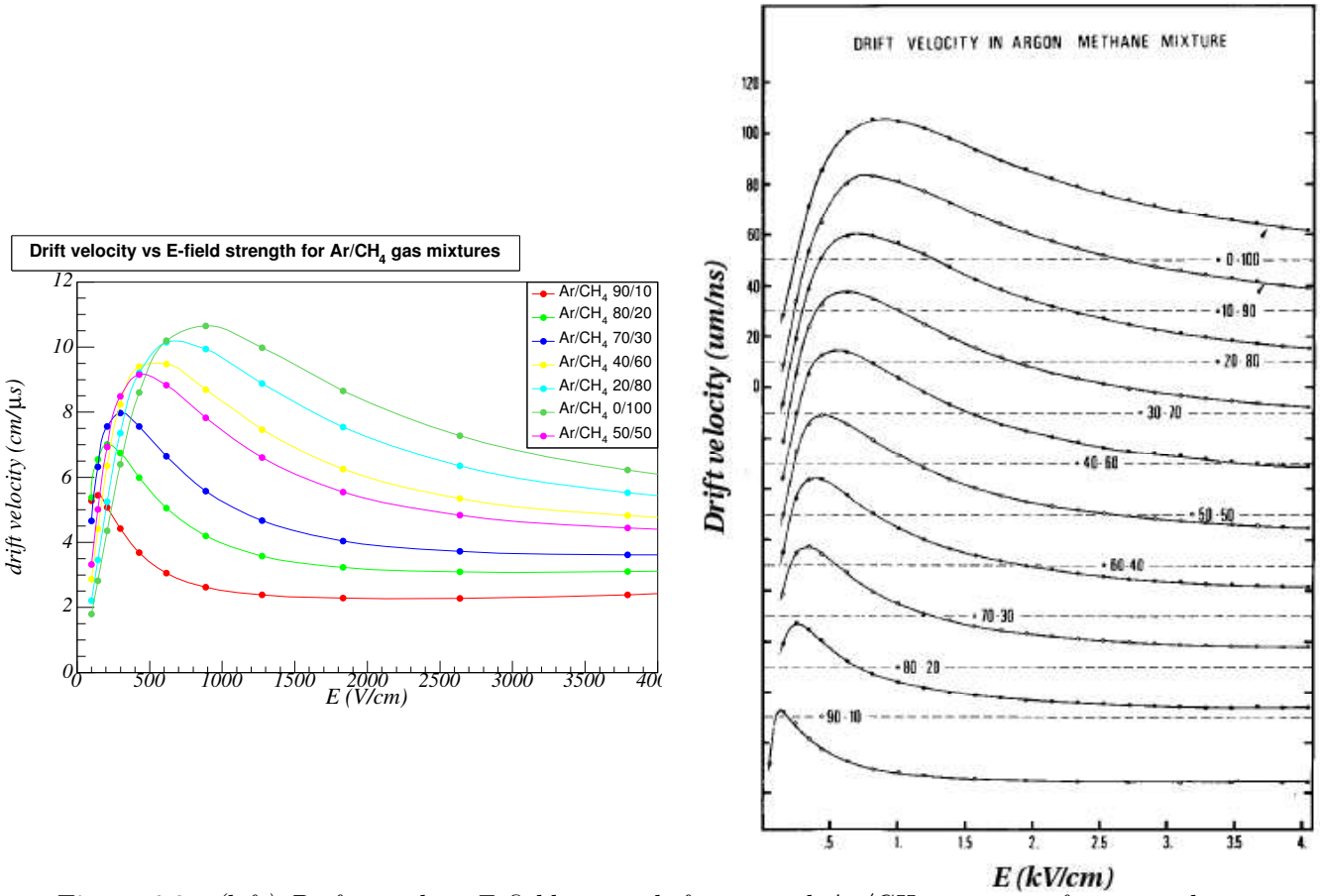

Figure 6.3: *(left) Drift speed vs E-field strength for several Ar/CH_4 mixtures from simulation, (right) from experiment [40].*

Figures 6.4 and 6.5 show reduced effective Townsend coefficient as a function of reduced electric field. The effective Townsend coefficients are larger for larger values of the electric field strength and lower pressures. This is logical, as lower pressures and larger field strengths allow the drifting electron to reach larger speeds between collisions and liberate more additional electrons per collision.

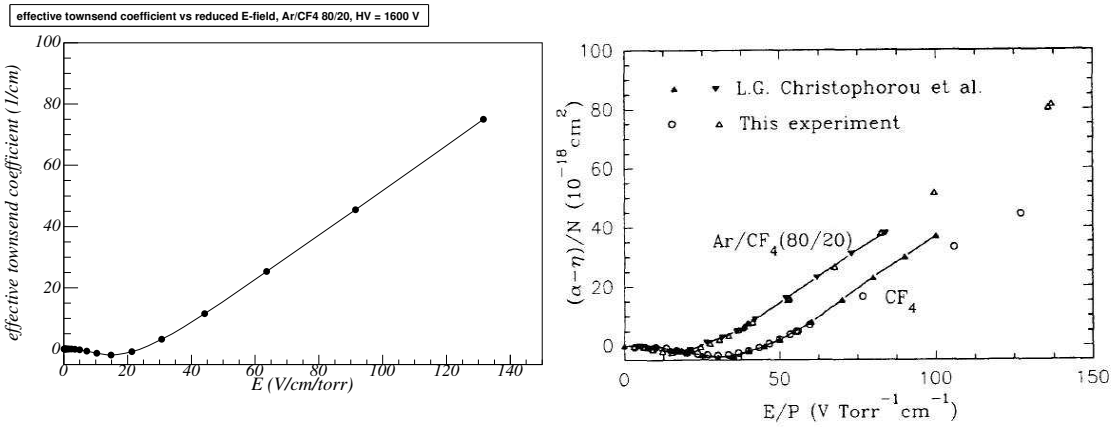

Figure 6.4: *(left) The reduced effective Townsend coefficient (Townsend coefficient - attachment coefficient, α-η/P) as a function of the reduced electric field E/P from simulation, (right) from experiment [38].*

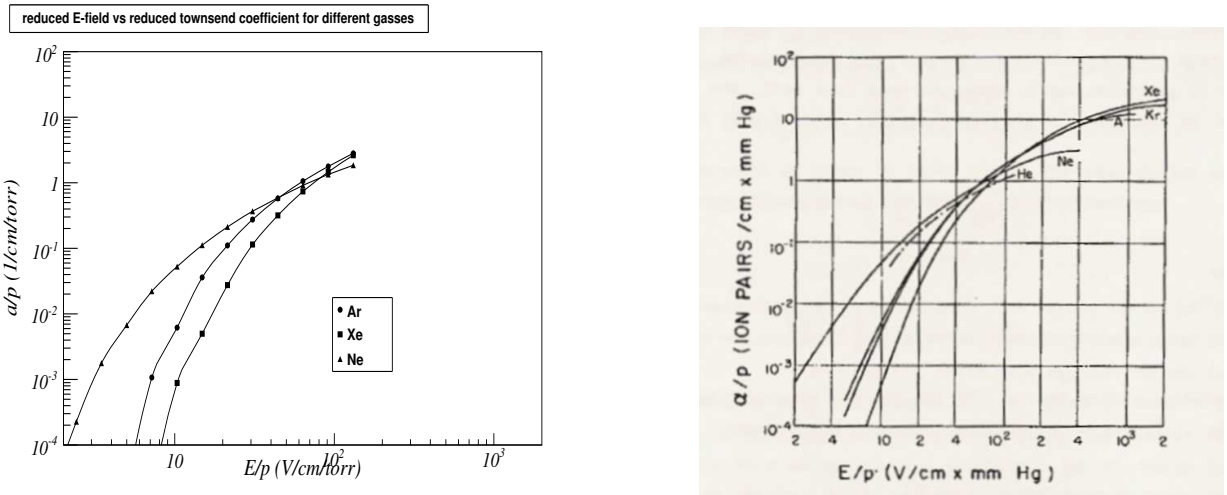

Figure 6.5: *(left) The reduced effective Townsend coefficient (Townsend coefficient - attachment coefficient, α-η/P) as a function of the reduced electric field E/P from simulation, (right) from experiment [38].*

6.4 Simulation of Ar/CO_2 70/30 in straw tubes

Now that we are confident that the gas transport parameters obtained from MAGBOLTZ and GARFIELD are valid and accurate, we can simulate the LHCb outer tracker straw tubes and compare the results with those of test beam measurements.

6.4.1 The arrival time distribution

GARFIELD produces the arrival time of the avalanche as a function of the radial distance of the primary ionization. This arrival time has also been measured in beam tests at several occasions [17, 42, 43]. The arrival time has been simulated for three Ar/CO_2 mixtures (65/35, 70/30, 25/75) and $Ar/CF_4/CO_2$ 70/15/10. These measurements, together with results from simulations, are shown in figure 6.6. It shows that the simulated and measured arrival times versus radius are in good agreement with the measurements and that small variations in the concentration of the gas mixtures have no significant effect on the arrival time.

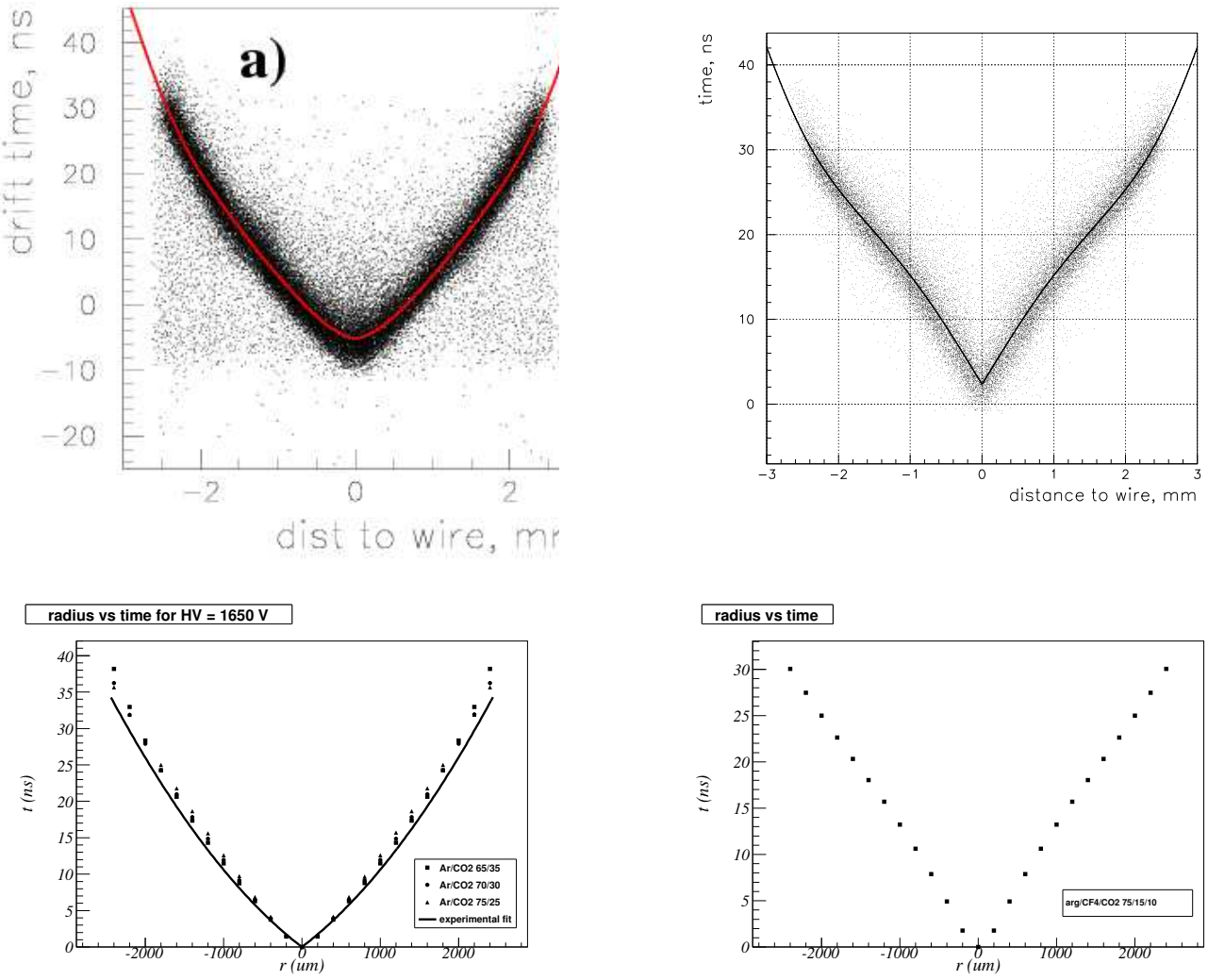

Figure 6.6: *(upper) r-t Relation with Ar/CO_2 comparison to test beam 2005 [43].*(lower) r-t Relation with CF_4, comparison to test beam 2000 [17, 42].

6.4.2 The gain

MAGBOLTZ produces the Townsend coefficient and attachment coefficient as a function of reduced electric field, so that they are independent of the geometry of the setup. Figure 6.7 (left) shows the electric field strength in the straw tube as a function of the distance from the anode wire, which is given by [44]:

$$E(r) = \frac{HV}{r \log(\frac{r_{cathode}}{r_{anode}})} \tag{6.2}$$

Equation 6.2 can be used to compute the effective Townsend coefficient as a function of the distance from the anode wire, $\alpha(r)$, which is shown in figure 6.7 (right). As was discussed in section 2.1.2, an avalanche only starts when the effective Townsend coefficient is nonzero. Figure 6.7 (right) shows that an avalanche is only formed if an electron comes within 400 μm of the anode wire. Using equation 2.4, $\alpha(r)$ can be used to calculate the gain.

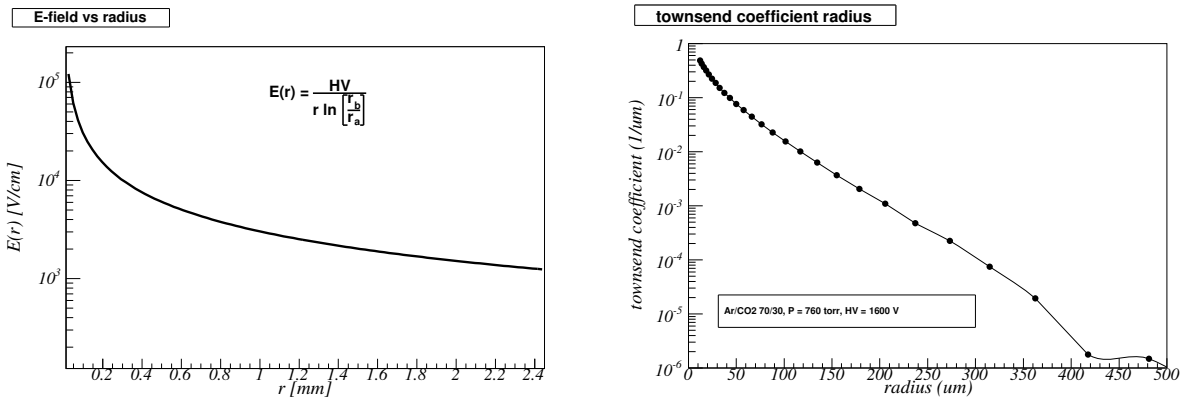

Figure 6.7: *(left) Electric field as a function of the distance to the anode wire. (right) Townsend coefficient, α, as a function of the distance to the anode wire.*

Figure 6.8 shows the gain that is obtained from simulation in case no Penning effect (see section 2.1.2) and maximum Penning effect (every excited argon atom ionizes a CO_2 atom) [28] take place as well as the gain measured with the test beam experiment. The gain without Penning effect is significantly lower than the measured one. On the other hand, the gain with maximum Penning effect assumed, agrees well with experiment. For the occurrence of maximum Penning effect, every excited argon molecule would have to ionize a carbon dioxide molecule, which is an unrealistic scenario.

The discrepancy between simulation and measurement might be explained by some amount of Penning effect. The remaining discrepancy might be attributed to the photon feedback as shown in figure 6.9. Photon feedback can not be taken into account by MAGBOLTZ. This means that only the first avalanche is simulated, while the pulse induced on the straw tube anode wires is caused by both avalanches. The gain derived from these simulations is therefore the gain that would be measured without photon feedback, thus, underestimating the size of the avalanche and

producing too small a value for the gain. The effect of photon feedback might play a role when oxygen is added (see section 6.5).

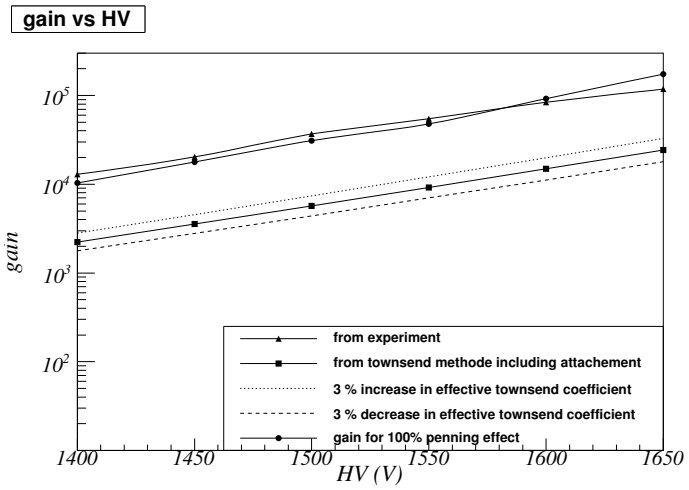

Figure 6.8: *Gain vs HV for gas mixture Ar/CO_2 70/30 The contribution to the gain by the photon feedback is not taken into account. The dotted lines represent the gain when the effective Townsend coefficients are 3% higher or lower.*

Figure 6.9 shows a series of pulses induced on the anode wire as a function of time for a given avalanche. The bump at 45 ns suggests that a second avalanche arrives, which is exactly the time it takes for an electron to drift from the anode to the cathode. This indicates that the outer tracker modules exhibit photon feedback (see section 2.1.2).

6.5 Effects of O_2 on the arrival time distribution and gain

In the last section the simulated arrival time distribution was shown to agree with the results of the test beam experiment [42, 43]. Figure 6.10 shows the maximum arrival time of the avalanche as a function of oxygen concentration of the counting gas, obtained from simulation. It shows that the time it takes the electrons to drift from the cathode to the anode does not significantly depend on the O_2 concentration.

Figure 6.11 shows the gain obtained from simulation, using equation 2.4, for several O_2 concentrations. No variation of the gain is observed for oxygen concentrations between 0% and 5%. This does not agree with the measurements of the signal response in section 5.7.1, which showed that adding 4.5% O_2 to the counting gas lowers the signal response with 28%. This is explained by the fact that the reduction of the pulse height is caused by the loss of drifting primary electrons before reaching the avalanche region. On the other hand, here the gain is calculated from the properties of the avalanche region itself, where very few electrons are captured.

The gain depends strongly on the values of the Townsend and attachment coefficients. The dotted lines in figure 6.11 indicate the gain computed for 3% lower and higher effective Townsend

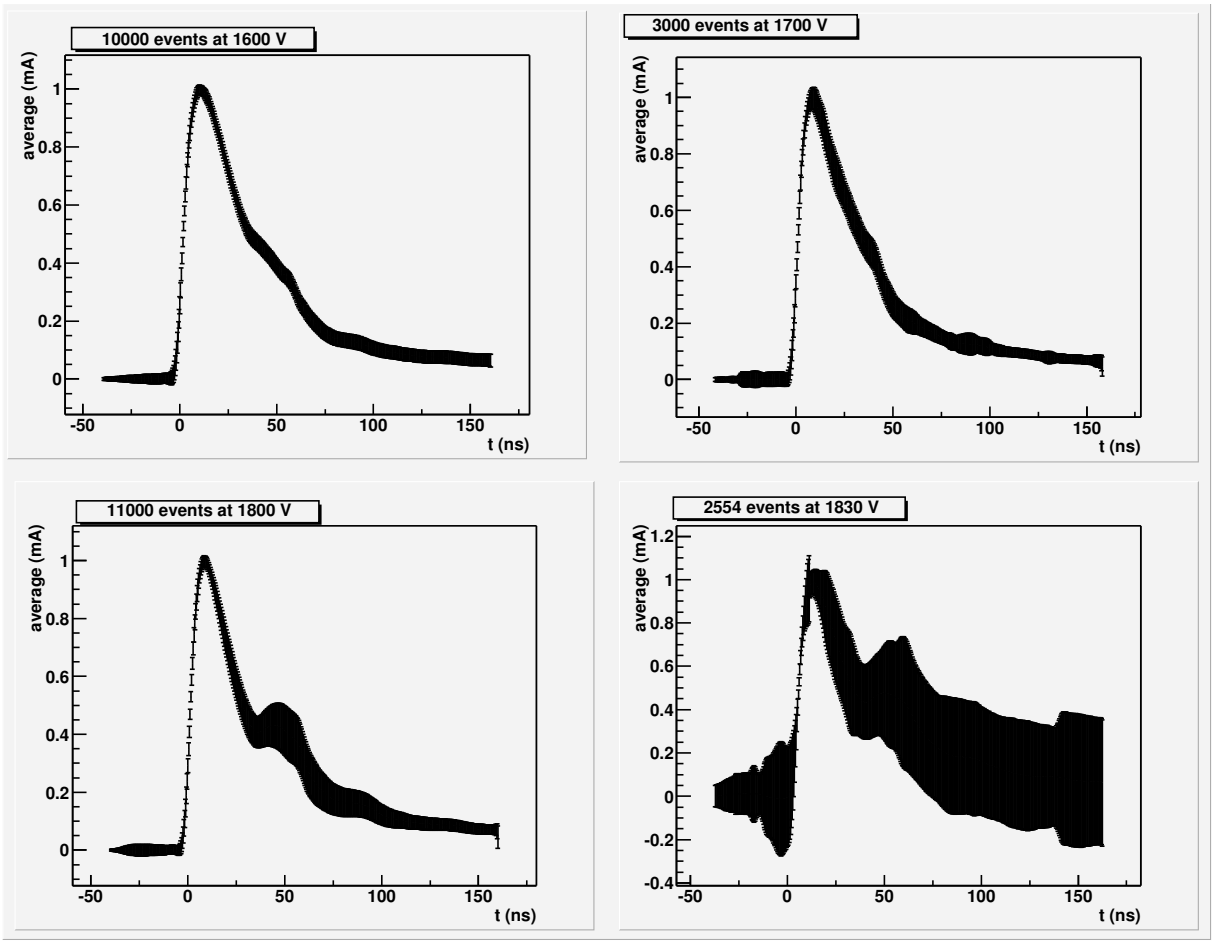

Figure 6.9: *A series of pulses, overlapped, for several values of the high voltage. The photon feedback is seen from the pulse shape by the contribution at* $t > 30$ *ns [45].*

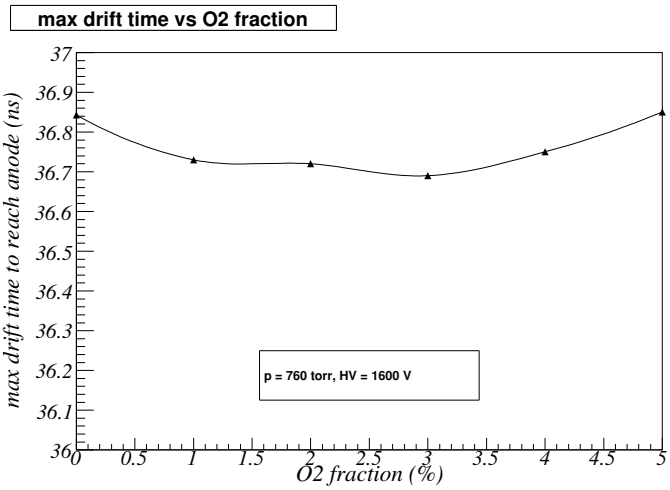

Figure 6.10: *The maximum arrival time of the avalanche for O_2 concentrations between 0% and 5%.*

coefficients. A 3% increase of the effective Townsend coefficient gives rise to a 25% increase of the gain. An error in the simulated Townsend coefficient would have a strong effect on the calculated gain. As expected, no dependence on the O_2 concentration has been observed. Reliable results for the gain can only be obtained from experiments.

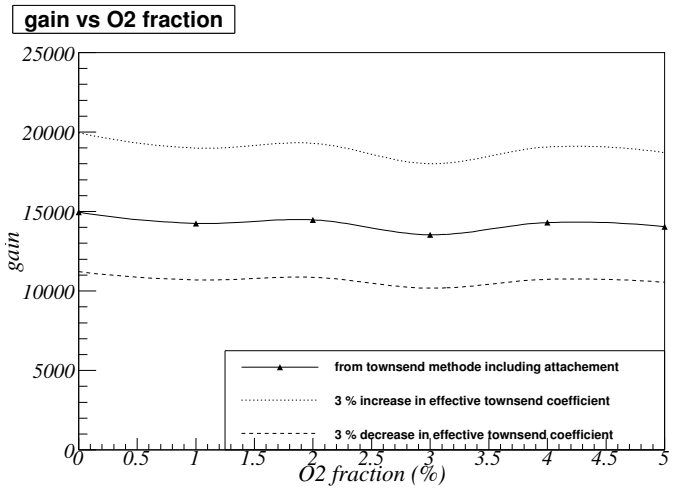

Figure 6.11: *The gain computed with the Townsend method, using simulated data from GARFIELD. The gain is also calculated for 3% lower and higher Townsend coefficients.*

6.6 Summary

Experimental values for Townsend and attachment coefficients taken from literature can be reproduced accurately by simulation with GARFIELD interfaced with MAGBOLTZ and the simulated gas transport properties of the outer tracker straw tubes agree well with test beam measurements. The gain obtained from calculating the size of the avalanche is sensitive for deviations in the Townsend coefficients; an over-, or underestimate of 3% results in an increase or decrease in the gain of 25%.

Simulation of the drift properties of the counting gas for several oxygen concentrations show that the drift time does not depend on the O_2 concentration.

In contrast, the gain calculations are not reliable. Furthermore, photon feedback takes place in the straw tubes, because CO_2 is not a good quench gas. This effect is not taken into account in the simulation and could account for the difference between measured and simulated gain.

Since the addition of oxygen to the counting gas decreases the ageing rate [15] and does not affect the drift velocity, 3% of oxygen can safely be added to the outer tracker gas mixture, despite the 25% loss of signal response.

Chapter 7

Further investigation of heating, flushing and HV training

In chapter 5 the effects of adding some gases and liquids to the gas mixture were investigated. Ageing does not necessarily need to be prevented by additions to the counting gas; other potential solutions that prevent or reverse ageing exist. Some which have shown promise, but need further investigation are: heating, flushing and HV training.

Measurements with a revised heating setup have been undertaken. Many modules have been flushed continuously at Nikhef since April 2007. A reference irradiation has been made to determine their current condition. Repeatedly HV training the anode wires might damage them. To estimate this potential danger of HV training a trained wire as been inspected with a Scanning Electron Microscope (SEM). The results of these investigations are given in this chapter.

7.1 Heating

Outgassing of the glue, Araldite AY 103-1, has been shown to be the cause of the ageing of the outer tracker. This glue is an epoxy. Hardening of the adhesive is caused by a reaction with the resin, HY 991. Should outgassing result from this chemical reaction heating the module may accelerate the chemical process. If the hardening is completed, outgassing and ageing may significantly decrease. If, on the other hand, ageing is caused by evaporation of the hardened glue, ageing might not decrease by heating.

Heating tests performed at the Physikalisches Institut der Universität Heidelberg showed promising results [21]. Modules that had not yet been irradiated (modules HD7 and HD20) were wrapped in four electric blankets, which were automatically regulated via a temperature sensor. A 300 μm aluminum plate was placed between the blankets and the modules to distribute the heat equally and bubble wrap was used to thermally isolate the ensemble. The modules were flushed for several days, after which two simultaneous reference irradiations, with a duration between 160 and 230 hours, were made. Subsequently, the modules were heated to a temperature of 40 – 45°C for 10 – 12 days, during which time they were flushed with pure CO_2 at a rate of one volume exchange per hour. After this heating procedure the modules were allowed to cool down for 1 – 2 days, while being flushed with the normal Ar/CO_2 70/30 gas mixture. Again two simultaneous

irradiations were performed to see whether the ageing rate had improved. These measurements showed that after the heating treatment, the decrease of the ageing rates of the modules could not be explained solely by the longer flushing time. But, despite many attempts, these results could not be reproduced at Nikhef [18].

The effect of heating seems to differ from module to module. This could be caused by the different ways in which the glue was mixed for the modules built in Warsaw, Heidelberg and Amsterdam, influencing the speed of the hardening process. This is corroborated by the fact that the modules from the various construction sites exhibit the tendency to age at different rates.

On the other hand, the failure to reproduce the results from Heidelberg might be caused by a difference in heating procedure. In the heating setup at Nikhef [18], the temperature sensor that regulated the temperature was placed at the middle of the module. When the temperature was kept at 40°C, the temperature at the end of the modules, where most of the glue is situated, may have been lower. The heating test was redone with module 1 with the sidewall removed. The sensors were placed at the end of the module, both inside the spacer and inside the module next to the straws, close to the spacer (see figure 7.1).

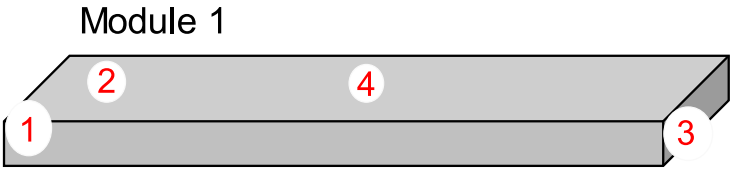

Figure 7.1: *Sketch of the module to indicate the location of the sensors used to monitor and regulate the temperature in the module during the heating test.*

- 1 – Left, 1 m from the edge on top of the module surface. When the temperature was maintained at 45°C the measured temperature was 39.4 – 39.9°C.
- 2 – Left, on top of module. When the temperature was maintained at 45°C the measured temperature was 35.4 – 35.7°C.
- 3 – Right of module, in hole between feed through boards insulated with a special paste. This sensor is used to regulate the temperature during the heating procedure. When the temperature was maintained at 45°C the measured temperature was 44.6 – 45.2°C.
- 4 – On top of module. When the temperature was maintained at 45°C the measured temperatures was 40.5 – 41.9°C.

When the temperature is maintained on 45°C the temperatures measured by the four sensors were between 35.4 and 45.2°C and had a daily variation of 0.6°C. This shows that the temperature

in the different parts of the module may differ significantly from the desired one and seem to be lower further away from the regulating sensor.

The setup used for this test is shown in figure 7.2. Module 1 was wrapped in electric blankets and an aluminum plate was placed between the module and the blanket to improve the conductance of the heat and distribute it over the module. The temperature was monitored with a sensor placed at the end of the module and automatically maintained at a value of 40 – 45°C.

The module was heated in this way for 12 days at a temperature of 40°C and subsequently another 21 days at 45°C. During this period the side wall was removed so that the gas released by the glue could exit the module expeditiously. For this reason the module could not be flushed during the heating procedure. Subsequently, the module was flushed abundantly. After a flushing period of 8 days at a flow rate of one volume exchange per hour, a reference irradiation of 22 hours was made. The damage profile of this irradiation is shown in figure 7.3 (left). The maximum gain loss is 83% and the characteristic crescent-moon shape of the damage is no longer apparent. After flushing the module for an additional 46 days it was again irradiated for 20 hours, which produced the damage shown in figure 7.3 (right). This time the gain had decreased with 52%. A reference irradiation before the heating treatment invoked a similar maximum gain loss of 52%.

The ageing rate of the module significantly increased a few days after the heating treatment, but decreased with flushing time (see table 7.1). This observation is consistent with the hypothesis that heating expedites the release of pollution into the counting gas, which was expected. But

Figure 7.2: *Photo of heating setup at Nikhef.*

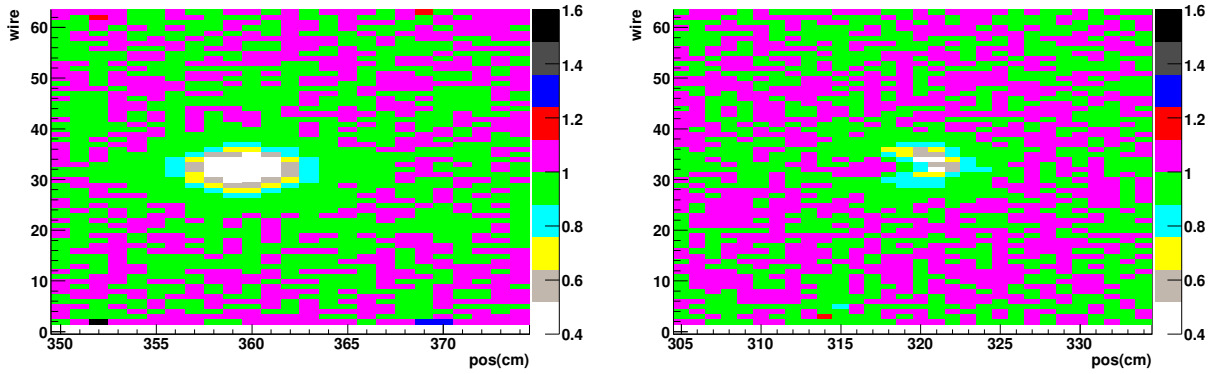

Figure 7.3: *Ageing induced after heating module 1A for 33 days: (left) 22 hours of irradiation after 8 days of flushing. Maximum damage is 83%, (right) 20 hours of irradiation after 54 days of flushing. Maximum damage is 52%. [Left: Module 1A, 27/06/2008 – 28/06/2008. Right: Module 1A, 12/08/2008 – 14/08/2008]*

because the module was not flushed during the heating procedure, all the emitted pollution remained in the module, causing the ageing rate to be very large. When the module was flushed, the pollution left the chamber and the ageing rate decreased. This means that, if ageing is the result of outgassing from the hardening process and not from evaporation of the hardened glue, heating accelerates the outgassing and should shorten the time the modules need to be flushed to stop all outgassing.

	Gain loss
Before heating	52%
After heating	83%
After flushing	52%

Table 7.1: *Summary of maximum damage from 20 hours of irradiation.*

7.2 Flushing

Flushing the outer tracker modules removes pollution from the counting gas and reduces their ageing rate [18]. Flushing modules 2 for 150 days and module 3 for 250 days reduced the maximum damage caused by an irradiation of 20 hours from 72% to about 15% and 3% respectively [18]. Furthermore, figure 7.4 shows the minimum relative gain of module 121A after a 20 hour irradiation measured at different times. Except for the last measurement, less ageing occurs if

the module has been flushed longer. The ageing rate has increased between the 10^{th} and 27^{th} week. This is due to the fact that in 24^{th} – 26^{th} week the module was not flushed, allowing the contamination level to rise and the ageing rate to increase. The observation that the ageing rate deteriorated when the module was not flushed is consistent with the findings in section 7.1.

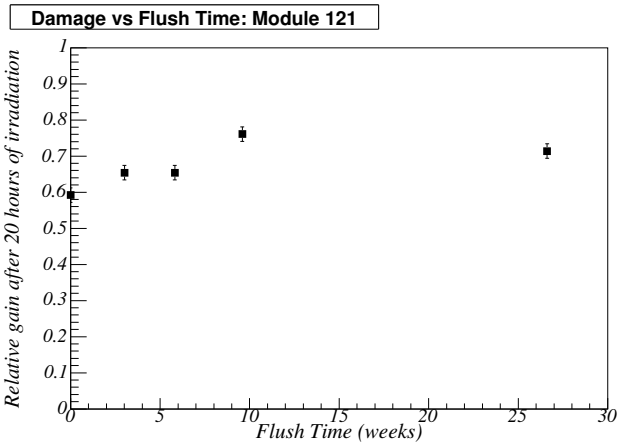

Figure 7.4: *The minimum relative gain of module 121A caused by 20 hour irradiations with a 2mCi ^{90}Sr source at different times. The decrease in ageing rate is attributed to longer flush time*[2].

Therefore, several modules are being flushed at Nikhef since April 2007. Although there can be large module-to-module variations, the ageing rate of two S3 modules can be compared: S3-099A, that was irradiated before flushing in April 2007 and S3-117B, that had been flushed for 1.5 years.

Figure 7.5 (right) shows the relative gain after a 20 hour reference irradiation of module, 99A, made in April 2007. Then, the maximum gain loss of that irradiation was 73%. To determine their current status, one of these modules, 117-88B, has been irradiated for 42 hours after it had been flushed for 14 months. The relative gain of the module after this irradiation is shown in figure 7.5 (left). The maximum gain loss is 2%, which is approximately 1% per 10 – 20 hours (given the uncertainty of the damage increase as a function of time). We therefore conclude that flushing the modules has a beneficial effect on the ageing rate.

It seems that the improvement of the ageing rates due to flushing diminishes gradually with time. This is consistent with the hypothesis of section 7.1 that flushing first removes the pollution already emitted by the glue from the gas system and is subsequently limited by the outgassing rate of the glue. After the contamination that had built up over time has been removed from the gas system, the ageing rate decreases because less pollution is emitted, which is then rapidly

[2]Module 121 has been used a lot in our ageing investigation. It has been flushed from May 2007 – September 2007 during which time several HV trainings have been undertaken as well as a study of the effects of oxygen. Between September 2007 and June 2008 the module was not flushed. From June 2008 the module was flushed again. Since it has been hydrated with water/H_2O_2 50/50 (8100 ppm), 0.4% N_2O had been added to gas mixture and the influence of ethanol (2000 ppm) investigated.

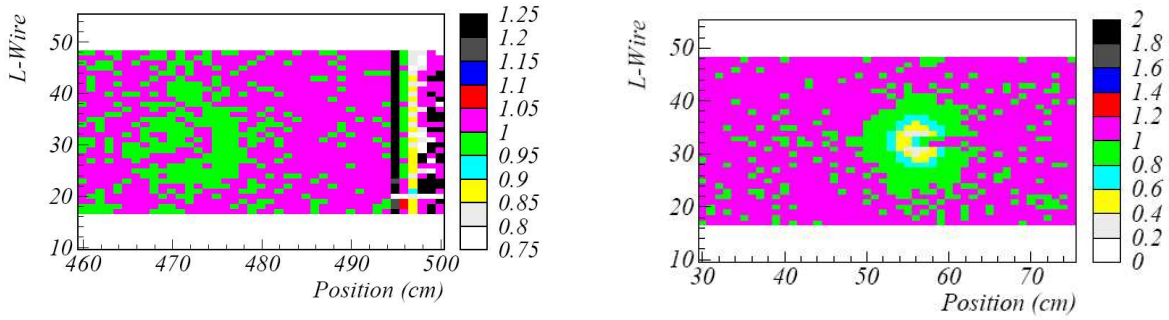

Figure 7.5: *(left) Relative gain of module 117-88B after 42 hours of irradiation with a 2mCi ^{90}Sr source. The gas flow is from right to left. (right) Relative gain of module 99A after 20 hours of irradiation with a 2mCi ^{90}Sr source. Gas flow is from left to right. [Left: Module 88B, 03/10/2008 – 08/10/2008. Right: Module 99A, 16/02/2006 – 17/02/2006]*

transported out of the straw tubes. Some amount of ageing persists, because outgassing of the glue does not stop.

7.3 HV training

7.3.1 Influence of water on the effects of HV training

Prevention as a result of HV training the anode wires of the straw tubes and in some cases even reversal of gain loss has been observed [18], but is unpredictable and unreliable as, for unknown reasons, it does not always work for all wires.

When a voltage between 1800 and 1950 V is applied to the anode wires (normal operation is 1520 V), a strong current between 10 and 30 μA per wire is induced and discharges between the anode and cathode take place. We envision that the insulating layer is removed directly by these discharges, or evaporates due to local increase in temperature of the anode wire as a result of the high currents.

Introducing water into the module would increase the conduction of the damage and therefore, might stimulate discharges and promote recovery of the signal response. To test this hypothesis, water was added to the gas mixture by leading it through a bottle of water before entering the module. The vapor pressure of the counting gas was monitored with a dew point meter placed at the gas outlet of the module. [3] A schematic representation of the setup is shown in figure 7.6.

[3]The dew point is the temperature at which the water in the gas condensates. This relies directly on the vapor pressure. A table relating the vapor pressure to the dew point may be found in appendix A.

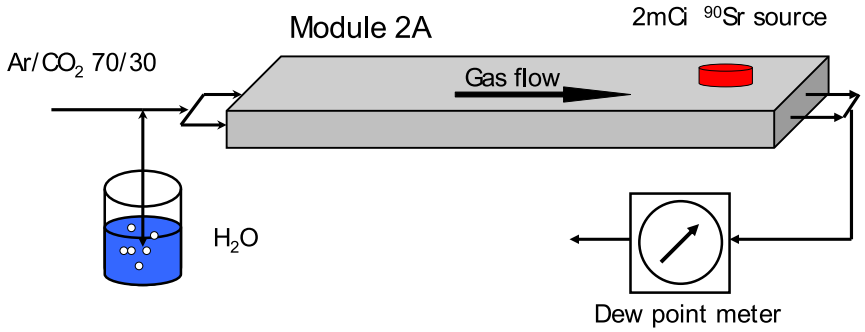

Figure 7.6: *Setup to add water to the counting gas and monitor its concentration.*

Figure 7.7 shows the damage of module 2A before HV training. The module had severely aged 110 cm from the gas inlet (left in figure 7.7). Multiple attempts of HV training at 1900 – 1920 V with normal, dry counting gas did not repair the damage [46].

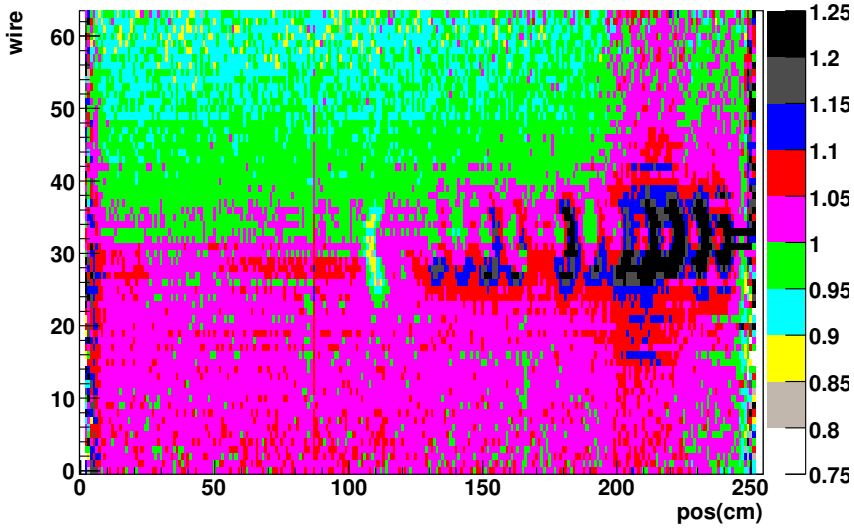

Figure 7.7: *Relative signal response of module 2A before HV training. The module has been aged on several locations. All but the ageing spot at 110 cm have been repaired by HV training. [Module 2A, 17/04/2008 – 27/06/2008]*

Half of the wires of module 2A were HV trained twice at elevated humidity. The first training lasted for 30 hours with 40.000 ppm of water present in the module (dew point = -5°C). The result of this training is shown in figure 7.9. The second training had a duration of 20 hours with 4000 ppm water (dew point = -29°C). The currents drawn from the anode wires 1 – 32 during these trainings are shown as a function of time in figure 7.8. The relative gain of the module

after this training is shown in figure 7.10.

The relative gain is not precisely 1 in both figure 7.9 and 7.10. The variations of the current in the various wires is due to a varying dark current caused by the humidity in the module. Figures 7.9 and7.10 show that neither of the trainings cured the damaged areas visible in figure 7.7.

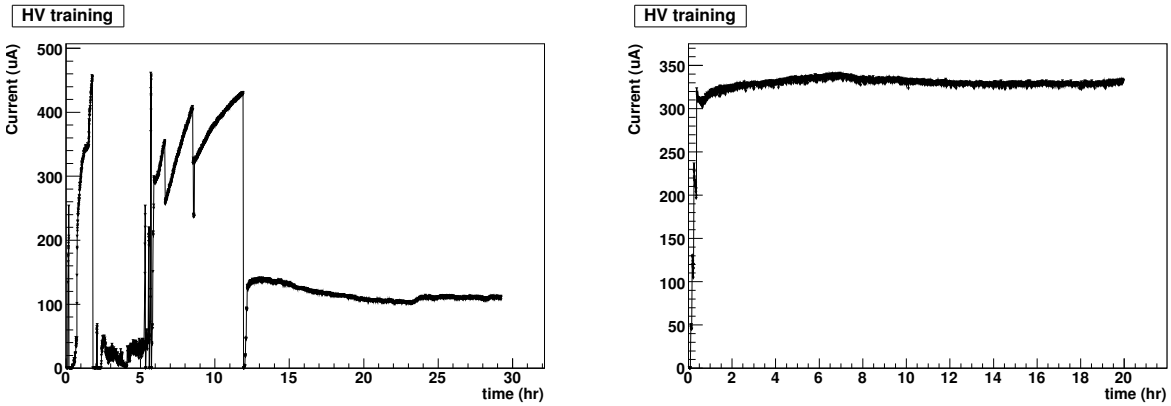

Figure 7.8: *Current in 32 wires during HV training of hydrated module 2A (left) 40.000 ppm, (right) 4000 ppm.*

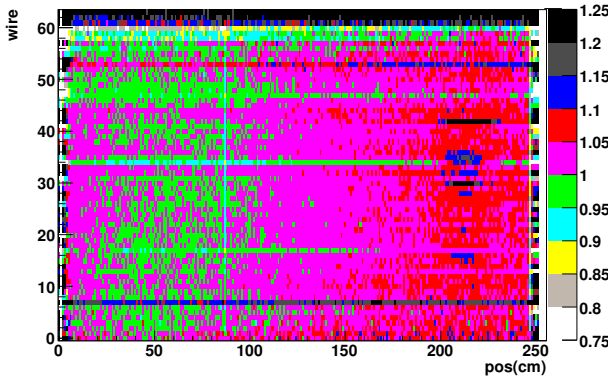

Figure 7.9: *Relative gain of module 2A after 30 hrs HV training 40.000 ppm H_2O. The scans before and after the training were made at the same humidity. [Module 2A, 08/07/2008 – 11/07/2008]*

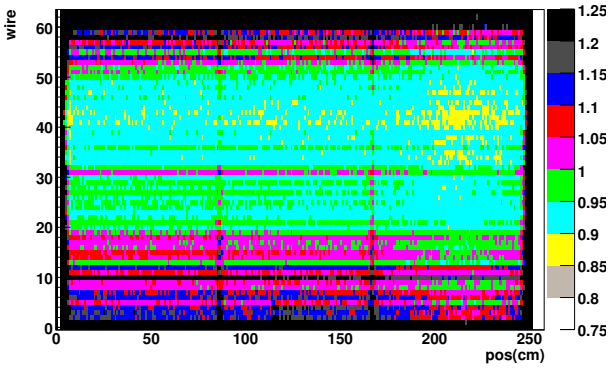

Figure 7.10: *Relative gain of module 2A after 20 hrs HV training 4000 ppm H_2O. The horizontal structures indicate that the dark currents are no longer negligible and vary from wire to wire. [Module 2A, 24/07/2008 – 25/07/2008]*

7.3.2 Wire damage from HV training

HV training the anode wires increases the durability of the detector, prevents ageing and sometimes even recuperates the module. However, this aggressive treatment with large currents potentially forms a risk for the protective gold layer on the anode surface. Before HV training can be used to repair the outer tracker modules any sign of mechanical damage needs to be excluded.

A special module, module 501, from which the anode wires can be removed and replaced, has been constructed [18]. Part of this module was irradiated for 713 hours with a 20 mCi ^{90}Sr source to invoke ageing. The damage caused by this irradiation is depicted in figure 7.12). [4] The four wires situated in the middle of the module (wires 29, 31, 33, 35) were trained at $50\mu A/wire$ for 40 hours. The current as a function of time for this training is depicted in figure 7.11. The relative gain after these procedures is shown in figure 7.13. It is clear that the HV training of the wires reversed their ageing.

[4] The sharp border of the damage at a position of 42 cm is due to a metal bar between the ageing source and the module.

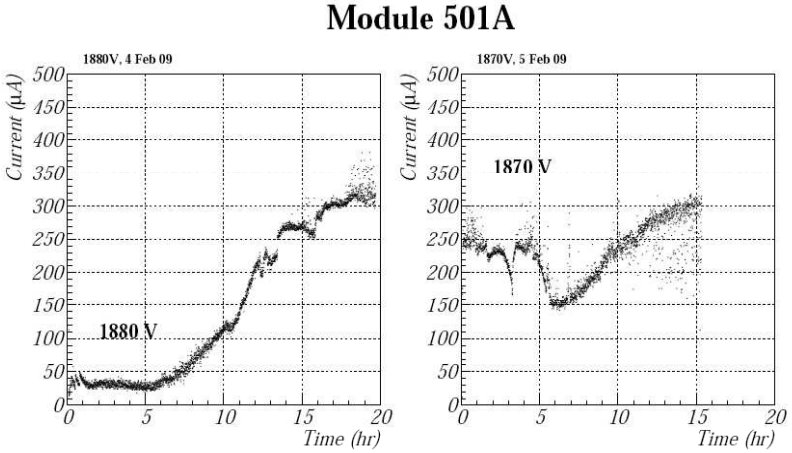

Figure 7.11: *Current drawn from wires 29, 31, 33 and 35 during HV training of module 501.*

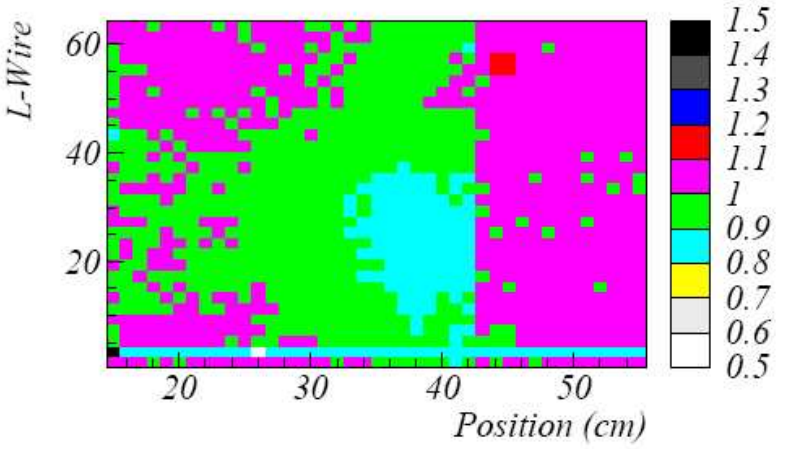

Figure 7.12: *Relative gain loss of module 501A after 713 hours of irradiation with the 20 mCi ^{90}Sr scanning source. [Module 501A, 23/12/2008 – 03/02/2009]*

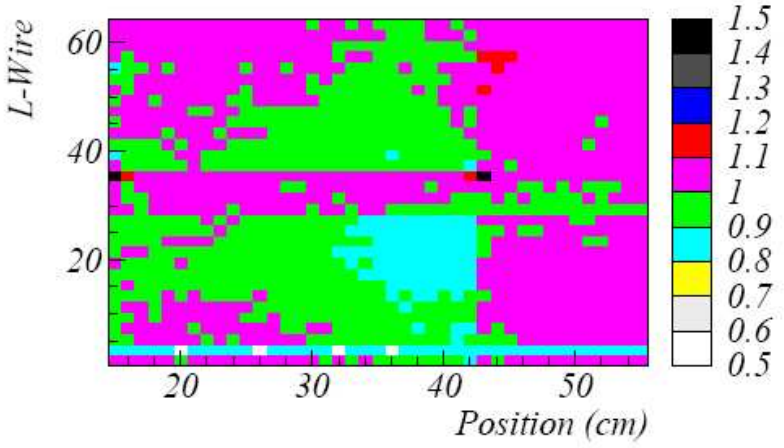

Figure 7.13: *Relative gain loss of module 501A after 713 hours of irradiation and 40 hours of HV training wires 29, 31, 33, 35. Wires from this module were investigated with a SEM. [Module 501A, 23/12/2008 – 05/02/2009]*

To determine the possible damaging effects of HV training, several wire samples were taken from the module to inspect them with a Scanning Electron Microscope (SEM). These samples, shown in figures 7.14 – 7.18, are listed in table 7.2.

Wire	Position from gas inlet (cm)	Figure	Comment	Sample number
27	37	7.14	Aged, but not trained	1
27	180	7.15	Not aged, not trained	3
29	37	7.17	Aged and trained	4
-	-	7.16	New wire taken from spool WIR 051014-15	7
29	180	7.18	Trained, not aged	6

Table 7.2: *Summary of wire samples that were investigated with a scanning electron microscope.*

Figures 7.14 and 7.15 show photos of two wire samples made with the SEM. The sample in figure 7.14 has aged as a result of 713 hours of irradiation with a 20 mCi ^{90}Sr source. Figure 7.15 shows a second sample of the same wire, but from a part that was not irradiated. The surface of the irradiated part is covered with the insulating layer. The light square in the photo is caused by illumination of the SEM, which has removed some of the coating, making it more transparent to the photons emitted by the wire. The surface of the wire that was not aged looks as clean as the new wire, shown in figure 7.16. The black square is again caused by illumination of the SEM. However, this time the SEM deposited a layer on the wire (caused by the polluted vacuum) indicating that the wire surface was initially clean.

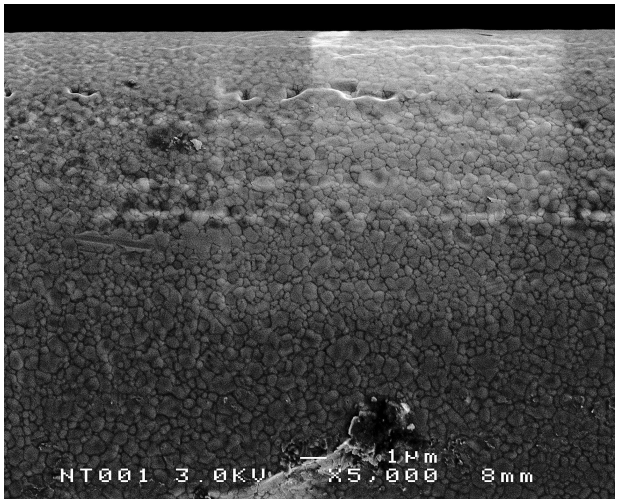

Figure 7.14: *Picture made with a Scanning Electron Microscope of wire 27 from module 501A. The wire was aged by the ^{90}Sr scanning source. The source position was 57 cm from the gas inlet, the sample was taken 37 cm from lower end. This part had aged, but the wire was not trained.*

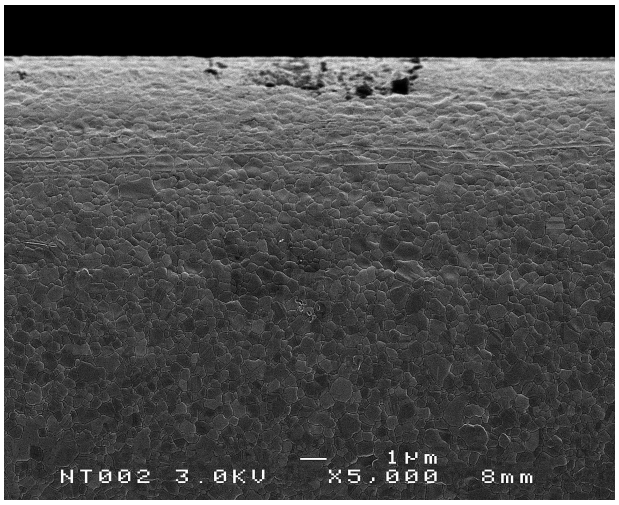

Figure 7.15: *Picture made with a Scanning Electron Microscope of wire 27 from module 501A. The wire was aged by the ^{90}Sr scanning source. The source position was 57 cm from the gas inlet, the sample was taken 180 cm from lower end. This part had not aged and the wire had not been trained.*

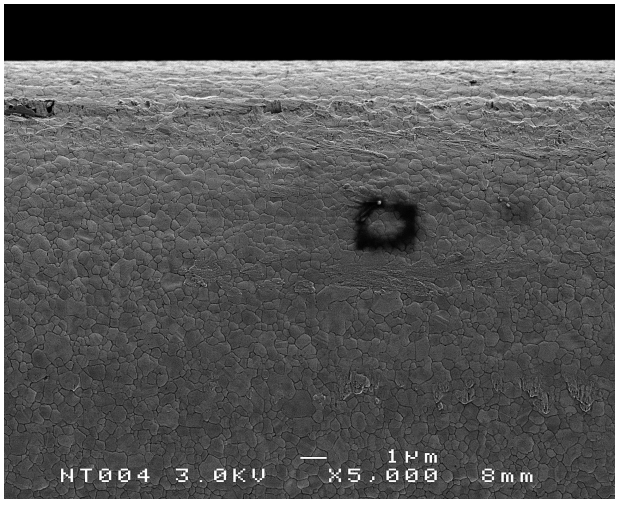

Figure 7.16: *Picture made with a Scanning Electron Microscope of a piece of new wire taken straight from spool WIR 051014-15. It has not been in the module.*

Figures 7.17 and 7.18 show photos of two wire samples made with the SEM. The sample in figure 7.17 has aged as a result of 713 hours of irradiation with a 20 mCi ^{90}Sr source and was afterward submitted to a HV training of 40 hours. The sample in figure 7.18 comes from the same wire, but from a part that was not irradiated.The black squares visible in figures 7.17 and 7.16 are carbon deposits caused by illumination with the SEM. These deposits make the surface less transparent to photons emitted by the wire surface. The fact that this matter accumulates on the wire surface indicates that all ageing deposits had been removed. Indeed the trained sample of figure 7.17 looks as clean as the sample of the new, unused wire in figure 7.16. The wire cleaned by HV training shows no signs of damage from the severe treatment. The black spots along the length of the wire are probably carbon deposits, which might have been caused by the HV training. However, these spots do not form a threat to the detector performance.

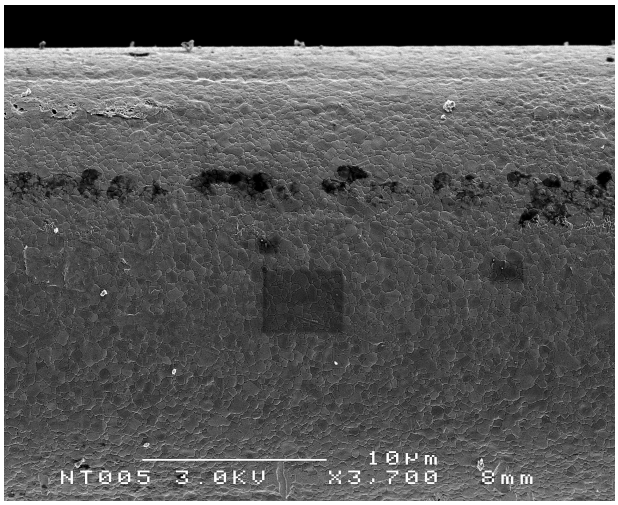

Figure 7.17: *Picture made with a Scanning Electron Microscope of wire 29 from module 501A. The wire was aged by the ^{90}Sr scanning source. The source position was 57 cm from the gas inlet, the sample was taken 37 cm from lower end. This part had aged and had been trained.*

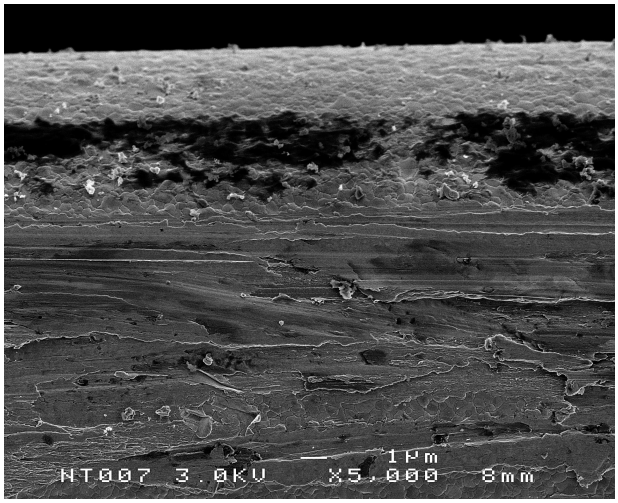

Figure 7.18: *Picture made with a Scanning Electron Microscope of wire 29 from module 501A. The wire was aged by the ^{90}Sr scanning source. The source position was 57 cm from the gas inlet, the sample was taken 180 cm from lower end. This part had not aged, but the wire had been trained. The mechanical scratches are most probably made when the wire was extracted from the module. This part of the wire had to pass through two wire locators during the extraction.*

Apart from the visual inspection of the wire surface, using the SEM images, also the EDX spectra of all wire samples have been analyzed (see figure 7.19). The Au (gold) peak has not decreased for the HV trained sample, which is another indication that the gold layer has not been affected.

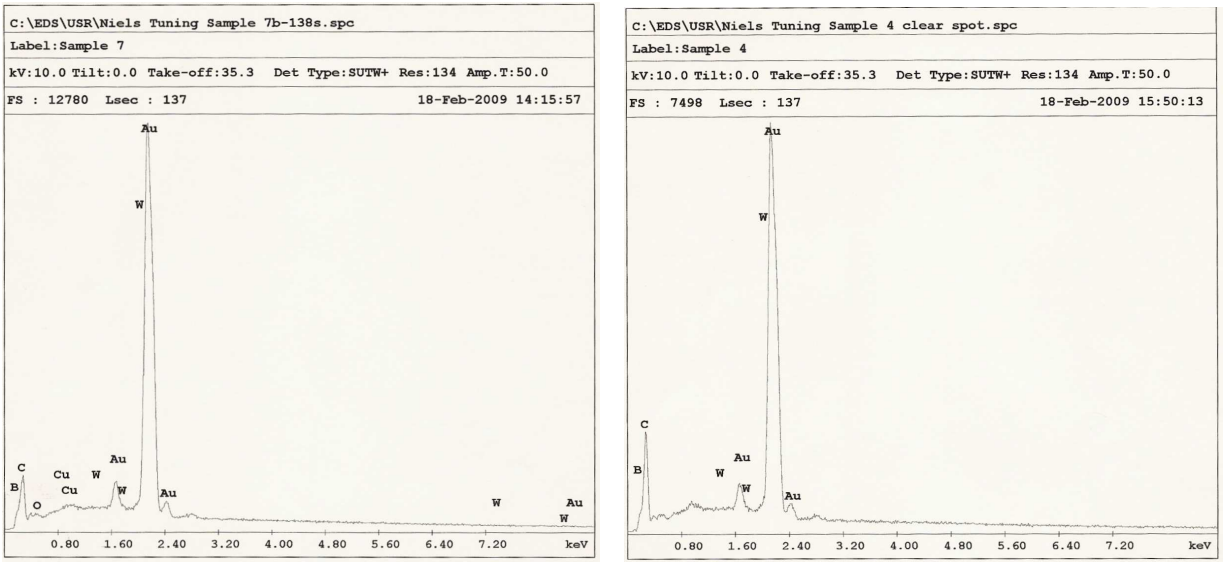

Figure 7.19: *EDX spectra of new (left) and trained (right) anode wire.*

7.4 Summary

If outgassing is a result of the hardening process of the adhesive, the modules will stop ageing when this process is complete. Heating the outer tracker modules has shown to accelerate the outgassing from the glue. Although no module at Nikhef has yet reached an acceptable ageing rate.

Flushing the outer tracker modules for some weeks or months has been shown to decrease the ageing rate strongly, but as the module is flushed for a much longer period of time the improvement of the ageing rate diminishes. This indicates that the observed reduction in ageing rate after a longer flushing time is due to a decrease of the outgassing speed of the glue, which agrees with the outgassing measurements in chapter 3. Flushing only transports the pollution out of the detector and its effect is therefore limited by the outgassing speed of the glue.

Adding water to the counting gas does not enhance the effect of HV training. The success of HV training does not depend on humidity, but is apparently governed by a different parameter.

No damage or other negative effects as a result of HV training the anode wires of the straw tubes has been observed with the SEM. Repeatedly training the wires to increase their radiation hardness or restore the detector response should be save from a mechanical point of view.

Chapter 8

Conclusion

The modules of the LHCb outer tracker suffer from ageing. The glue used for their construction contaminates the gas system and forms an insulating coating on the anode wires during irradiation. The mass spectrum of the glue obtained with a quadrupole mass spectrometer is consistent with the presence of several substances likely to be either emitted by the glue, or to originate from the residual gas in the vacuum. These are: water, air, N_2 , H_2, CO_2, methane, ethane, propane, butane, epichorohydrin, hydrolyzable chlorine, bound chlorine, α-glycol, solid epoxy group (figure 3.14), trimethylbutane and trimethylhexane. Water being the most abundant. The mass spectrum of trabond should also be tested for the presence of these compounds.

An upper limit for the rate at which these gasses are emitted by araldite in the outer tracker modules has been determined to be 2.6 10^{-6} $mbarLs^{-1}$. This rate implies that the maximum concentration of pollution in the outer tracker gas system is roughly 141 ppm, most of which is water. Furthermore, the outgassing rate of both araldite and trabond has been observed to decreases with a characteristic time of 14 – 15 days. This timescale does not agree with that of the decrease of the ageing rate of the detector and is therefore thought to be the rate at which water is drained from the glue samples by the vacuum in stead of the natural rate at which the glue hardens.

N_2O, H_2O_2 and ethanol have been tested for their ability to prevent ageing. Some improvement has only been observed with H_2O_2, but is attributed to the formation of O_2. N_2O has no effect on the ageing rate and ethanol accelerates the ageing process.

Heating the outer tracker modules has shown to accelerate the outgassing from the glue. If contamination of the outer tracker gas system arises from hardening of the glue, the process may be accelerated by heating and ageing will stop when hardening is complete.

The ageing rates of the outer tracker modules, that have been flushing at Nikhef since April 2007, have decreased significantly, but have not vanished. This is consistent with the results from the outgassing measurements, showing that the outgassing rate decreases. Flushing would then only remove pollution from the module that has already been emitted by the glue and its positive effects on the ageing rate would be limited by the outgassing speed of the glue.

Increasing the humidity of the outer tracker gas mixture does not enhance the effect of HV training. The success of HV training is apparently governed by a different parameter. Furthermore, no structural damage resulting from HV training has been observed with the SEM and

reversing ageing effects by drawing strong currents from the anode wires should be harmless to the detector.

The addition of a small percentage of O_2 has been shown to reduce the ageing rate, but O_2 is notorious for its ability to capture electrons. Determination of the pulse height spectrum with ^{55}Fe showed that adding 2.5% and 4.5% O_2 reduced the signal repsonse of the straw tubes with 11% and 28% respectively. The influence on the response to a ^{90}Sr source has been shown to be stronger, 20% and 45% gain loss.

Effects of the addition of O_2 on other gas transport properties have been obtained from simulation with GARFIELD interfaced with MAGBOLTZ. Neither drift velocity, arrival time, or gain have been observed to depend on the oxygen concentration. The independence of the gain on the oxygen concentration does not agree with the measurements of the signal response to ^{55}Fe . This apparent inconsistency is due to the fact that the signal response is reduced,because of the loss of drifting primary electrons. The gain of the surviving drifting electrons in the avalanche region is unaffected.

Appendix A

Dew Point vs H_2O concentration

Dew point (°C)	H_2O concentration (ppm)
-81.48	5.33
-79.4494	7.47
-77.4188	10.27
-75.3882	14
-73.3576	19.07
-71.327	25.86
-69.2964	34.8
-67.2658	46.53
-65.2352	61.86
-63.2046	81.86
-61.174	107.72
-59.1434	141.32
-57.1128	183.98
-55.0822	237.31
-53.0516	306.64
-51.021	393.97
-48.9904	503.96
-46.9598	641.28
-44.9292	811.93
-42.8986	1023.91
-40.868	1287.89

Dew point (°C)	H_2O concentration (ppm)
-38.8374	1611.86
-36.8068	2009.16
-34.7762	2497.12
-32.7456	3090.4
-30.715	3811.68
-29.6997	4226.31
-28.6844	4679.6
-27.6691	5186.23
-26.6538	5732.85
-25.6385	6346.13
-24.6232	7012.74
-23.6079	7732.68
-22.5926	8532.61
-21.5773	9399.2
-20.562	10345.8
-19.5467	11385.7
-18.5314	12518.9
-17.5161	13745.5
-16.5008	15092
-15.4855	16545.3
-14.4702	18145.1
-13.4549	19865
-12.4396	21758.2
-11.4243	23798
-10.409	25997.8
-9.3937	28410.9
-8.3784	31010.7
-7.3631	33823.8
-7.16004	34410.4
-6.95698	35010.4
-6.3478	36863.5
-5.3325	40169.9
-4.3172	43729.6
-3.3019	47569.3
-2.2866	51728.9
-1.2713	56221.9
-0.256	61048.1

Table A.1: *Relation between dew point and concentration.*

Bibliography

[1] A. Sakharov, "Violation of CP invariance,C asymmetry, and baryon asymmetry in the universe," *Pisma Zh. Eksp. Toer. Fis.*, vol. 5, pp. 32 – 35, 1967.

[2] I. Bigi and A. Sanda, *CP Violation*. Cambridge University Press, Cambridge, 2000.

[3] M. Kobayashi and T. Maskawa, "CP violation in the renormalizable theory of weak interaction," *Prog. Theor. Phys.*, vol. 49, p. 652, 1973.

[4] J. Christenson, J. Cronin, V. Fitch, and R. Turlay, "Evidence of the CP asymmetry amplitude $\sin 2\beta$ with B^0 mesons," *Phys. Rev. Lett.*, vol. 13, pp. 138 – 140, 1964.

[5] S. Bachmann, I. Bagaturia, H. Deppe, F. Eisele, T. Haas, L. Hajduk, U. Langenegger, J. Michalowski, A. Nawrot, G. Polok, *et al.*, "The straw tube technology for the lhcb outer tracking system," *Nuclear Inst. and Methods in Physics Research, A*, vol. 535, no. 1-2, pp. 171 – 174, 2004.

[6] P. Vankov, *Study of the B-meson lifetime and the performance of the outer tracker at LHCb*. PhD thesis, Vrij Universiteit, Amsterdam, 2008.

[7] W. Leo, *Techniques for Nuclear and Particle Physics Experiments: A How-To Approach*. Springer, 2nd ed., 1994.

[8] F. Sauli, *Principles of Operation of Multiwire Proportional and Drift Chambers*. European Organization for Nuclear Research, 1977.

[9] K. Kleinknecht, *Detectors for particle radiation*. Cambridge University Press, 2nd ed., 1998.

[10] L. Hommels, *The Tracker in the Trigger of LHCb*. PhD thesis, University of Amsterdam, Amsterdam, 2006.

[11] S. Korff, *Electron and Nuclear Counters*. Van Nostrand, 1955.

[12] G. Knoll, *Radiation detection and measurement*. Wiley New York, 1989.

[13] D. R. Lide, *CRC Handbook of Chemistry and Physics*. CRC Press LLC, Boca Raton, Florida, 84th ed., 2003.

[14] S. Biagi, "A multiterm boltzmann analysis of drift velocity, diffusion, gain and magnetic-field effects in argon-methane-water-vapour mixtures," *Nuclear Instruments and Methods in Physics Research Section A*, vol. 283, no. 3, pp. 716 – 722, 1989.

[15] M. Blom, I. Mous, and N. Tuning, "Effects of adding oxygen to the outer tracker gas mixture," *LHCb*, vol. 064, 2008.

[16] G. v. Apeldoorn, "Outer tracker module production at nikhef - quality assurance," *LHCb*, vol. 078, 2004.

[17] P. Marinho, I. Bediaga, A. Barbosa, J. Magnin, J. De Miranda, A. Massafferi, A. Reis, R. Silva, S. Amato, P. Colrain, *et al.*, "Lhcb outer tracker technical design report," *CERN/LHCC*, vol. 24, 2001.

[18] I. Mous, "Aging in the lhcb outer tracker." CERN-THESIS-2008-005.

[19] S. Bachmann *et al.*, "The straw tube technology for the lhcb outer tracking system," *Nuclear Inst. and Methods in Physics Research*, vol. 535, pp. 171 – 174, 2004.

[20] E. Simioni. PhD thesis. to be published.

[21] T. Haas, *Alterungsstudien und Studium der Betriebseigenschaften des Outer Trackers des LHCB-detektors*. PhD thesis, Ruprecht-Karls-Universitat, Heidelberg, 2007.

[22] B. Storaci *et al.*, "Ageing studies on an outer tracker module constructed with tra-bond glue," *LHCb*, vol. 017, 2008.

[23] M. Capeans, "Aging and materials: lessons for detectors and gas systems," *Nuclear Inst. and Methods in Physics Research, A*, vol. 515, no. 1-2, pp. 73 – 88, 2003.

[24] J. O'Hanlon, *A user's guide to cvacuum technology*. John Wiley & Sons, New York, 1980.

[25] A. Chambers, F. R.K., and B. Halliday, *Basic vacuum technology*. Institute of physics publishing, Bristol and Philadelphia, 2nd ed., 1998.

[26] Huntsman Advanced Materials (Europe), Everslaan 45, 3078 Everberg, Belgium, *Safety data sheet – araldite AY 103*, October 2004. Private communication.

[27] A. international handbook committee, *Engineerd materials handbook - volume 3 - adhesives and sealants*. ASM international, Metals park, Ohio, 3th ed., 1990.

[28] M. Chefdeville, *Development of micromegas-like gaseous detectors using a pixel readout chip as collecting anode*. PhD thesis, Universiteit van Amsterdam, 2008.

[29] Y. Bagaturia. private communication.

[30] C. Färber, "New results from ageing studies," tech. rep., University of Heidelberg, 2008. Presentation LHCb week, Sep. 2008.

[31] T. H. . S. TNO Arbeid, Vereniging van de Nederlandse Chemische Industrie VNCI, *Chemiekaarten - Gegevens voor veilig werken met chemicalien*. Uitgever Chemiekaarten, Den Haag, 14th ed., 2004.

[32] J. Va'vra, "Review of wire chamber ageing," *Nuclear Inst. and Methods in Physics Research*, vol. A252, pp. 547 – 563, 1986.

[33] R. Veenhof, "Garfield, recent developments," *Nuclear instruments & methods in physics research. Section A, Accelerators, spectrometers, detectors and associated equipment*, vol. 419, no. 2-3, pp. 726 – 730, 1998.

[34] R. Veenhof, 2010. http://garfield.web.cern.ch/garfield/.

[35] H. Tolsma, *The Honeycomb Strip Chamber: a Two Coordinate and High Precision Muon Detector*. PhD thesis, Universiteit Twente, 1996.

[36] S. Biagi, 2000. http://ref.web.cern.ch/ref/CERN/CNL/2000/001/magboltz.

[37] S. Biagi, "Monte carlo simulation of electron drift and diffusion in counting gases under the influence of electric and magnetic fields," *Nuclear Inst. and Methods in Physics Research*, vol. 421, pp. 234 – 240, 1999.

[38] W. Anderson, J. Armitage, E. Dunn, J. Heinrich, C. Lu, K. McDonald, J. Weckel, and Y. Zhu, "Electron attachment, effective ionization coefficient, and electron drift velocity for cf 4 gas mixtures," *Nuclear Instruments and Methods in Physics Research Section A*, vol. 323, no. 1-2, pp. 273 – 279, 1992.

[39] J. Armitage, S. Beingessner, R. Carnegie, E. Ritchie, and J. Waterhouse, "A study of the effect of methane and carbon dioxide concentration on gas amplification in argon based gas mixtures," *Nuclear Instruments and Methods in Physics Research Section A*, vol. 271, no. 3, pp. 588 – 596, 1988.

[40] B. Jean-Marie, V. Lepeltier, and D. L'Hote, "Systematic measurement of electron drift velocity and study of some properties of some gas mixtures: A-C2H4, A-C2H6, A-C3H8 ," *Nuclear Inst. and Methods in Physics Research*, vol. 159, pp. 213 – 219, 1979.

[41] H. Fulbright, "Ionization chambers in nuclear physics," *Encyclopedia of Physics, S. Fliigge, ed., Springer-Verlag, Berlin*, p. 1, 1958.

[42] I. Gouz *et al.*, "Beam tests of lhcb outer tracker prototypes in 2000," *LHCb*, vol. 011, 2001.

[43] G. v. Apeldoorn, S. Bachmann, T. Bauer, E. Bos, Y. Guz, T. Haas, J. Knopf, J. Nardulli, T. Ketel, A. Pellegrino, *et al.*, "Beam Tests of Final Modules and Electronics of the LHCb Outer Tracker in 2005," tech. rep., CERN-LHCB-2005-076, 2005.

[44] D. Griffiths, *Introduction to Electrodynamics, 3th edition*. Prentice Hall, New Jersey, 1999.

[45] V. Suvorov *et al.*, "Avalanche and streamer production in arco2 mixtures," *LHCb*, vol. 038, 2005.

[46] B. Storaci. Private communication.

Acknowledgments

First of all, I would like to sincerely thank Niels Tuning for supervising this research project. Especially, for always making time to have fruitful discussions, giving me direction and making my graduation project such a pleasant one. I enjoyed working with you a lot this past year.

Also, I would like to thank Marcel Merk for letting me participate in his research group and giving me the chance to work on such a prominent project.

I would like to thank Piet Blankert for taking the time to be the second reader of my Masters thesis.

Many thanks to Tjeerd Ketel, my master coordinator, for all his efforts.

Furthermore, I would like to thank the entire B-physics group for making my time at Nikhef pleasant, for many productive discussions, great fun during breaks and, not in the least, for always finding time to answer questions which I had on a variety of topics. In particular, I would like to thank: Besma, Serena, Ivan, Aras, Chiara, Edwin, Daan, Barbara, Gabriel, Fabian, Eduard and everyone I have forgotten when I made that list (sorry). Eduard and Edwin I owe special thanks for the darting sessions between the long periods of writing this report.

In no particular order, I would like to thank: Jorn Boomsma, Thomas van Dijk, Wilco den Dunnen, Tomàš Ježo and Thijs Stegeman (they will agree these acknowledgments would not be complete without mentioning Raymond and Jacques) for great fun during borrels, coffee and lunch breaks, a student time to remember and for always putting up a good fight when playing M**** K***.

Above all, I would like to thank my parents, Lieneke and Ronald, my brothers, Vincent and Christiaan, and my lovely girlfriend, Julia, for their unlimited patience and support.

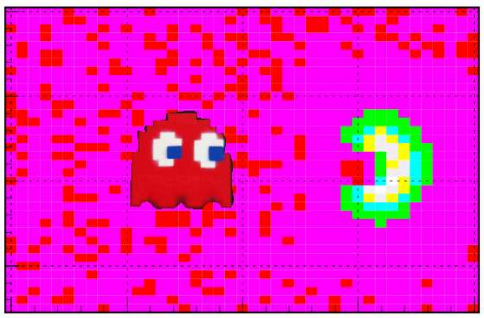

Our ageing is shaped like...? Pac-man